CHEMICAL ENGINEERING SCIENCE
GENIE CHIMIQUE

VOL. I DECEMBER 1952 No. 6

Etudes d'equilibres liquide-vapeur

A. Système dichloréthane-1,4 dioxane (1 atm)

B. Système monométhylamine-diméthylamine (10 atm)

A. DELZENNE

Laboratoire de Recherches des Etablissements Kuhlmann, La Madeleine, Paris

(Received 21 June 1952)

Summary—Vapour-liquid equilibrium data has been determined for the two binary systems:—
Dichloroethane-1.4 Dioxane at 1 atm.
Monomethylamine-Dimethylamine at 10 atm.
There is satisfactory agreement between the experimental activity coefficients and those calculated by the VAN LAAR equation.

Résumé—Détermination expérimentale du diagramme d'équilibre liquide-vapeur des deux binaires:
— dichloréthane-1,4 dioxane sous 1 atm.
— monométhylamine-diméthylamine sous 10 atm.
Les résultats sont comparés avec ceux déduits de l'équation théorique GIBBS-DUHEM-VAN LAAR.

A. Système dichloréthane-1,4 dioxane

I. PURETÉ DES CONSTITUANTS

Comme l'indique le Tableau 1 de constantes physiques, le dichlorethane et le dioxane utilisés ont été obtenus à un degré de pureté satisfaisant par rectification dans une colonne à grand pouvoir séparateur *.

* La colonne dont nous nous servons couramment dans notre Laboratoire pour la purification de nos produits peut être considérée comme équivalente à 46 plateaux théoriques dans le cas du mélange binaire *n-heptane — methylcyclohexane* avec un débit dans la colonne de 100 cc/h/cm², débit maintenu constant sur toute la hauteur de la colonne dans des conditions de reflux total.

Les analyses ont été effectuées après une période de fonctionnement de 8 heures.

Les indices de réfraction ont été déterminés au moyen du réfractomètre FERY-V URABOURG donnant la précision de la 4ème décimale.

Les densités ont été déterminées au moyen d'un picnomètre.

II. TENSIONS DE VAPEUR

Le Tableau 2 reproduit les valeurs des tensions de vapeur des constituants purs trouvées dans la littérature. Pour l'interpolation nécessaire à nos calculs, nous nous sommes bornés à l'emploi de la formule $\log P = f\left(\frac{1}{T}\right)$ se traduisant par une droite sur un diagramme à grande échelle.

Tableau 1

	Dichlorétane		*Dioxane*	
	Expérimental	*Littérature*	*Expérimental*	*Littérature*
Indice de réfraction n_D^{20}	1,4445	1,4443 [1]	1,4226	1,4232 [1]
Densité α_4^{20}	1,248	1,2529 [2]	1,036	1,0336 [3]

Tableau 2

	Constituant 1: Dichloréthane [4]									
Pression en mg Hg	1	5	10	20	40	60	100	200	400	760
Température en °C	−44,5	−24	−13,6	−2,4	+10	+18,1	+29,4	+45,7	+64	+83,5

	Constituant 2: 1,4 Dioxane [5]									
Pression en mm Hg	1	5	10	20	40	60	100	200	400	760
Température en °C	−35,8	−12,8	− 1,2	12	25,2	33,8	45,1	62,3	81,8	101,5

III. ANALYSE DES ECHANTILLONS

L'analyse des échantillons a été faite par réfractométrie, la courbe $n = f(x)$ ayant été déterminée au préalable (Tableau 3 et Fig. 1a).

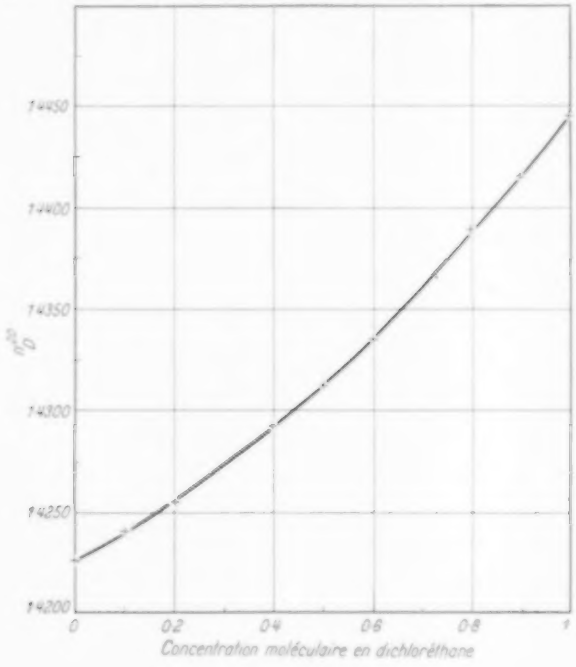

Fig. 1a. Courbe $n_D^{20} = f(x)$.

Tableau 3. Indice de réfraction n_D^{20} en fonction du titre moléculaire en dichloréthane

Titre moléculaire en dichloréthane	*Indice de réfraction*
0	1,4226
0,100	1,4240
0,200	1,4255
0,400	1,4293
0,500	1,4314
0,600	1,4335
0,800	1,4388
0,900	1,4415
1	1,4445

IV. METHODE EXPERIMENTALE

La détermination de la courbe d'équilibre liquide-vapeur a été faite en utilisant l'appareil de Stage [6] représenté sur la Fig. 2a. Le mélange liquide est chauffé à ébullition au moyen d'un chauffe ballon électrique recouvrant entièrement le bouilleur. Le distillat condensé est retenu par une cuvette annulaire entourant le col. C'est un appareil simple et robuste dont l'exactitude a parfois été contestée en lui attribuant un léger pouvoir de fractionnement. Toutefois il a été constaté dans notre laboratoire au cours de l'étude du système eaudioxane que l'appareil de Stage a donné des résultats en accord avec la littérature [7].

La température est déterminée au moyen d'un thermocouple ferconstantan connecté à un potentiomètre portatif, capable de donner une précision de 0,01 millivolt (0,2° C). Toutes les expériences ont été faites au voisinage de 760 mm; mais le températures du mélange en ébullition ont été corrigées et ramenées aux valeurs qu'elles auraient eues sous 760 mm.

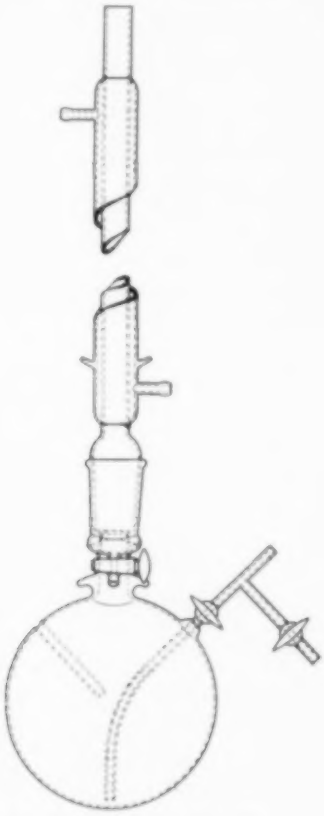

Fig. 2a. Appareil de stage.

Une charge totale de 200 cc est utilisée pour chaque essai; le régime est établi au bout de deux heures d'ébullition environ. On prélève alors un échantillon de la phase liquide et un échantillon de la phase vapeur condensée (échantillons de 1 cc).

V. RESULTATS

Les résultats expérimentaux sont rassemblés dans le Tableau 4 et représentés sur les Fig. 3a et 4a. La Fig. 3a concerne le faisceau d'ébullition et de rosée;

Tableau 1. Données expérimentales de l'equilibre liquide-vapeur du systeme dichloréthane-1,4 dioxane

Température °C	x_1	y_1	γ_1	γ_2	log γ_1	log γ_2
100,1	0,05	0,130	1,445	1	0,15987	0
98,7	0,110	0,220	1,285	0,995	0,10890	0,00218
96	0,225	0,385	1,150	1,005	0,06070	0,00217
94	0,325	0,495	1,105	1,008	0,04336	0,00346
92,4	0,420	0,580	1,050	1,010	0,02119	0,00432
90	0,555	0,715	1,040	1,010	0,01703	0,00432
87,1	0,740	0,865	1,015	1,025	0,00647	0,01072
84,8	0,900	0,945	1	1,065	0	0,02735

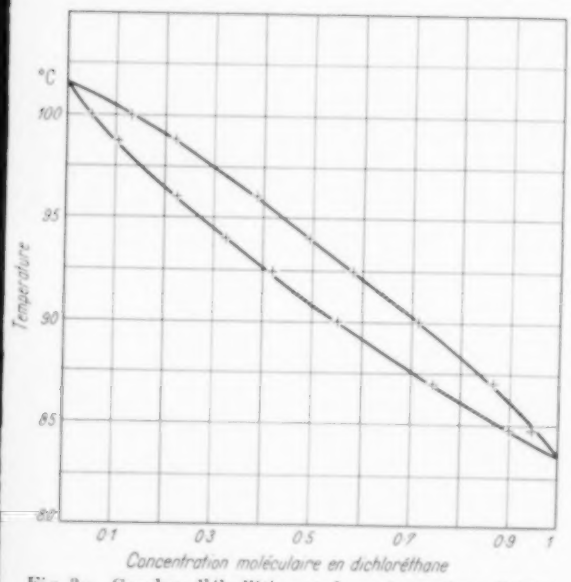

Fig. 3a. Courbes d'ébullition et de rosée système dichloréthane-1,4 dioxane.

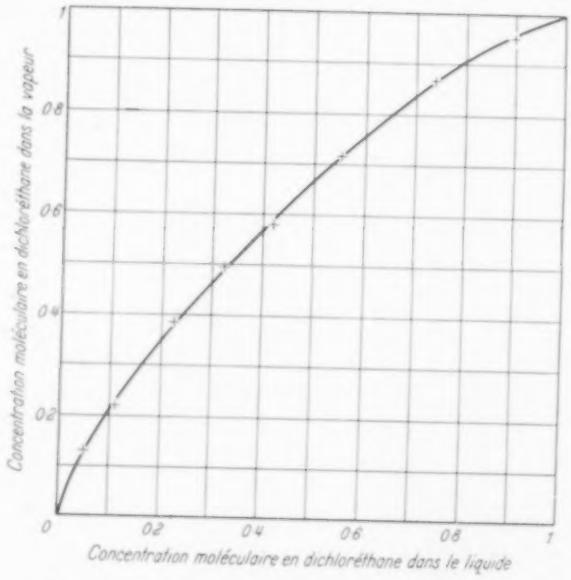

Fig. 4a. Courbe d'équilibre liquide-vapeur systeme dichloréthane-1,4 dioxane.

la Fig. 4a traduit la relation $y = f(x)$ indépendamment de la température.

Les coefficients d'activité ont été calculés d'après les relations suivantes:

$$\gamma_1 = \frac{P y_1}{p_1^0 x_1}, \qquad (1a)$$

$$\gamma_2 = \frac{P y_2}{p_2^0 x_2} \qquad (1b)$$

et les résultats obtenus sont représentés par les courbes de la Fig. 5a.

VI. Verification et Controle

Les résultats expérimentaux ont été vérifiés au moyen des équations de van Laar déduites de la relation générale de Gibbs-Duhem:

$$\log \gamma_1 = \frac{A}{\left(1 + \frac{A x_1}{B x_2}\right)^2}, \qquad (2a)$$

$$\log \gamma_2 = \frac{B}{\left(1 + \frac{B x_2}{A x_1}\right)^2}. \qquad (2b)$$

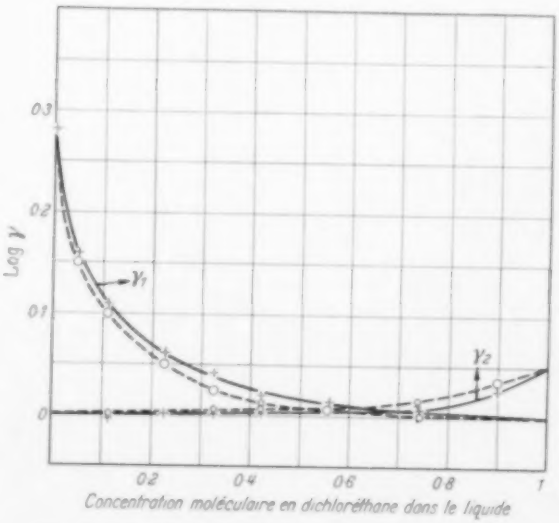

Fig. 5a. Courbe log γ: ♄(○) système dichloréthane-1,4 dioxane.

où A et B sont des constantes du système considéré, dans un faible intervalle de température.

Il convient de faire remarquer que ces équations, aussi bien celle de DUHEM que celles de VAN LAAR ont été établies en partant de conditions isothermes et ne s'appliquent strictement qu'à des résultats de ce type. Mais on sait qu'il est possible d'utiliser ces équations dans le cas de systèmes dont les composants ont, sous une pression determinée, des points d'ébullition voisins, ce qui est le cas pour le système étudié ici, puisque l'écart est inférieur à 20°.

Les valeurs des constantes A et B ont été obtenues graphiquement en prolongeant les courbes représentatives des coefficients d'activité en fonction du titre, jusqu'aux points extrêmes $x_1 = 0$ et $x_1 = 1$.

On trouve de cette façon:

$$A = 0{,}280\,,$$

$$B = 0{,}050\,.$$

Les courbes résultant de l'application des équations de VAN LAAR à partir de valeurs précédentes de A et B sont représentées en pointillés sur la Fig. 5a. L'accord entre ces dernières et les courbes expérimentales (en trait plein) est aussi satisfaisant que le permet l'emploi des équations (2a) et (2b).

B. Système monométhylamine-diméthylamine

I. PURETÉ DES CONSTITUANTS

La monométhylamine est obtenue par dégazage d'une solution aqueuse à 40% d'origine américaine. Toutes les précautions ont été prises pour obtenir un produit pur et anhydre, les vapeurs de monométhylamine passant sur de la soude caustique en pastilles pour éliminer les entrainements d'eau éventuels. De plus le récepteur était protégé de l'humidité atmosphérique par un piège contenant du chlorure de calcium.

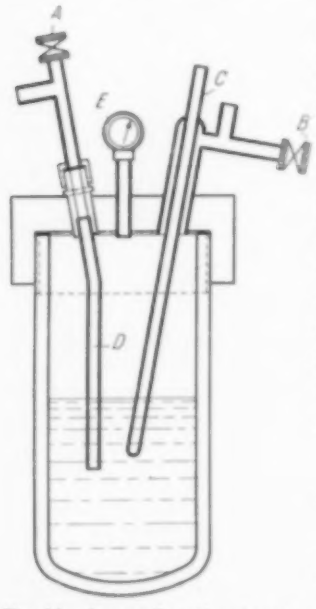

Fig. 1b. Appareil statique pour la determination des equilibres vapeur jous pression. *A* Vanne pour paise echantillom phase liquide; *B* Vanne pour paise echantillom phase vapeur. *C* Gaime pyrometrique; *D* Tube plongeur dans liquide; *E* Manometre.

La diméthylamine est obtenue dans les mêmes conditions à partir d'une solution à 25%.

La pureté des produits, déterminée par analyse chimique (acidimétrie) a atteint 99,9%.

II. TENSIONS DE VAPEUR

Nous rapportons dans le Tableau 5 les valeurs des tensions de vapeur des constituants purs.

III. APPAREILLAGE

L'appareil d'OTHMER nous ayant donné des mécomptes, nous avons préféré employer un appareil statique. Il s'agit d'un autoclave (Fig. 1b) d'une capacité de 1200 cc environ, muni d'un manomètre et d'une gaine pyrométrique permettant le contrôle de la pression et de la température. Au moyen de deux vannes, on prélève simulanément d'une part un échantillon de la phase liquide par un tube plongeant, d'autre part un échantillon de la phase vapeur.

On fait d'abord le vide dans l'autoclave; on le remplit ensuite jusqu'à moitié (600 cc). L'autoclave est alors plongé dans un bain d'eau ou d'huile et l'on chauffe jusqu'à atteindre la pression désirée. Le système est maintenu pendant trois heures environ à cette température et sous cette pression en agitant fréquemment (basculement) de façon à obtenir un très

Tableau 5. Tensions de vapeur des constituants purs

	Constituant 1: Monométhylamine [8]							
Pression en atm.	1	2	5	10	30	50	60	$P_c = 73{,}6$
Température en °C	−6,3	10,1	36	59,5	106,3	133,7	144,6	$T_c = 156{,}9$

	Constituant 2: Diméthylamine [9]							
Pression en atm.	1	2	5	10	30	40	50	$P_c = 52{,}4$
Température en °C	−7,4	25	53,9	80	132,2	149,8	162,6	$T_c = 164{,}5$

VOL. 1 1952

bon équilibre des phases. On effectue alors une prise d'échantillon des deux phases, respectivement dans deux récipients contenant un poids d'eau connu et on dose l'alcalinité de chaque échantillon.

La vanne qui permet la prise d'échantillon de la phase vapeur est entourée d'une résistance chauffante, de façon à éviter toute condensation partielle.

Le manomètre, sensible à $\pm 0{,}100$ kg/cm² est vérifié et réétalonné avant et après chaque détermination. Les températures sont enregistrées au moyen d'un couple fer-constantan relié à un potentiomètre portatif donnant une précision de 0,01 millivolt (0,2 °C).

L'appareillage a été étalonné:

a) en déterminant la courbe de tension de vapeur d'un corps connu, le méthanol,

b) en déterminant les données d'équilibre liquide-vapeur sous pression d'un système connu (système eau-méthanol sous 10 atm.).

Comme en témoignent les Tableaux 6 et 7, les résultats expérimentaux sont en bon accord avec ceux données dans la littérature.

Tableau 6. Tensions de vapeur du methanol

Pression absolue en kg/cm²	*Température observée en °C*	*Température (Littérature) [1]*
1	64,5	64,7
2	84	84
3	95,5	96
4	104,7	104,5
5	113,4	113
6	119	119
8	130,8	130,5
10	138,7	138,5
12	146	146
14	152,5	153
15	155,9	155,5

Tableau 7. Equilibre liquide-vapeur du système eau-méthanol sous 10 atm.

x_1	y_1 *expérimental*	y_1^* *littérature [10]*
0,130	0,260	0,270
0,240	0,440	0,450
0,375	0,610	0,615
0,545	0,740	0,740

IV. Analyses

Pour déterminer les concentrations dans l'une et l'autre phase on a procédé à des dosages alcalimétriques en se basant sur les équations suivantes:

Si a_1 = poids du constituant 1 dans l'échantillon
a_2 = poids du constituant 2 dans l'échantillon
M_1 = masse moléculaire du constituant 1
M_2 = masse moléculaire du constituant 2
P = poids total de l'échantillon
A = alcalinité totale exprimée en grammes d'azote.

on a:

$$P = a_1 + a_2,$$

$$A = \frac{14}{M_1} a_1 + \frac{14}{M_2} a_2$$

od'ù l'on tire a_1 et a_{22} puis

x_1 et x_2

y_1 et y_2.

V. Resultats

Les résultats expérimentaux sont rassemblés dans le Tableau 8 et représentés sur les Fig. 2b et 3b. La

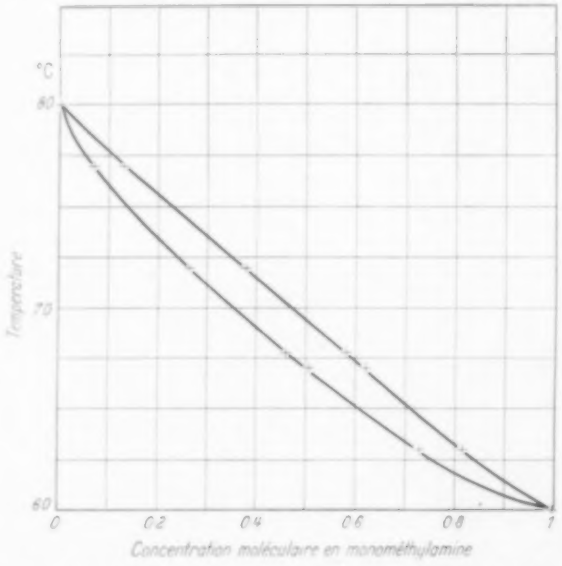

Fig. 2b. Courbes d'ébullition et de rosée système monomèthylamine-dimèthylamine.

Fig. 2b concerne le faisceau d'ébullition et de rosée; la Fig. 3b traduit la relation $y = f(x)$.

Les coefficients d'activité ont été calculés à l'aide des équations suivantes:

$$\gamma_1 = Z_1 \frac{P y_1}{p_1^0 x_1} \qquad (3a)$$

$$\gamma_2 = Z_2 \frac{P y_2}{p_2^0 x_2}. \qquad (3b)$$

En effet, la vapeur ne suivant pas les lois des gaz parfaits, on doit corriger les équations (1a) et (1b) par un facteur Z qui tient compte de la compressibilité.

Tableau 8. Données expérimentales d'équilibre liquide-vapeur du système monométhylamine-diméthylamine

Température en °C	x_1	y_1	γ_1	γ_2	$\log \gamma_1$	$\log \gamma_2$
77,1	0,070	0,130	1,260	1	0,10037	0
72	0,265	0,380	1,125	1,015	0,05115	0,00647
67,8	0,460	0,580	1,055	1,038	0,02325	0,01620
67	0,505	0,620	1,045	1,048	0,01912	0,02036
63	0,730	0,815	1,025	1,105	0,01072	0,04336

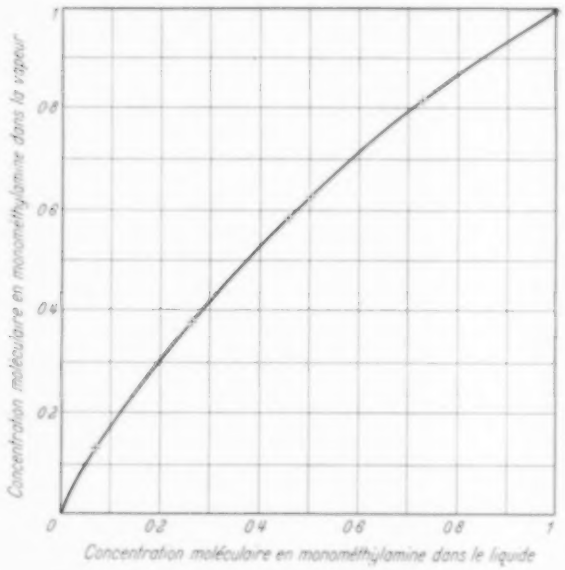

Fig. 3b. Systeme monométhylamine-diméthylamine.

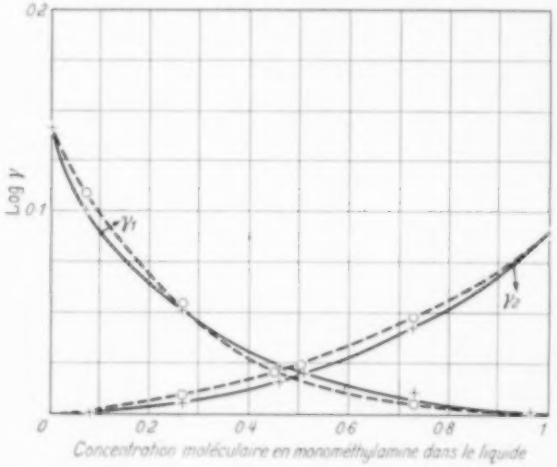

Fig. 4b. Systéme monométhylamine-diméthylamine.

D'après SCATCHARD et GILMANN [11], le facteur Z est calculable de la façon suivante:

$$\ln Z = \frac{(p^0 - P)(v - B)}{RT} \qquad (4a)$$

où:

v = volume moléculaire du liquide

B = second coefficient du viriel de l'équation d'état, dépendant de la pression réduite et de la température réduite et défini par:

$$B = \frac{RT_c}{P_c}\left(0{,}197 - 0{,}012\,T_r - \frac{0{,}400}{T_r} - \frac{0{,}146}{T_r\,3{,}27}\right). \qquad (5a)$$

Ce facteur Z peut également être lu sur un diagramme (12).

Les valeurs de γ_1 et γ_2 ainsi calculées ont été rapportées dans le Tableau 8 et l'on a tracé sur la Fig. 4b, les courbes traduisant la relation $\log \gamma = f(x_1)$.

VI. VERIFICATION ET CONTROLE

De la même façon que pour le système dichloréthane-dioxane, on a vérifié ces résultats expérimentaux au moyen des équations de VAN LAAR (2a) et (2b).

Les valeurs de A et B, valeurs de $\log \gamma_1$ et de $\log \gamma_2$ aux points extrêmes, déterminées graphiquement sont les suivantes

$$A = 0{,}140$$

$$B = 0{,}090.$$

Les courbes résultant de l'application des équations de VAN LAAR à partir de ces valeurs de A et B, sont représentées en pointillés sur la Fig. 4b. L'accord avec les courbes expérimentales est satis-faisant.

CONCLUSIONS

Le système dichloréthane-1,4 dioxane n'est pas un système idéal, non plus que le système monométhylamine-diméthylamine.

Les légères différences que l'on observe dans les courbes des coefficients d'activité entre les valeurs expérimentales et les valeurs calculées d'après les équations de VAN LAAR sont dues en partie à l'appareillage, et en partie à la non isothermicité des séries d'expériences. Néanmoins l'accord est très acceptable.

VOL. 1 1952

NOMENCLATURE

x_1 = titre moléculaire dans le liquide en constituant le plus volatil

y_1 = titre moléculaire dans la vapeur en constituant le plus volatil

γ = coefficient d'activité

P = pression totale

p° = tension de vapeur d'un constituant à une température déterminée

A et B = constantes des équations de VAN LAAR

Z = facteur de correction intervenant dans le calcul des coefficients d'activité.

LITTERATURE CITEE

[1] Handbook od Chemistry and Physics (Chemical Rubber Publishing Co.). [2] COULSON, E. A., HALES and HERINGTON, E. F. G.; Trans. Faraday Soc. 1948 **44** 636. [3] SCHÜTZ, Z.; Z. physik Chem. B 1938 **40** 156. [4] FIFE and REID; Ind. Eng. Chem. 1930 **22** 513–515. [5] GALLAUGHER and HIBBERT; J. Amer. Chem. Soc. 1937 **59** 2521–2525. [6] Öl und Kohle 1944 **40** 126. [7] Chemie Ingenieur Technik 1950 **21** 453–476. [8] ASTON, J. G., SILLER, C. W. and MESSERLY, G.; J. Amer. Chem. Soc. 1937 **59** 1743–1751. [9] SCHUMB and BICKFORD; J. Amer. Chem. Soc. 1934 **56** 852–854. [10] OTHMER, D. F. and MORLEY, F.; Ind. Eng. Chem. 1946 **38** 751–756. [11] SCATCHARD, G. and GILMANN; J. Amer. Chem. Soc. 1938 **60** 1284. [12] SCHEIBEL, E. G.; Ind. Eng. Chem. 1949 **41** 1077.

Channelling in packed columns

S. HILL, M.A., F. Inst. P., F.S.S.

Tate & Lyle Research Laboratory, Keston, Kent

(Received August 1952)

Summary.—Experiments on the displacement of sugar liquors by water from columns of granular bone charcoal (sweetening off) have led to a theory which accounts for the channelling which sometimes occurs when one fluid follows another along a uniformly packed column. The existence or absence of a tendency towards channelling is shown to depend upon the linear velocity of flow. A critical velocity can be defined in terms of the viscosities and densities of the two fluids. The interface between the two fluids may be (1) inherently stable, (2) inherently unstable, (3) stable or unstable according to the relation between the actual and the critical velocities. In the case of "sweetening off"—an important operation in sugar refining—channelling occurs if the velocity of flow exceeds the critical velocity. Experimental evidence is quoted in support of the theory.

Résumé—Etudiant le déplacement par l'eau des jus sucrés dans les colonnes à noir animal, l'auteur propose une théorie qui rend compte des court-circuits qui se produisent parfois lorsqu'un fluide en déplace un autre dans une colonne à garnissage uniforme. Il définit une vitesse critique fonction des viscosités et densités des deux fluides.

La surface de séparation de deux fluides peut être: 1. essentiellement stable — 2. essentiellement instable — 3. tantôt stable, tantôt instable, suivant le rapport entre la vitesse actuelle et la vitesse critique. Dans le cas de la décoloration des jus sucrés, le court-circuitage se produit si la vitesse d'écoulement dépasse la vitesse critique.

La théorie paraît en accord avec les faits expérimentaux cités par l'auteur.

INTRODUCTION

Refining of raw sugar, beet or cane, necessitates a sequence of processes which are devised to reduce the concentration of non sugars. After affination the raw sugar is dissolved and the solution is purified by carbonatation and filtration. Before crystallisation of granulated sugar by boiling in vacuum pans the sugar liquors are further purified by downward percolation through granular bone charcoal (char) in deep vertical cylindrical "cisterns". In this process adsorption of non-sugars, colouring matters, salts etc. takes place and as percolation proceeds the adsorptive power of the char is progressively reduced and the effluent from the cistern becomes less pure. When the purity of the effluent, as indicated by its colour density, has decreased to an established limit, beyond which the liquor would not be suitable for production of market quality granulated sugar, the cistern is sweetened off—*i.e.* the sugar liquor remaining in the cistern is displaced downwards by water.

Any mixing of the liquor and the water during sweetening off is undesirable. The liquor to be displaced usually contains about 67 % of sucrose. Ideally the percentage concentration (° Brix) of the effluent should follow the broken curve of Fig. 1, the discontinuous reduction to zero Brix taking place when the water-liquor interface reaches the bottom of the cistern.

In practice some departure from this ideal cannot be entirely prevented. The continuous curve is typical of practical cases. In the *Tate and Lyle* Refineries it has been customary to accept liquor for crystallisation until the concentration falls to about 45° Bx. Liquors below 45° Bx can be used for sweetening

off other cisterns [1]. Alternatively they can be concentrated by evaporation, in which case it is important to minimise the quantity of light liquors (liquors of concentration less than 45° Bx) in order to economise in time and cost of evaporation. As also the evaporated lights are of much lower purity

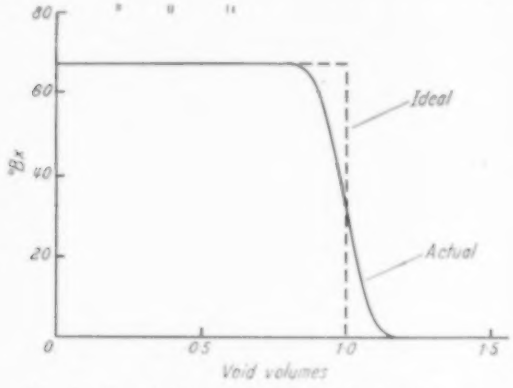

Fig. 1. Sweetening off—Ideal and actual curves.

than the liquor from which they originated, through desorption from the char of previously adsorbed impurities, they cannot be utilised directly for production of granulated sugar.

Production of Light Liquors During Sweetening Off

Hitherto two main factors have been recognised as contributing to the formation of lights. These are (1) mixing of the water and the liquor by diffusion at the horizontal interface and (2) the time taken for the sugar liquor to drain and diffuse out of the pores of the granules. Turbulence has been mentioned as a third contributory factor [2] but we consider that this is improbable. The Reynolds number under Refinery conditions of operation is well below the limit at which turbulent flow can arise. As a matter of long established experience the quantity of lights can only be kept down to a reasonable level by sweetening off with a very small velocity of flow. This indicates that diffusion of liquor from the pores of the granules is the limiting factor.

Recent laboratory and pilot scale experiments [3] have shown that the rate of adsorption of colour (impurities) during percolation can be greatly increased by using char of smaller granular size than has been usual hitherto. Therefore there is a considerable incentive to use fine grist char. Considerations of the pressure gradient required to generate the flow of liquor will limit the extent to which the char size can be reduced. A limiting mean aperture (M.A.) of the order of 0·01 in. is imposed by this factor. However a more serious difficulty has been encountered during pilot scale experiments with fine grist char [4]. *viz.*: the excessive quantity of lights formed when sweetening off proceeds at a rate of flow that is satisfactory for the normal grist of char.

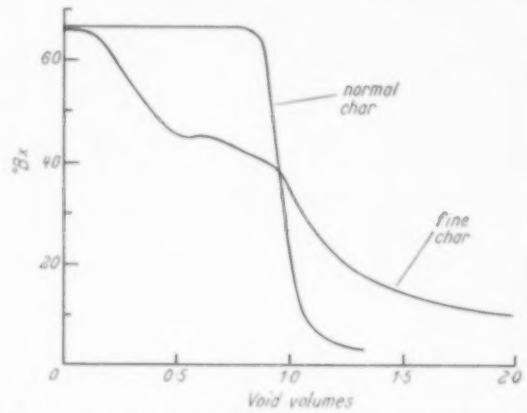

Fig. 2. Sweetening off—Pilot plant curves for normal grist and fine grist char.

Two char cisterns were operated in parallel. One of these contained char of normal size and the other a fine grist char. The size distributions of the chars were approximately Gaussian (normal) with respect to weight. The mean aperture of the normal char was 0·039 in. and that of the fine char was 0·011 in. The coefficients of variation (C.V.) were about 52% (normal) and 35% (fine). Figs. 2 and 3 show, respectively, the curves obtained when the chars were sweetened off and sweetened on. Sweetening on is the inverse of sweetening off. Char may sometimes be settled into water. Sweetening on is the displace-

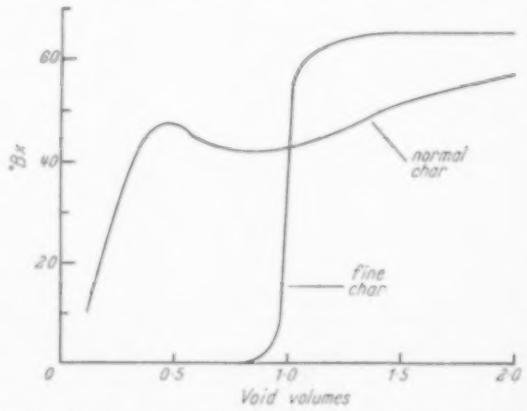

Fig. 3. Sweetening on—Pilot plant curves for normal grist and fine grist char.

VOL. 1 1952

ment of this water by sugar liquor, in this case by downward flow.

We see that at the flow velocities used the normal char gives a satisfactory sweetening off curve and an unsatisfactory curve for sweetening on, while the opposite is the case for the fine char. A theoretical explanation of these phenomena is advanced in the following.

THEORY OF CHANNELLING

When a mobile fluid (*e.g.* water) displaces a viscous fluid (*e.g.* sugar liquor) from the voids of a uniform packing the difference between the viscosities tends to cause instability.

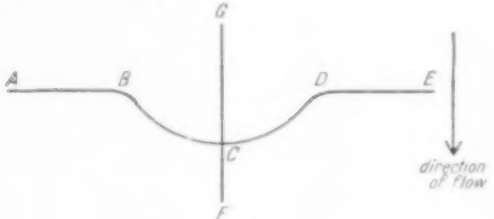

Fig. 4.

Consider the interface A B C D E (Fig. 4) between the two fluids. B C D is a bulge which is supposed to have developed in the interface. The line G C F which is perpendicular to A E is a path of minimum resistance to flow so that the velocity through C increases and the depth of the bulge also increases. Therefore the difference between the viscosities tends to make the interface unstable during the process of sweetening off. Conversely this factor has a stabilising influence on the interface during sweetening on.

If, during the operation of sweetening off or sweetening on, the less dense fluid is above the denser one the difference between the densities of the fluids tends to keep the interface horizontal. On the other hand it tends to cause instability of the interface if the denser fluid is uppermost.

Sugar solutions are denser and more viscous than water, and from a consideration of these two factors (density and viscosity) it follows that upward sweetening off is an inherently unstable process while upward sweetening on is inherently stable. The other two processes—sweetening off and on by downward flow—may be stable or unstable according to which of the two factors predominates.

The theory may be formulated quantitatively as follows.

Consider a fluid of viscosity μ_2 and density ϱ_2 displacing a fluid of of viscosity μ_1 and density ϱ_1 by downward flow (Fig. 5).

The velocity of flow $= v$.

Suppose that a shallow depression C D, of depth δx, develops in the interface A B.

Let p_0 = pressure at the level A B,
p_1 = pressure just below C D,
p_2 = pressure just above C D.

The depression will disappear if $p_1 > p_2$, and will increase in depth if $p_2 > p_1$.

Now

$$p_1 = p_0 + g\varrho_1\delta x - k\mu_2 v\delta x$$

and

$$p_2 = p_0 + g\varrho_2\delta x - k\mu_2 v\delta x$$

where k = resistance constant of the char, and g = acceleration due to gravity.

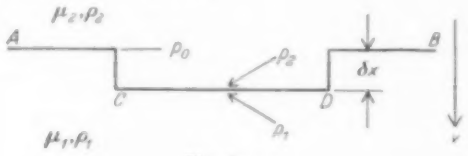

Fig. 5.

The condition for stable flow is therefore:

$$p_1 - p_2 = g(\varrho_1 - \varrho_2)\delta x - kv(\mu_1 - \mu_2)\delta x > 0.$$

That is

$$g(\varrho_1 - \varrho_2) > kv(\mu_1 - \mu_2)$$

or

$$v < \frac{g(\varrho_1 - \varrho_2)}{k(\mu_1 - \mu_2)}.$$

Apart from k all of the quantities in this expression are known. k must be determined experimentally.

$\frac{g(\varrho_1 - \varrho_2)}{k(\mu_1 - \mu_2)}$ will be called the critical velocity, v_c.

If $\varrho_1 > \varrho_2$ and $\mu_1 > \mu_2$ (downward sweetening off) the flow is unstable if v exceeds the critical value. In the case of downward "sweetening on" ($\varrho_2 > \varrho_1$ and $\mu_2 > \mu_1$) the flow is stable if (and only if) the velocity exceeds the critical value.

Note that conditions that yield stable sweetening off cause unstable sweetening on and vice versa. Note also that laboratory experiments designed to test sweetening off and on must be done at the correct linear velocity.

The differences between the curves for fine and normal char in Figs. 2 and 3 can now be accounted for by the difference between the two values of k. The fine char has a greater value of k and therefore a smaller critical velocity.

Owing to lack of exact data the critical velocities could only be roughly estimated but Table 1 shows that within the limits of uncertainty the curves conform to the theory.

VOL. 1 1952

SWEETENING OFF

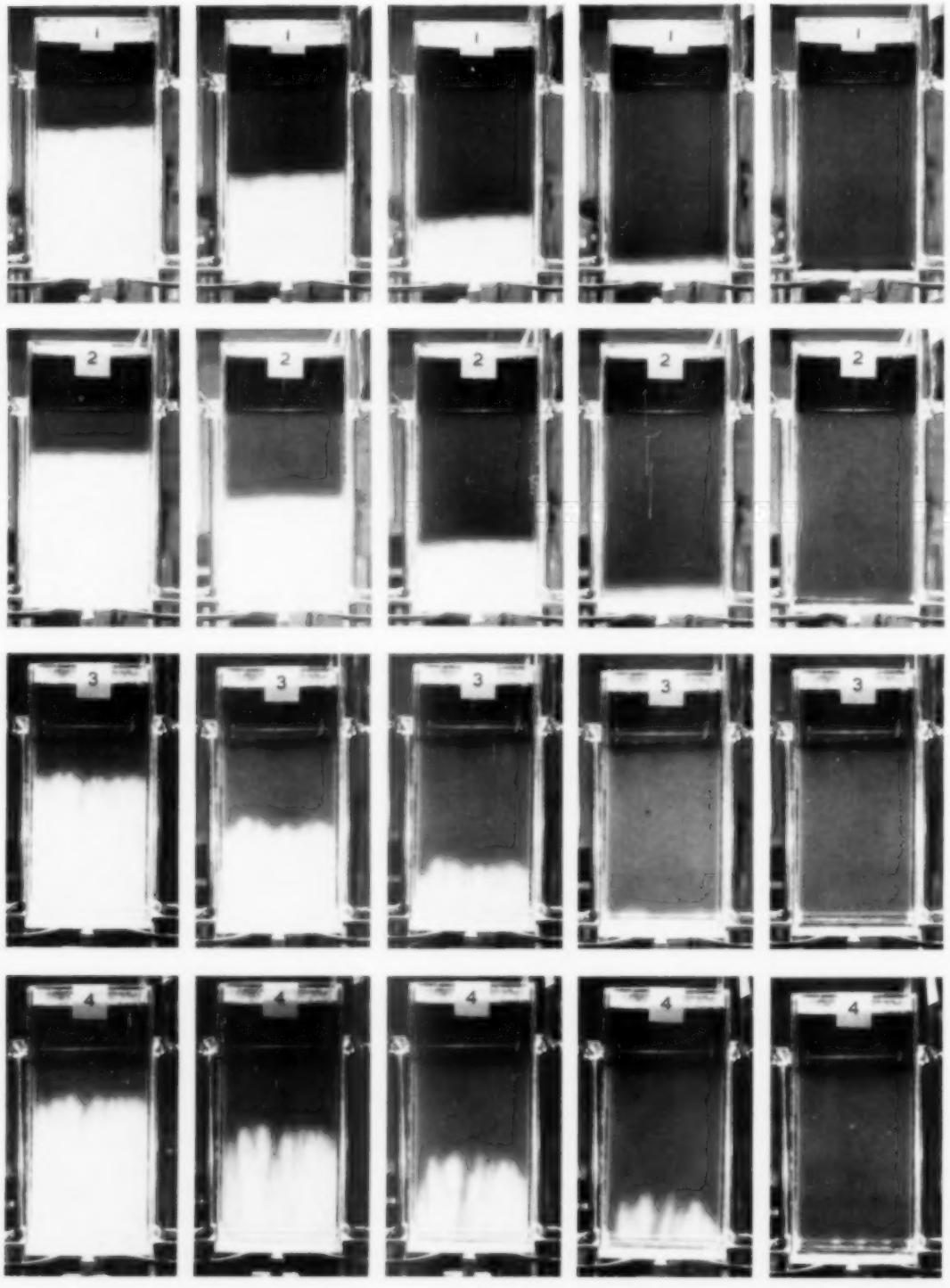

PLATE I

SWEETENING ON

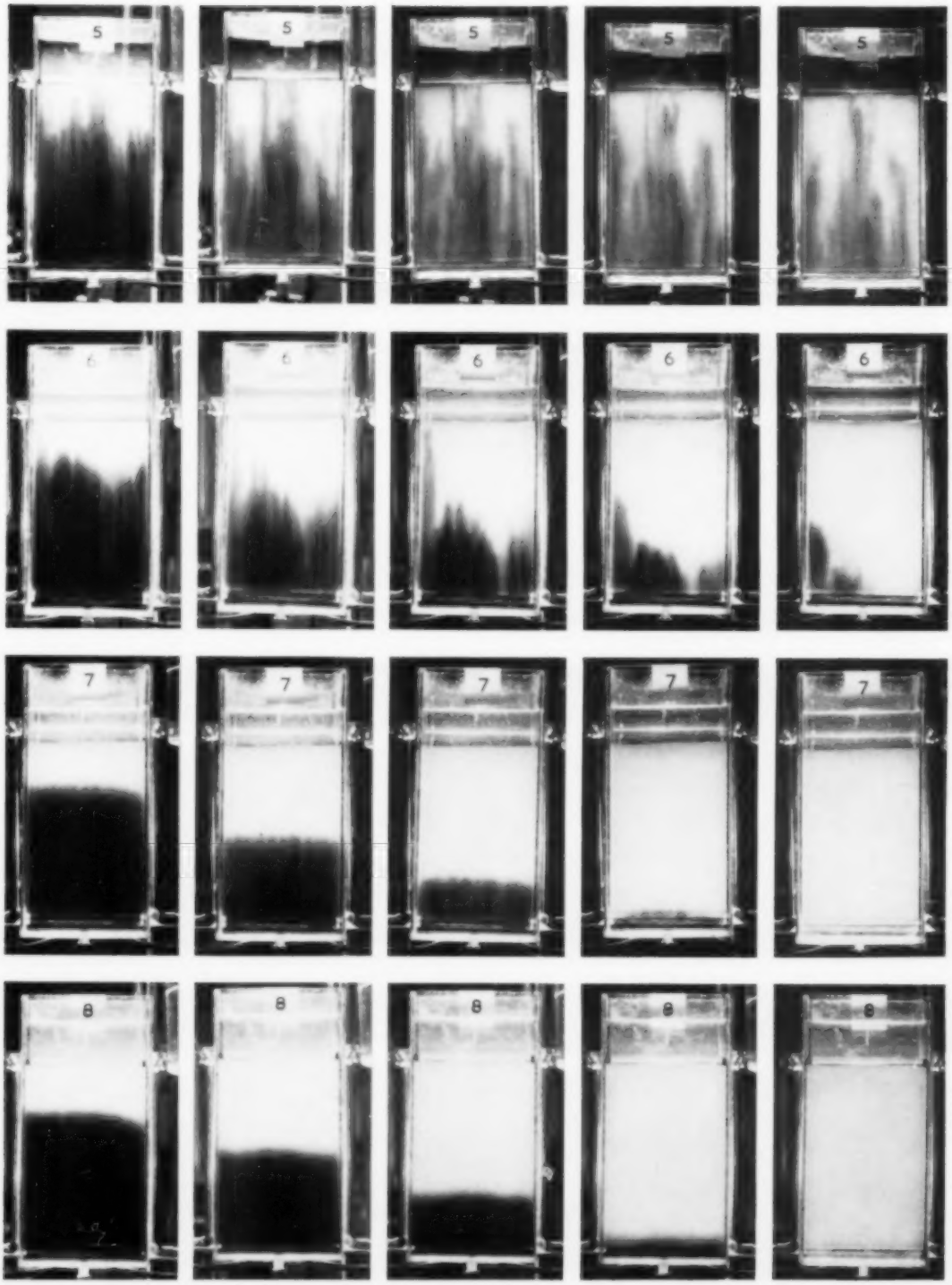

$V = \frac{1}{4}V_c$

$V = V_c$

$V = 2V_c$

$V = 4V_c$

PLATE 2

Two direct tests of the theory have been made. In the first test a transparent perspex cell of height = 13 in., breadth = 6 in. and thickness = 1 in. and containing sugar solution was packed to a depth of 9 in. with glass spheres of 0·4 mm diameter (Plates 1 and 2). The value of k for the packing was determined and the critical velocity calculated. The cell was then sweetened off by adding coloured water at the top

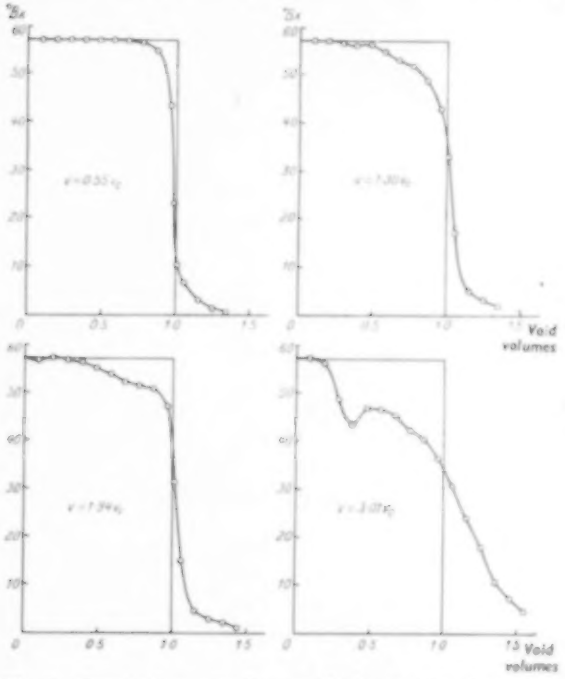

Fig. 6. Sweetening off—Curves obtained with the 1 ft laboratory column.

from a constant level device and running off the sugar solution from the bottom. The cell was suitably illuminated and photographs were taken when the volumes of liquor displaced were $\frac{1}{4}$, $\frac{1}{2}$, $\frac{3}{4}$, 1 and 1$\frac{1}{4}$ times the void volumes of the packing—Plate 1. The dark areas of the cell are occupied by the coloured water and the light areas by the sugar solution. Sets numbered 1, 2, 3 and 4 of Plate 1 show the results obtained when the velocities of flow were respectively $\frac{1}{2}$, 1, 2 and 4 times the critical velocity. Satisfactory separation of the liquid is maintained in sets 1 ($v = \frac{1}{2} v_c$) and 2 ($v = v_c$), but channelling occurs in sets 3 ($v = 2 v_c$) and 4 ($v = 4 v_c$). Similar sets of photographs, shown in Plate 2, were made while sweetening on. In this case the results of sets 5

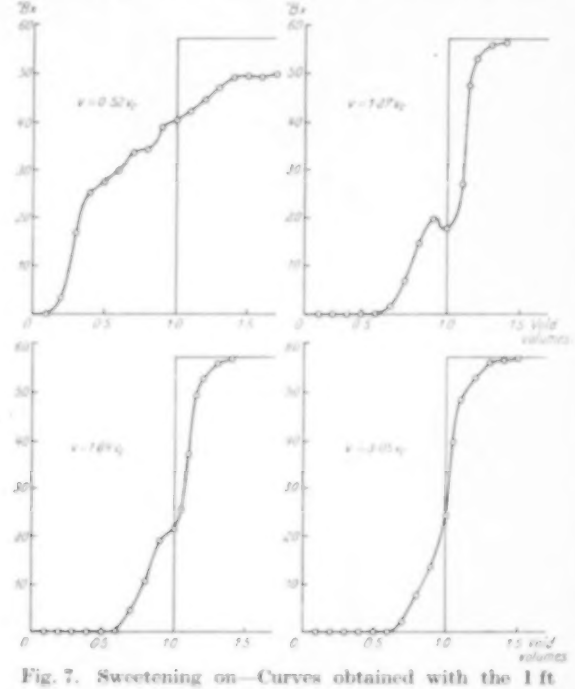

Fig. 7. Sweetening on—Curves obtained with the 1 ft laboratory column.

($v = \frac{1}{2} v_c$) and 6 ($v = v_c$) are unsatisfactory, while sets 7 ($v = 2 v_c$) and 8 ($v = 4 v_c$) show good separation.

In the second test a column 1 ft high and $2\frac{7}{8}$ in. in diameter was packed with char of M.A. = 0·0138 in., and C.V. = 25%. The char was sweetened off and on at velocities varying from $\frac{1}{2} v_c$ to $3 v_c$. For convenience the experiment was made with 57° Bx sugar solution at 30° C. Under these conditions $v_c = 0{\cdot}2$ ft/hr open tube velocity. The two groups of curves, Figs. 6 and 7 show the results, which also conform to the theory. Satisfactory sweetening off is achieved only if $v < v_c$ and satisfactory sweetening on if $v > v_c$.

The effects described are in dependentof small inhomogeneities in the packing.

Table 1

Grist	*Sweetening*	*Liquor velocity (ft/hr)*		*Result*	
		Actual	*Critical*	*Expected*	*Observed*
normal	off	0·26	0·9	good	good
	on	0·51		bad	bad
fine	off	0·26	between 0·12 and 0·32	?	bad
	on	0·51		good	good

Refinery Considerations

We may now consider the quantitative nature of this problem as it affects Refinery operations. A char cistern in which liquor is decolourised by char will

deliver a quantity of liquor which depends on the time taken to pass one cistern volume of liquor. If this time is 3 hrs in the case of carbonatated liquor on char of M.A. = 0·014 in. the volume of acceptable liquor produced is of the order of 20 cistern volumes so that the cistern is decolourising liquor for about 60 hrs. In the Refinery 67° Bx liquor is processed at 70° C. Such liquor has a critical open tube velocity through a packing of this char of about 0·4 ft/hr. Assuming 60% voids in the char this gives a critical linear velocity of 0·67 ft/hr. A separate experiment has shown that the concentration of the effluent liquor does not fall to the value 1·8° Bx (at which it is turned to drain) until about 1·5 cistern void volumes have been displaced. Thus the time taken to sweeten off at the critical velocity is 1·5/0·67 = 2·25 hrs/ft of column.

Conventional char cisterns are from 16 to 20 ft deep so that sweetening off would take from 36 to 45 hrs. Comparing this with the 60 hrs of decolourisation we see that the non-effective time is a substantial fraction of the whole. On a shorter cistern the fraction would, of course, be correspondingly smaller.

The practical sweetening off of fine char is therefore still an incompletely solved problem. It is also one of considerable importance. The procedure customary with normal char has been found inadequate. Slow sweetening off of short columns may be an acceptable compromise but a really satisfactory solution is still awaited.

Acknowledgments—Acknowledgment is made for the information supplied by D. R. DICKINSON and G. PAYNE from the experiments carried out by them in the Pilot Plant Char Department at the *Tate & Lyle* Plaistow Refinery and to the Directors of *Tate & Lyle* for permission to publish this paper incorporating work carried out in the Research Laboratory.

NOTATION

° Bx = % concentration of a sugar solution.
M.A. = Mean aperture = Sieve aperture through which 50% of the char can be passed.
C.V. = Coefficient of variation = $\frac{100 \times (\text{Standard deviation})}{(\text{M. A.})}$ %.
μ_1 = Viscosity of the fluid being displaced.
ϱ_1 = Density of the fluid being displaced.
μ_2 = Viscosity of the displacing fluid.
ϱ_2 = Density of the displacing fluid.
p_0 = Hydrostatic pressure at the plane part of the interface.
p_1 = Hydrostatic pressure just below the bottom of the bulge.
p_2 = Hydrostatic pressure just above the bottom of the bulge.
g = Acceleration due to gravity.
k = Resistance constant of the packing = Pressure gradient required to generate flow at unit velocity of a fluid of unit viscosity.
δx = Depth of an incipient bulge in the interface.
v = Open tube velocity of flow.
v_c = Critical velocity of flow.

REFERENCES

[1] DE WHALLEY, H. C. S.; *Sugar Industry Technicians, Inc.*, May 1951. [2] BABCOCK, A. B. and BASTONE, H. J.; Proceedings of the Technical Session on Bone Char, 1949, p. 149. [3] DE WHALLEY, H. C. S. and ALBON, N.; Int. Sugar J. 1946 **48** 125. THOMPSON, H. M. *et al.*; Private communication. DICKINSON, D. R. and PAYNE, G.; Private communication. [4] DICKINSON, D. R. and PAYNE, G.; Private communication.

Transport of solids through horizontal rotary cylinders

L. VÀHL and W. G. KINGMA

Research Department for Chemical Engineering of Werkspoor N.V., Amsterdam, Netherlands

(Received August 1952)

Summary—Equations based on theoretical considerations have been developed to give the volume transported per minute, the loading in the drum, the time of passage and the power requirements for the transport of granulated solids through horizontal rotary cylinders without flights or any other lifting devices. The simple equations are suitable for practical purposes. Experiments have shown that the results of the calculations are in reasonable accordance with the values obtained from the experiments.

Résumé—Des considérations théoriques ont conduit à des équations permettant de calculer le volume transporté par minute, la charge du cylindre, la durée de passage et la puissance consommée pour le déplacement de solides en grains au travers de cylindres rotatifs horizontaux dépourvus de chicanes ou de tout autre dispositif élévatoire. Des équations simples suffisent pour les applications pratiques. Les résultats expérimentaux sont en bon accord avec les valeurs calculées.

1. INTRODUCTION

For handling a continuous flow of granulated material in drying, humidifying, mixing, heating, cooling or calcining processes, in chemical reactions with gases, etc. rotary cylinders are often used, through which the granules are transported.

In many cases the interior of the rotary cylinders contains flights or other lifting devices causing an intensive contact between the granulated material and the gases that flow through the drum in counter-current or in parallel current with the granules.

The most simple construction of rotary drums, however, is that without any flights or lifter blades inside the cylinder. This type of cylinder is often used in industry, *e.g.* for the manufacture of cement, for burning light granules of clay and so on.

The design of rotary cylinders involves the calculation of:

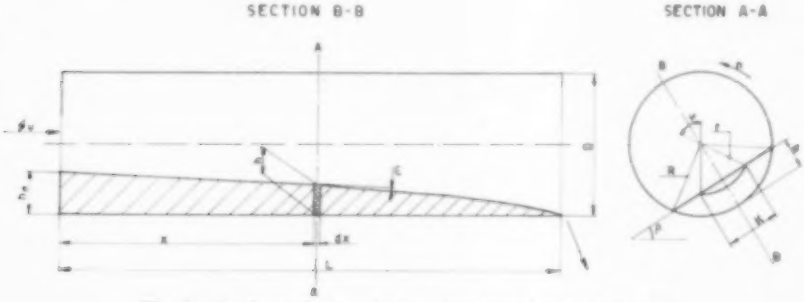

Fig. 1. Surface of material in a horizontal rotary cylinder.

1. The amount of material flowing through the drum;

2. The loading in the drum as a percentage of the total volume;

3. Time of passage of the material through the drum.

These quantities have to be determined as functions of:

1. Dimensions and other constructional data of the drum;

2. Properties of the material to be transported;

3. Operating conditions of the plant.

In horizontal drums, without flights and without flow of gases, transport of granulated materials takes place because of the difference of the levels of the material at the entrance and discharge end of the drum [1]. Calculation of the volume transported per minute Φ_v gave the equation:

$$\Phi_v = a \left(\frac{h_0}{D}\right)^b \cdot \frac{D^3\, n \,.\, \cot \beta}{L} \qquad \text{(A)}$$

where a and b are constants. For the meaning of the other symbols, see list of notations.

This result contradicts the empirical equation of SULLIVAN, *et al.* [2] according to which the transport would be nil in horizontal rotary kilns.

Last year SAEMAN published a theory of the transport of material through rotary cylinders [3]. For lightly loaded kilns an equation is derived resembling that of SULLIVAN. Due to the simplifications introduced into the calculations, SAEMAN's theoretical considerations do not give results than can be used for horizontal rotary cylinders. For the transport of material at heavy kiln loads and in horizontal cylinders no solution is given.

Eq. (A) gives figures for the transport of material through *horizontal* rotary cylinders, that are in good agreement with the experiments, even for heavy loads. It is interesting to note that this equation has been developed on the same theoretical assumptions as used two years later by SAEMAN. The different result is mainly due to the fact that the simplifications, necessary for the mathematical development of eq. (A), have been chosen more fortunately than those used by SAEMAN. The results of the theory for the calculation of material transport, load, time of passage and power requirements,—already published in part in 1949 [1]—can immediately be used for practical purposes and will, therefore, be given in some detail in the present paper.

VOL. 1 1952

2. EQUATION FOR TRANSPORT RATE OF MATERIAL

The surface of the granulated material in a horizontal rotary drum without flights is shown schematically in Fig. 1. The feed rate should be sufficient to keep the bed depth at the entrance constant (measured along B–B). It is assumed that the particles do not slide along the cylinder wall.

The particles cascade quickly down in a thin layer on the surface of the bed along chord k and are then carried back again in the bulk of the bed to the surface. The position of the surface with respect to the horizontal plane is determined by the angle of repose β of the material. The angle of repose depends on the physical properties of the material, as friction coefficient of the particles, distribution of size of particles and bulk density. The axial component of the path of the cascading particle can be determined by geometrical considerations as a function of the path k, the angle of repose β and the angle ε:

$$s = k \frac{\cos \beta \,.\, \sin \beta \,.\, \tan \varepsilon}{\tan^2 \varepsilon + \sin^2 \beta} .$$

The angle ε being small, $\tan^2 \varepsilon$ may be neglected against $\sin^2 \beta$, so

$$\frac{s}{k} = \cot \beta \,.\, \tan \varepsilon \,, \tag{1}$$

where

$$\tan \varepsilon = - \frac{dh}{dx} \,.$$

A particle on a circle with radius r travels along the arc $q\,r$ in the time $\frac{q\,r}{n \,.\, 2\pi r}$. When the particle arrives at the surface of the bed, it cascades along a path of a length equal to chord k in a time that may be neglected with respect to the time needed for travelling along the arc of the circle. The average axial transport velocity v_r of this particle during the complete cycle will therefore be

$$v_r = - k \,.\, \cot \beta \,.\, \frac{dh}{dx} \,.\, \frac{2\pi n}{q} \,. \tag{2}$$

This equation is valid for all particles in a cross-section of the area $q\,r \cdot dr$ and the flow of material through this elementary section is

$$d\Phi_v = v_r \,.\, q \,.\, r \,.\, dr = - n \,.\, \cot \beta \,.\, \frac{dh}{dx} \,.\, k \,.\, 2\pi r \,.\, dr \,. \tag{3}$$

The total flow of material through a section of the drum is

$$\Phi_v = - 2\pi n \,.\, \cot \beta \,.\, \frac{dh}{dx} \int_{R-h}^{R} k \,.\, r \,.\, dr \,, \tag{4}$$

where $k = 2\sqrt{r^2 - (R-h)^2}$.

Integration of (4) gives the equation

$$\Phi_v = - \frac{4}{3} \pi R^4 n \,.\, \cot \beta \left\{ 2 \frac{h}{R} - \left(\frac{h}{R} \right)^2 \right\}^{\frac{3}{2}} \frac{d \frac{h}{R}}{dx} \,. \tag{5}$$

Writing $\frac{h}{R} = \xi$, $\frac{h_0}{R} = \xi_0$ and $\frac{h_L}{R} = \xi_L$, where the subscripts indicate values at the entrance and the end of the drum respectively, the eq. (5) can be integrated:

$$\frac{\Phi_v}{\frac{1}{3}\pi R^4 \,.\, n \,.\, \cot \beta} \int_0^L dx = - \int_{\xi_0}^{\xi_L} (2\xi - \xi^2)^{\frac{3}{2}} \,.\, d\xi = F(\xi_0). \tag{6}$$

In cases where $h_L = 0$ the function $F(\xi_0)$ becomes:

$$\left. \begin{aligned} F(\xi_0) = - \frac{3}{8} \left\{ \sin^{-1}(1 - \xi_0) - \frac{\pi}{2} \right\} - \frac{1}{4} \times \\ \times (2\xi_0 - \xi_0^2)^{\frac{1}{2}} \,.\, (\tfrac{5}{2} + \tfrac{1}{2}\xi_0 - 3\xi_0^2 + \xi_0^3) \,. \end{aligned} \right\} \tag{7}$$

Fig. 2 shows $F(\xi_0)$ as a function of ξ_0. It can be seen in Fig. 2 that the rather complicated expression (7) can be replaced by the sufficiently close approximation:

$$F(\xi_0) \cong 0{\cdot}62 \,.\, \xi_0^{2{\cdot}08}$$

in the interval $0{\cdot}3 < \frac{h_0}{R} < 0{\cdot}9$ that is interesting for practical purposes.

Substitution of this approximation in eq. (6) gives for the volume transported per minute:

$$\Phi_v = 0{\cdot}68 \left(\frac{h_0}{D} \right)^{2{\cdot}08} \,.\, \frac{D^4 \,.\, n \,.\, \cot \beta}{L} \,. \tag{8}$$

for values in the interval $0{\cdot}15 < \frac{h_0}{D} < 0{\cdot}45$*.

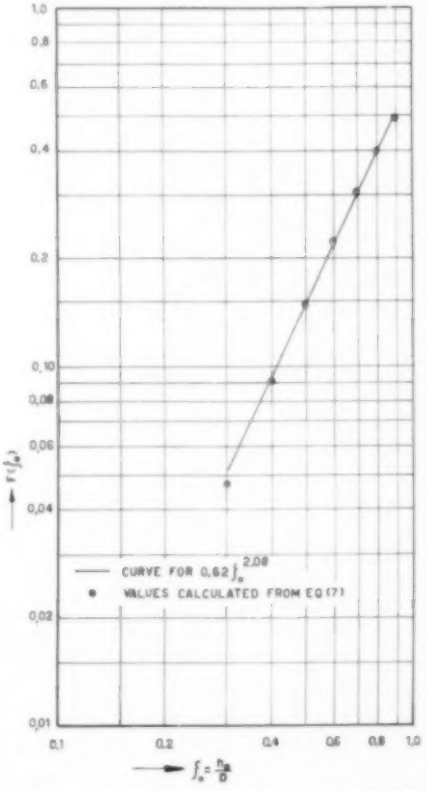

Fig. 2. Curve representing function $F(\xi_0)$.

3. Laboratory Experiments

a) *Description of apparatus*

For the experiments, glass and steel cylinders have been used, both with a diameter of 110 mm and a length of 650 mm (see Fig. 3). The constriction at the entrance was variable, and so experiments could be carried out with different values of h_0. The discharge end of the rotating cylinder was not constricted and no experiments have been made with such constrictions. A constant supply, necessary for the experiments, has been obtained by a simple but reliable control device.

* The development of eq. (8) here given is a simplification proposed by Prof. H. KRAMERS of the original development by the authors.

b) *Qualitative experiments*

Two materials have been used for the experiments *viz.* dry sharp sand (diameter of particles 0·2 to 1 mm) and rye (particles 7 mm long and 2 mm diameter).

For facilitating the study of the cascading of the granules the first experiments have been carried out in a glass cylinder. It turned out that in the glass cylinder the bed of sand, and even more so the rye, started sliding as one solid mass as soon as the depth h of the bed became less than a certain value ($h < 12$ mm), and no cascading of particles took place

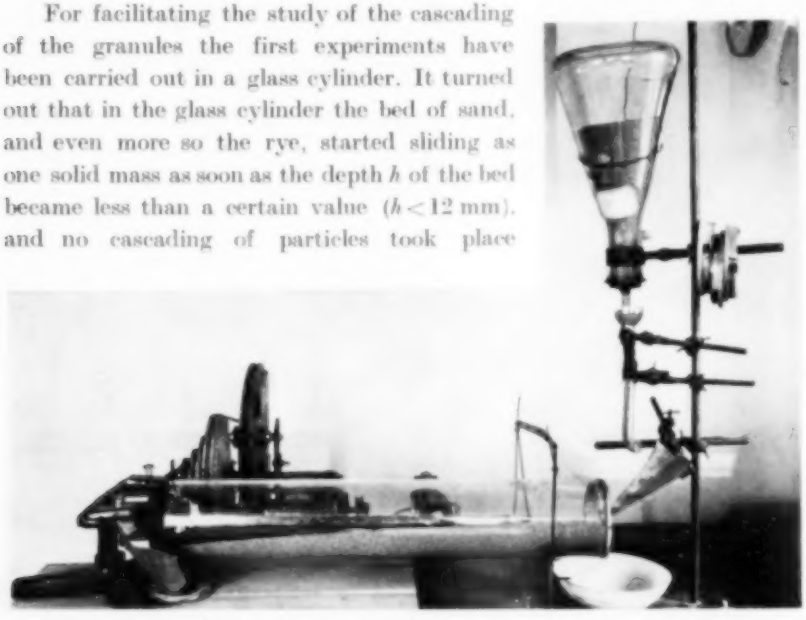

Fig. 3. Apparatus used for the experiments.

because the angle of repose of the material was not attained.

In the steel cylinder with a rough surface the particles cascaded, without sliding of the material as

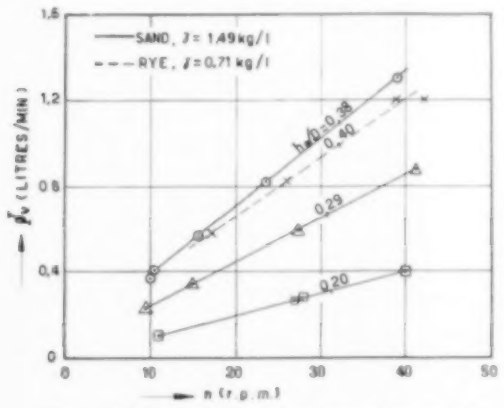

Fig. 4. Volume flow of transported material.

a whole, because the friction between the material and the wall was greater than the mutual friction between the granules.

The movement of the material in a cross section could be observed by using a transparent ring of celluloid at the entrance of the cylinder. At low speeds of the cylinder a particular granule described continuously about the same path. The layer of cascading granules gave the impression of a laminar flowing liquid. At higher speeds, $n > 15$ r.p.m., the straight cascading path changed into a wave line with a minimum in the middle.

c) *Quantitative experiments*

When a certain speed of the cylinder and a certain depth h_0 of the bed at the entrance had been set up, the feed of material was controlled in such a way that a small amount of material flowed over the ring out of the cylinder. The steady state was soon obtained and then the transported material would be collected for some time and weighed. The accuracy of the measurement was about 2%.

Fig. 4 shows curves of the measured quantities of transported material. The load of the rotating cylinder was determined by weighing its contents at the end of each experiment.

d) *Bulk density*

In the beginning of this study the bulk density has been determined by means of a calibrated measuring glass. The values obtained in this way showed large variations, depending on the manner of filling the measuring glass. Careful filling or prolonged stamping of the contents resulted for sand in values varying from 1·45 to 1·62 kg/l. Therefore another method of measuring the bulk density has been adopted. A cylinder of 110 mm diameter, closed by glass discs at both ends, was charged with a certain amount of material. After rotating the cylinder for some time the depth of the bed of material was measured accurately and the volume of the bed calculated. From the weight of the contents of the cylinder the bulk density under actual conditions in a rotary drum could then be computed.

The bulk density measured in this way was for sand 1·49 kg/l and for rye 0·71 kg/l.

The angle of repose β has been measured in rest. After slowly revolving the cylinder by hand until cascading of the granulated material started, the

VOL. 1 1952

angle between the bed surface and a horizontal plane could be determined with an accuracy of 1°. The value of the angle of repose was for sand 33° and for rye 40°.

4. Comparison of the Results of Calculations and Experiments

The results of the experiments are given in Fig. 4, which shows for each value of h_0/D a linear relationship between the volume transported per minute and the speed of the rotating cylinder. From these results an experimental coefficient f_{exp} can be determined for each value of h_0/D (see Fig. 5):

$$f_{exp} = \Phi_v \frac{L}{D^3 . n . \cot\beta} = 0{\cdot}74 \left(\frac{h_0}{D}\right)^{2{\cdot}05}.$$

Comparing the results of the experiments, shown in Fig. 4, with those of the theoretical calculation (eq. (8)], it appears that the experimental values are approximately 13% higher than the theoretical ones. As the measured values in Fig. 5 are lying rather close on a straight line, the following empirical equation can be given for the volume Φ_v transported per minute:

$$\Phi_v = 0{\cdot}74 \left(\frac{h_0}{D}\right)^{2{\cdot}05} . \frac{D^3 . n . \cot\beta}{L}, \qquad (9)$$

which equation is for values $0{\cdot}15 < \frac{h_0}{D} < 0{\cdot}45$ in accordance with eq. (8), except for the exact values of the coefficients.

5. Calculation of the Loading in the Drum

If X be the area of any cross-section of the bed (Fig. 1), then the load H in m³ of the rotary cylinder is

$$H = \int_0^L X . dx. \qquad (10)$$

The calculation of H is simplified by using an approximation instead of the exact formula for the area of the segment X. The equation

$$X \cong 1{\cdot}14 D^2 \left(\frac{h}{D}\right)^{1{\cdot}42} \qquad (11)$$

gives for values $h/D < 0{\cdot}45$ an approximation with an accuracy of 3%.

The flow of material Φ_v being the same through every cross-section it can be found by using eq. (9) that:

$$\left(\frac{h}{h_0}\right)^{2{\cdot}05} = \frac{L-x}{L}. \qquad (12)$$

By substituting eqs. (11) and (12) in eq. (10), the latter can be integrated:

$$H = 0{\cdot}67 D^2 \left(\frac{h_0}{D}\right)^{1{\cdot}42} . L. \qquad (13)$$

The load ratio of the rotary drum is defined as

$$\eta_l = \frac{\text{loading in cylinder}}{X_0 . L},$$

where X_0 is the segmental area of the cross-section through the bed at $x = 0$. From (11) and (13) the value of η_l can be calculated:

$$\eta_l = \frac{0{\cdot}67 D^2 (h_0/D)^{1{\cdot}42} L}{1{\cdot}14 D^2 (h_0/D)^{1{\cdot}42} L} = 0{\cdot}59.$$

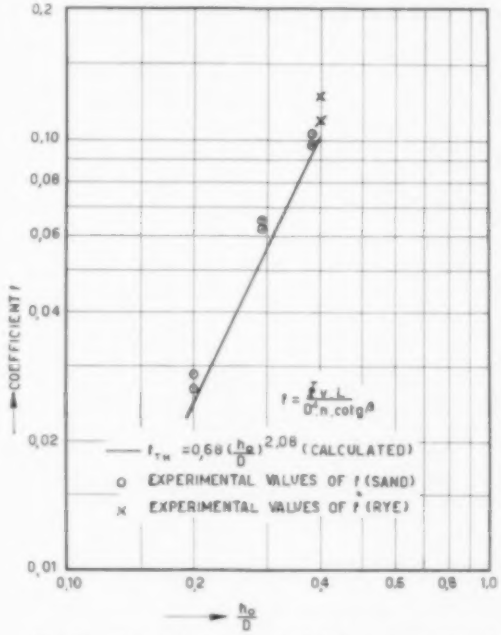

Fig. 5. Comparison of calculated and measured coefficients f.

This shows that the load ratio has a constant value, independent of size and operating conditions of the rotary cylinder and independent of the properties of the transported material. The loading H in the cylinder has been determined in some of the experiments. Table 1 shows the results of the measurements and the values of η_l as calculated from the measured data.

Table 1. Experimental values of the load ratio

h_0/D	0·20		0·29		0·38		
n	11	16	10	41	9	38	r.p.m.
H_{exp}	0·52	0·55	1·00	1·07	1·47	1·55	litres
$X_0 . L$	0·90	0·90	1·55	1·55	2·30	2·30	litres
η_{exp}	0·58	0·61	0·645	0·695	0·64	0·675	—

6. Calculation of Time of Passage

The average time of passage τ of the particles is

$$\tau = \frac{H}{\Phi_v} = 0{\cdot}91 \left(\frac{L}{D}\right)^2 \left(\frac{D}{h_0}\right)^{0{\cdot}57} \frac{\tan\beta}{n} \text{ (min)}. \qquad (14)$$

7. Calculation of Power Requirements

A particle cascading along a chord of length k (see cross section, Fig. 6) is lifted again over a height of $k \sin\beta$. The amount of work done on a particle entering the bed at P and leaving it at Q is

$$\gamma \,.\, r \,.\, d\varphi \,.\, dr \,.\, dx \,.\, k \,.\, \sin\beta \ \text{(kg m)}.$$

Per revolution, the volume entering at P is

$$dr \,.\, dx \int_0^{2\pi} r \,.\, d\varphi = 2\pi r \,.\, dr \,.\, dx.$$

The power required for displacing the material in a bed segment of thickness dx, at n r.p.m. is found by integration:

$$dp = \frac{n}{60} \,.\, \gamma \,.\, 2\pi \sin\beta \,.\, dx \int_{R-h}^{R} k \,.\, r \,.\, dr.$$

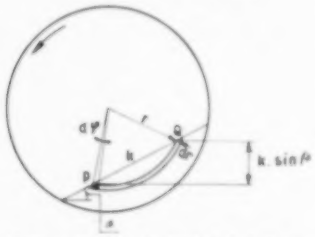

Fig. 6. Cross-section through bed of material.

The solution of the integral in this equation is

$$\int_{R-h}^{R} k \,.\, r \,.\, dr = \frac{2}{3} R^3 \left\{ 2\frac{h}{R} - \left(\frac{h}{R}\right)^2 \right\}^{\frac{3}{2}}.$$

With an accuracy of 5% this integral can be replaced, for values $0{\cdot}2 < h/R < 0{\cdot}8$, by the equation:

$$\frac{2}{3} R^3 \left\{ 2\frac{h}{R} - \left(\frac{h}{R}\right)^2 \right\}^{\frac{3}{2}} \cong \frac{2}{3} R^3 \,.\, 1{\cdot}24 \,.\, \frac{h}{R}.$$

Using this approximation the power requirements are

$$p = \frac{\pi n}{30} \gamma \,.\, \sin\beta \,.\, \frac{2}{3} R^2 \,.\, 1{\cdot}24 \int_0^L h \, dx, \qquad (15)$$

after substituting eq. (12) the integration of (15) gives

$$p = 0{\cdot}19\, n \,.\, \gamma \,.\, D^2 \,.\, L \,.\, h_0 \,.\, \sin\beta \quad \text{(metric h.p)}. \qquad (16)$$

8. Conclusions

a) Through a horizontal rotary drum with a depth h_0 of the bed of material at the entrance and with a free discharge at the other end of the drum, material is transported as a result of the difference of the levels of the material at both ends.

b) From theoretical considerations an equation for the nett volume transported per minute has been developed for values of h/D in the interval $0{\cdot}15 < h_0/D < 0{\cdot}45$:

$$\Phi_{v_{theor.}} = 0{\cdot}68 \left(\frac{h_0}{D}\right)^{2\cdot08} \frac{D^3 \,.\, n \,.\, \cot\beta}{L} \quad \text{(m}^3\text{/min)}.$$

Experiments gave about 13% higher values:

$$\Phi_{v_{exp}} = 0{\cdot}74 \left(\frac{h_0}{D}\right)^{2\cdot05} \frac{D^3 \,.\, n \,.\, \cot\beta}{L} \quad \text{(m}^3\text{/min)}.$$

c) The load ratio

$$\eta = \frac{H}{X_0 \,.\, L}$$

is 60 to 65% and is practically independent of the size of the drum, the operating conditions and the properties of the transported material.

d) The time of passage of the material through the drum is given by eq. (14):

$$\tau = 0{\cdot}91 \left(\frac{L}{D}\right)^2 \cdot \left(\frac{D}{h_0}\right)^{0\cdot6} \cdot \frac{\tan\beta}{n} \quad \text{(min)}.$$

e) The power needed for lifting the particles in the bed in the drum up to the cascading layer is given by eq. (16):

$$p = 0{\cdot}19\, n \,.\, \gamma \,.\, D^2 \,.\, L \,.\, h_0 \,.\, \sin\beta \quad \text{(metric h.p.)}.$$

Notation

- s = axial component of the path of a cascading particle
- ε = angle between drum axis and surface of material (Fig. 1)
- β = angle of repose of material
- γ = bulk density of material (kg/m³)
- h = depth of bed
- h_0 = depth of bed at entrance of drum,
- L = length of drum (m)
- x = axial distance of section to entrance of drum
- X = cross-sectional area of bed
- X_0 = cross-sectional area of bed at entrance ($x = 0$)
- k = length of path of cascading particle along chord of radius r
- φ = angle on chord k
- $R = D/2$ = radius of drum (m)
- n = speed of drum (revolutions per minute),
- v_r = average axial transport velocity of a single particle
- Φ_v = volume transported per minute (m³/min)
- H = load of drum (m³)
- η = load ratio of drum = $H/X_0 \,.\, L$
- τ = time of passage of a particle through the drum (min)
- p = power (metric h.p.)

References

[1] VÀHL, L.; Het transport in continu werkende droogtrommels. Chem. Weekbl. 1949 p. 325. [2] SULLIVAN, J. D., MAIER, C. G. and RALSTON, O. S.; U.S. Bur. Mines, Techn. Papers 1927, p. 384. [3] SAEMAN, W. C.; Chem. Eng. Prog. 1951 **47** 508.

The passage of granular solids through inclined rotary kilns

H. KRAMERS and P. CROOCKEWIT

Laboratorium voor Physische Technologie, Technische Hogeschool, Delft

(Received August 1952)

Summary—Starting from a simple mechanism of the movement of granular solids in a rotating cylinder, as first indicated by VÅHL, formulae are derived for the hold-up of an inclined rotary kiln, with and without end constrictions. A good agreement is found between the theoretical values and the experimental results.

Résumé—En utilisant la théorie simplifiée proposée par VAHL pour le déplacement des solides dans un cylindre tournant, l'auteur établit des formules rendant compte de la rétention dans un four rotatif incliné, muni ou non de chicanes. Les valeurs expérimentales sont en bon accord avec celles déduites de la théorie.

1. INTRODUCTION

In the design of rotary kilns one of the main problems is the calculation of the kiln dimensions and operating conditions for a given feed rate, and certain requirements as to the time of residence of the material.

The first attempts to find a correlation between these variables were made by SULLIVAN, MAIER and RALSTON [1] who experimented with small inclined kilns and relatively small feed rates. They derived an empirical formula for the time of passage through kilns without constrictions, whereas several corrections were indicated for use in kilns with constrictions. This well-known work has been followed by minor adjustments by BAYARD [2]. Recently, SAEMAN [3] published a paper in which a sound theoretical basis was put forward for the calculation of kiln hold-up, although he did not succeed in giving a general solution for practical use.

The theoretical results obtained in the present work are based on essentially the same mechanism of transportation as put forward by SAEMAN. They must, however, be considered as an extension of the ideas of Prof. VÅHL, the result of which was published in 1949 [4]. A full account of VÅHL's work for the case of *horizontal* rotating cylinders appears in this journal [5]. In our derivation of the hold-up relationships for *inclined* kilns we will refer as much as possible to the latter paper.

2. DERIVATION OF KILN FORMULAE

Transport mechanism

We start from the schematized description of the path of a particle which is transported through a rotating cylinder, as proposed by VÅHL [5] and by SAEMAN [3] (see Fig. 1): The bulk of material in the kiln has no relative motion with respect to it. So a particle at a distance r from the kiln axis describes a circular path in a plane perpendicular to the axis with the same angular velocity as the kiln wall. After it has reached the surface of the material it cascades down along a straight path having a "dynamic angle of repose" with respect to a horizontal plane. The latter movement has two components, one perpendicular to the kiln axis (k) and one parallel to it (s). Only s makes a contribution to the transport through the kiln.

The ratio between s and k depends on the angle of repose (β) of the material, the slope of the kiln

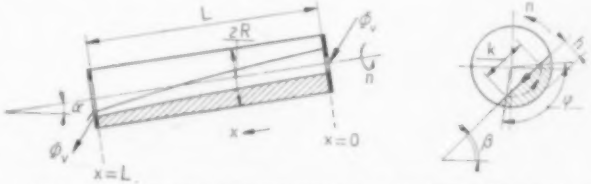

Fig. 1. Schematic representation of rotary kiln with symbols used.

(tan α) and the gradient of the surface with respect to the kiln axis $\left(-\frac{dh}{dx}\right)$. This relationship can be found from geometrical considerations and has been shown by SAEMAN to be:

$$\frac{s}{k} = \frac{\tan\alpha}{\sin\beta} - \frac{\cos\beta}{\sin\beta}\cdot\frac{dh}{dx}. \qquad (1)$$

It is valid for the small values of α encountered in practice and for small values of $\frac{dh}{dx}$.

With the same reasoning as used by VÅHL ([5], eq. (2), (3) and (4)) we arrive at the following formula for the volumetric flow of material through any cross-section of the kiln:

$$\Phi_v = \frac{4}{3}\pi n R^3\left(\frac{\tan\alpha}{\sin\beta} - \frac{dh}{dx}\cot\beta\right)\left(2\frac{h}{R} - \frac{h^2}{R^2}\right)^{3/2}, \qquad (2)$$

which is the basis for further calculations. It corresponds with eq. (18) in SAEMAN's paper.

Height of material along the kiln

Eq. (2) is a differential equation which relates the height of material h with distance x from the feed end

for given conditions of operation. As its solution is rather complicated we have simplified eq. (2) by replacing the function containing h/R by a linear one:

$$\left(2\,\frac{h}{R}-\frac{h^2}{R^2}\right)^{3/2} \cong 1{\cdot}24\,\frac{h}{R}\,. \qquad (3)$$

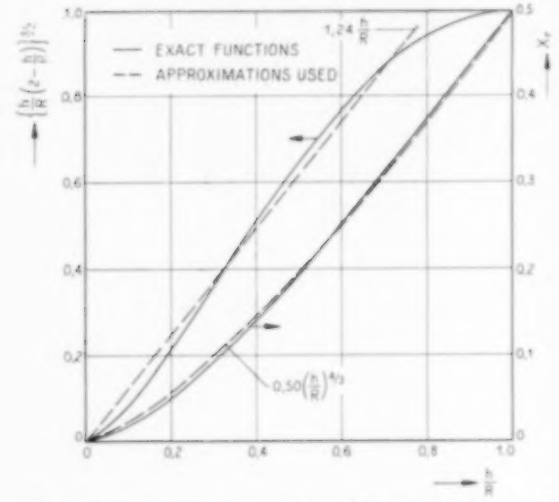

Fig. 2. Significance of approximations involved in eq. (3) and eq. (8).

Fig. 2 illustrates the degree of approximation obtained. The introduction of this approximation before

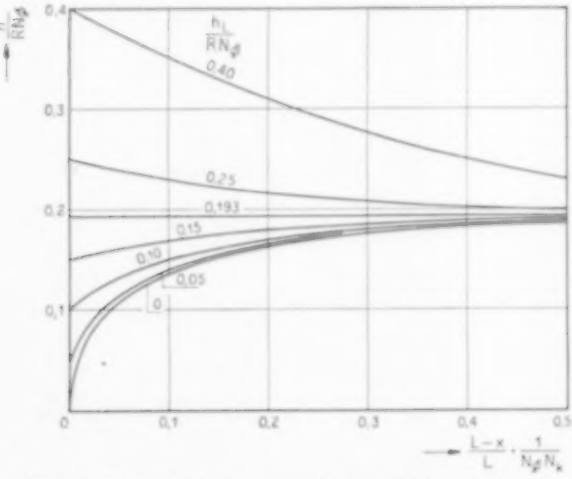

Fig. 3. Dimensionless representation of the relation between height of material and distance from discharge end, for various values of h_L.

integrating eq. (2) is at variance with VÅHL's derivation for horizontal kilns ($\alpha = 0$).

Further, if we use the following dimensionless combinations:

$$N_\Phi = \frac{\Phi_v \sin\beta}{n R^3 \tan\alpha} \quad \text{and} \quad N_k = \frac{R\cos\beta}{L\tan\alpha}\,, \qquad (4)$$

it can readily be seen that eq. (2) contains two variables only, *viz.*

$$\frac{h}{R N_\Phi} \quad \text{and} \quad \frac{x}{L N_\Phi N_k}\,.$$

The solution of (2) is fixed, if the terminal condition for the height of material is given:

$$h = h_L \quad \text{for} \quad x = L\,. \qquad (5)$$

We assume h_L to be equal to the height of an eventual diaphragm constriction. If no constriction is present at the discharge side of the kiln, $h_L = 0$.

After substitution of (3) and (4) and for the condition (5), eq. (2) gives the solution:

$$\frac{h_L}{R N_\Phi} - \frac{h}{R N_\Phi} + 0{\cdot}193 \ln \frac{\dfrac{h_L}{R N_\Phi} - 0{\cdot}193}{\dfrac{h}{R N_\Phi} - 0{\cdot}193} = \frac{L-x}{L N_k N_\Phi}\,. \qquad (6)$$

This rather complex relationship is represented by Fig. 3. It shows, in dimensionless form, the way in which the material height h changes with increasing distance from the discharge end, for various values of h_L.

A special case presents itself, when $h_L/RN_\Phi = 0{\cdot}193$, giving a constant height over the whole length of the kiln. For sufficiently small values of $N_\Phi N_k$ (low feed rate and long kiln with great slope) h_L approaches the value of $0{\cdot}193\,RN_\Phi$. For such cases the conditions at the discharge end represent a relatively unimportant end effect.

Calculation of fractional holdup $\overline{X}_r$

Once the relationship between h and x has been established, the calculation of hold-up involves no essential difficulties. If a cylinder of radius R is filled with material to a uniform height h, the fraction X_r of the cross sectional area occupied by material is:

$$\left.\begin{aligned} X_r &= \frac{1}{2\pi}(\varphi - \sin\varphi), \\ \frac{h}{R} &= 1 - \cos\frac{1}{2}\varphi\,. \end{aligned}\right\} \qquad (7)$$

whereas

This again is a complicated relationship between X_r and h/R. So we approximated it by the formula:

$$X_r \simeq \frac{1}{2}\left(\frac{h}{R}\right)^{4/3}. \qquad (8)$$

Fig. 2 shows the significance of this approximation. Actually a closer fit would have been obtained by a slight modification of the constants in (8) (compare [5], eq. (11)). However, we preferred the approxi-

mation given here because of its advantage for numerical calculations.

Since h varies through the kiln, the total relative hold-up $\bar{X}_r$ has to be found by integration:

$$\bar{X}_r = \frac{1}{L}\int_0^L X_r \, dx. \tag{9}$$

This operation was carried out graphically with eq. (6) as a starting point. Because of the approximation (8) the results are obtained in the form:

$\bar{X}_r N_\Phi^{-4/3} = f(N_\Phi N_k)$ for different values of $\frac{h_L}{R N_\Phi}$.

As we preferred to present a relationship between the two main variables $\bar{X}_r$ and Φ_v, we rearranged it so as to give a relation of the form:

$$\bar{X}_r N_k^{4/3} = f'(N_\Phi N_k) \tag{10}$$

for different values of $\frac{h_L}{R N_\Phi}$.

Table 1 gives the result of these calculations.

Table 1. Values of $\bar{X}_r N_k^{4/3}$

$N_\Phi N_k$ \ $\frac{h_L}{R N_\Phi}$	0	0·05	0·10	0·15	0·193	0·25	0·40
0·5	0·021	0·021	0·021	0·022	0·022	0·023	0·027
1	0·050	0·050	0·051	0·053	0·056	0·061	0·082
2	0·110	0·111	0·117	0·127	0·140	0·163	0·254
5	0·27	0·29	0·33	0·40	0·50	0·61	1·07
10	0·51	0·58	0·71	0·95	1·27	1·59	2·90
20	0·92	1·06	1·58	2·28	3·20	4·13	7·65

The relationship (10) is represented in Fig. 5 by the solid line for $h_L = 0$, *i.e.* for a kiln without a constriction at the end. For low and for high values of $N_\Phi N_k$ the curve approaches to different asymptotes. The former one corresponds to the case where the discharge conditions of the kiln are negligible, as mentioned before. For that case therefore, $\bar{X}_r$ can be calculated directly from (8), $\bar{X}_r = X_r$ and $h/R N_\Phi = 0{\cdot}193$, giving:

$$\bar{X}_r N_k^{4/3} = 0{\cdot}055\,(N_\Phi N_k)^{4/3} \quad \text{for} \quad N_\Phi N_k < 0{\cdot}1. \tag{11}$$

The asymptote for high values of $N_\Phi N_k$ refers to the case where the axial slope of the surface (dh/dx) is mainly responsible for the transport, *e.g.* when the kiln is nearly horizontal. Neglecting the term containing α in eq. (2) and using the proposed approximations, one finds:

$$\left.\begin{aligned}\bar{X}_r N_k^{4/3} = 0{\cdot}158\,(N_\Phi N_k)^{2/3} \quad &\text{for} \quad N_\Phi N_k \to \infty \\ &\text{and} \quad h_L = 0\end{aligned}\right\} \tag{12}$$

or $\bar{X}_r = 0{\cdot}158\,(N_\Phi/N_k^2)^{2/3}$, for $\alpha \to 0$ and $h_L = 0$. The latter equation no longer contains α as a variable.

Effect of end constrictions on hold-up

From Table 1 it can be seen that for relatively small values of $N_\Phi N_k$ the effect of an end constriction is only small, because for all values of h_L the eq. (11) is then approached asymptotically. In general, the effect of a constriction can be regarded as being a correction on the total hold-up calculated for $h_L = 0$. A correction factor f_{h_L} was defined by

$$(\bar{X}_r)_{h_L} = f_{h_L}(\bar{X}_r)_{h_L=0}. \tag{13}$$

Fig. 4 gives a plot of f_{h_L} as a function of $N_\Phi N_k$ for different values of $h_L/R N_\Phi$. Thus the total hold-up

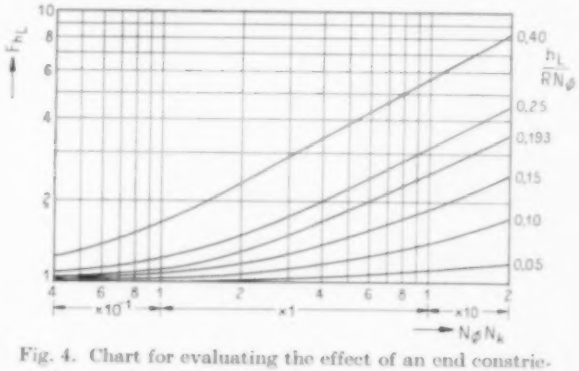

Fig. 4. Chart for evaluating the effect of an end constriction on the hold-up as found from Fig. 5 ($h_L = 0$).

of a kiln with end constriction, or with a given height h_L at the discharge end, can be calculated by first deriving $(\bar{X}_r)_{h_L=0}$ from Fig. 5 and afterwards correcting it by using Fig. 4. Both graphs are based on the numerical results contained in Table 1.

3. Experimental Part

After the above calculations had been set up tentatively, we compared them with Sullivan's data for $h_L = 0$ (Tables 1, 2, 5, 6, 7 and 8 in reference [1]). The agreement appeared to be very good, as can be seen from Fig. 5 (crosses). It was then decided to carry out some more hold-up measurements, in particular in the range $2 < N_\Phi N_k < 20$, *i.e.* at relatively greater loads than those investigated by Sullivan *et al.*

The experiments were performed in a rotating cylinder with an inner diameter $2R = 0{\cdot}197$ m and length $L = 1{\cdot}78$ m. It was mounted on the base of a semi-technical cement kiln having the means for adjusting the kiln slope α between 0·5 and 5°

and the rotational speed n between 0·04 and 0·25 r.p.s.*. The necessary precautions were taken to ensure a constant feed rate of material. In each experiment, after steady conditions had been reached, the feed was stopped and the hold-up of the cylinder was determined by weighing its contents. We used river sand and ground coke. The properties of these materials are shown in Table 2.

Table 2. Properties of materials used

Material	*River sand*	*Ground coke*
Particle size .	90% between 0·6 and 1·2 mm	95% between 0·5 and 1·5 mm
Bulk density (Loosely packed) . .	1480 kg/m³	560 kg/m³
Dynamic angle of repose . .	36°	40°

This table shows that the materials were of rather uniform particle size. The density was taken for maximum percentage of voids which is probably nearest to the density actually occurring in the kiln. Since both feed rate and hold-up were measured by weighing and Φ_v and $\overline{X}_r$ are approximately proportional to each other (see Fig. 5), a small error in density does not materially affect the experimental results. The angle of repose was measured during the experiments at different places in the kiln. No greater deviation than $\pm 5\%$ from the values indicated was observed. In all experiments the rotational speed of the kiln was sufficiently high to cause continuous movement of the material.

Table 3 summarizes the experimental results for the cylinder without end constriction ($h_L = 0$). As

* This piece of equipment was manufactured by *F. L. Smidth & Co.*, Copenhagen, for the Laboratory of Chemical Technology, Delft. It was kindly put at our disposal by Professor H. I. WATERMAN.

Table 3. Experimental results for $h_L = 0$

Slope tan α	*n* (*r.p.s.*)	*Feed rate* (10^{-3} *kg/sec*)	*Hold-up* (*kg*)	$(\overline{X}_r)_{exp}$	$\overline{X}_r N_k^{1.3}$	$N_\Phi N_k$	$(\overline{X}_r)_{calc.}$
			Sand				
0·0094	0·059	5·15	8·10	0·101	0·795	18·3	0·111
	0·090	2·68	5·00	0·062	0·488	6·25	0·054
	0·195	13·2	7·75	0·097	0·763	14·2	0·088
	0·232	7·24	3·85	0·048	0·378	6·55	0·043
0·0100	0·040	6·38	13·3	0·166	1·22	29·7	0·169
	0·040	5·00	11·2	0·140	1·03	23·2	0·144
	0·069	9·20	10·6	0·132	0·97	24·8	0·150
	0·069	6·53	8·5	0·106	0·782	17·6	0·113
	0·106	15·0	12·2	0·152	1·12	27·8	0·162
	0·159	12·0	7·49	0·093	0·686	14·0	0·092
	0·238	15·5	7·48	0·093	0·686	12·1	0·083
	0·238	11·9	6·13	0·076	0·561	9·22	0·068
0·0130	0·156	19·4	7·88	0·098	0·500	13·6	0·130
	0·156	10·0	5·66	0·071	0·362	6·96	0·073
	0·238	31·9	11·2	0·140	0·714	14·6	0·137
	0·238	15·0	6·02	0·075	0·382	6·88	0·062
0·0230	0·156	20·0	7·63	0·095	0·226	4·50	0·103
	0·156	11·4	4·49	0·060	0·143	2·57	0·058
	0·238	21·5	5·82	0·073	0·174	3·16	0·072
	0·238	14·2	4·00	0·050	0·119	2·09	0·048
0·0320	0·046	11·2	9·90	0·123	0·189	4·40	0·159
	0·077	9·60	4·75	0·059	0·091	2·26	0·080
	0·139	39·4	10·3	0·128	0·197	5·13	0·183
	0·180	28·0	7·77	0·097	0·149	2·82	0·100
	0·175	9·09	2·74	0·034	0·0526	0·94	0·029
	0·202	12·7	3·15	0·039	0·0605	1·14	0·037
	0·238	26·8	5·70	0·071	0·109	2·04	0·073
	0·238	8·49	1·45	0·018	0·0279	0·646	0·018
0·0533	0·141	27·7	6·47	0·081	0·0632	1·30	0·085
	0·140	10·2	2·40	0·030	0·0233	0·483	0·026
	0·233	21·1	3·10	0·039	0·0302	0·602	0·033
	0·238	12·9	1·81	0·023	0·0176	0·360	0·017
0·0556	0·048	10·6	6·80	0·058	0·0627	1·32	0·094
	0·068	29·2	13·1	0·163	0·120	2·58	0·239
	0·111	26·9	7·50	0·094	0·069	1·45	0·106
	0·114	46·2	14·8	0·185	0·137	2·43	0·169
			Coke				
0·0100	0·083	2·28	2·8	0·092	0·632	14·0	0·099
0·0135	0·235	14·9	5·1	0·168	0·775	17·8	0·182
0·0150	0·157	3·21	1·8	0·060	0·240	4·64	0·063
0·0232	0·157	13·6	5·2	0·172	0·386	8·26	0·191
0·0232	0·158	5·46	2·4	0·079	0·177	3·28	0·081
0·033	0·235	3·57	0·90	0·030	0·042	0·71	0·024
0·053	0·141	15·0	3·9	0·129	0·095	1·93	0·145

can be seen from Fig. 5 both SULLIVAN's and our own results agree well with the theoretical curve, deviations greater than 30% seldom occurring. In Fig. 6 the experimental and theoretical values of the total relative hold-up $\overline{X}_r$ are compared. This figure clearly shows that there is some systematic deviation, the calculated value being somewhat too low for small $\overline{X}_r$ and too high for great $\overline{X}_r$. In the region between 5 and 10% hold-up, the average agreement is best.

We also checked our results with SULLIVAN's empirical formula which can be written in the

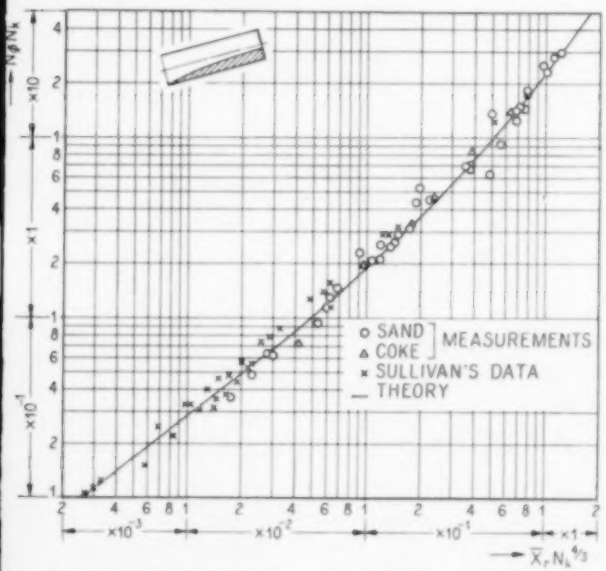

Fig. 5. General hold-up relationship for inclined kilns without end constriction.

following form:

$$\overline{X}_r = 0{\cdot}038\,\frac{\Phi_v\,\beta^{1.2}}{\pi\,R^2\tan\alpha}\,, \qquad (14)$$

and where β is expressed in radians. For hold-up values greater than 5%, and in particular for small angles of inclination eq. (14) gives values for $\overline{X}_r$ that are too high, sometimes by a factor 2.

Two series of measurements were carried out with diaphragms at the discharge end of the cylinder, which had inner diameters of 0·177 and 0·158 m ($h_L/R = 0{\cdot}10$ and 0·20 respectively). The results are shown in Table 4. For purpose of comparison we calculated $\overline{X}_r$ for the different experimental conditions, using first the theoretical line of Fig. 5 and correcting afterwards for h_L by means of Fig. 4. A comparison between the experimental and calculated hold-up values is presented by Fig. 7. This graph also includes the measurements of SULLIVAN *et al.* with end constriction (tables 25, 26, 28 and 35 of their paper). The agreement between $(\overline{X}_r)_{calc}$ and $(\overline{X}_r)_{exp}$ is good, even somewhat better than for the case $h_L = 0$ (Fig. 6).

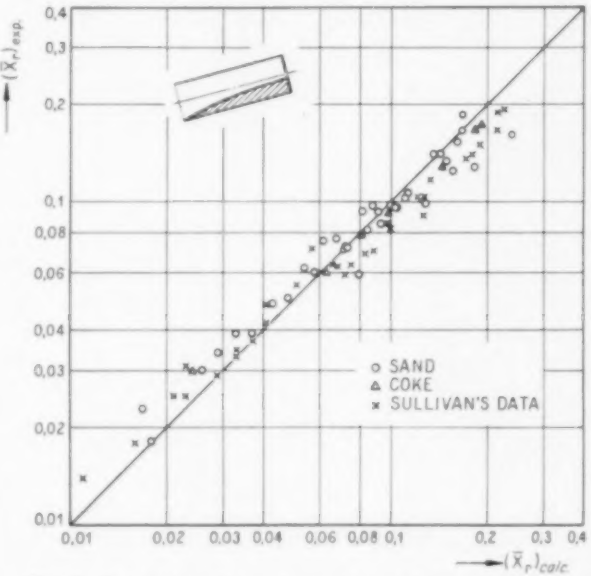

Fig. 6. Comparison between experimental and calculated hold-up values for kiln without end constriction.

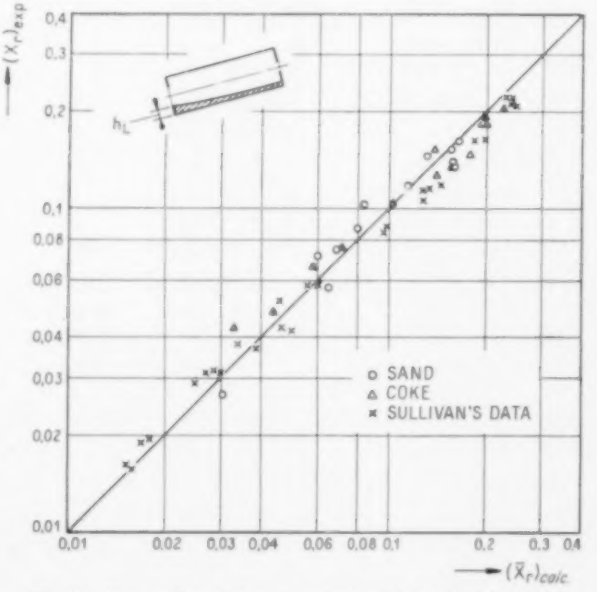

Fig. 7. Comparison between experimental and calculated hold-up values for kilns with end constrictions.

4. DISCUSSION OF THE THEORY

It is rather surprising that such a simple model of operation as described in section 2 yields results which appear to be useful for practical design work. However, the actual motion of the solids is much

Table 4. Experimental results for $h_L/R = 0{\cdot}10$ and $0{\cdot}20$

Slope tan α	*n* (*r.p.s.*)	*Feed rate* (10^{-3} *kg/sec*)	*Hold-up* (*kg*)	$(\bar{X}_r)_{exp}$	$\frac{h_L}{RN\Phi}$	$N_\Phi N_k$	$(\bar{X}_r)_{calc}$
			Sand, $h_L/R = 0{\cdot}10$				
0·0100	0·040	15·5	10·8	0·135	0·017	25·6	0·160
0·0135	0·156	8·7	6·0	0·075	0·058	5·65	0·069
0·0135	0·235	33·4	11·7	0·146	0·022	14·4	0·132
0·0230	0·157	31·8	13·0	0·162	0·027	7·1	0·164
0·0230	0·157	11·1	5·8	0·072	0·078	2·48	0·060
0·0535	0·141	21·7	4·6	0·057	0·081	1·03	0·065
			Sand, $h_L/R = 0{\cdot}20$				
0·0100	0·040	5·17	12·3	0·153	0·037	24·0	0·156
0·0135	0·156	9·9	8·2	0·102	0·108	6·12	0·084
0·0150	0·238	31·7	11·2	0·140	0·047	14·6	0·159
0·0240	0·156	20·0	9·5	0·118	0·090	4·13	0·115
0·0240	0·156	13·5	7·0	0·087	0·134	2·77	0·080
0·0315	0·238	10·0	2·11	0·026	0·36	0·78	0·031
0·0508	0·141	20·4	5·7	0·071	0·192	0·91	0·060
			Coke, $h_L/R = 0{\cdot}10$				
0·0100	0·083	4·95	5·6	0·185	0·014	30·6	0·191
0·0135	0·157	6·17	3·85	0·127	0·026	11·9	0·140
0·0135	0·238	16·5	5·6	0·185	0·016	19·3	0·199
0·0230	0·157	15·6	6·2	0·204	0·019	9·6	0·226
0·0230	0·157	4·67	2·30	0·076	0·065	2·86	0·073
0·0325	0·238	5·84	1·45	0·048	0·11	1·19	0·044
0·0535	0·141	16·4	4·00	0·132	0·038	2·06	0·154
			Coke, $h_L/R = 0{\cdot}20$				
0·0100	0·085	1·82	3·10	0·104	0·078	10·9	0·102
0·0135	0·157	2·33	2·35	0·077	0·152	4·15	0·070
0·0135	0·238	9·71	4·58	0·151	0·056	11·4	0·139
0·0230	0·157	12·9	5·8	0·191	0·046	7·9	0·199
0·0230	0·157	3·38	2·00	0·066	0·20	1·89	0·058
0·0325	0·238	3·69	1·30	0·043	0·36	0·73	0·033
0·0535	0·141	16·8	4·45	0·147	0·074	2·13	0·178

more complicated than would appear from the assumptions made. Moreover, a number of simplifications have been introduced in the calculations, the significance of which for the final results cannot easily be seen. A few of these points will be discussed here.

a) *Movement of the particles*

In reality, the surface of a granular material in a rotating cylinder is not flat but wave-like. This form of surface is connected with the fact that, once a particle has reached the surface it first is accelerated, then reaches a more or less constant velocity and finally slows down near the bottom of the slope. It appears that the angle of "repose" decreases throughout this process. We believe that the assumption of a flat surface introduces no serious error, as long as the average angle of repose under actual conditions of operation is used, and the centrifugal acceleration caused by rotation is negligible with respect to gravity.

The assumption of an infinite cascading velocity of the particles might, on the other hand, seriously affect the results. A limited average velocity causes the calculated hold-up to be too small, because the layer of material flowing down represents an additional hold-up not taken care of by the theory. In separate experiments in a 10 cm diameter cylinder, we measured superficial velocities of the order of 30 cm/sec. In this case the material involved in this movement was about 20% of the total hold-up. From the mechanism of flow, which is not unlike that of liquid films, this percentage may be expected to decrease with increasing kiln diameter. This was ascertained by measurements in three small cylinders of 2·4, 4·6 and 11·7 cm diameter at constant h/R values.

b) *Gradient along the kiln*

From eq. (2) which has been derived for small gradients, it follows that $-dh/dx$ can become very great for relatively small values of h/R. In reality this value cannot exceed tan β. For cases where $h_L = 0$ and the end effect is relatively important ($N_\Phi N_k > 1$) this will lead to calculated hold-up values which are too high.

On the other hand, for kilns with a thin diaphragm at the discharge side, as used in our experiments, the calculated hold-up will be too low. The constriction gives rise to a very complicated flow pattern. It results in a positive contribution to the theoretical $-dh/dx$ value, due to the restricted passage. The latter effect also decreases as the end correction becomes less important.

c) *Simplifications used*

Whereas the approximation of eq. (8) is sufficiently accurate, the substitution eq. (3) is rather crude, especially for low values of h/R. It would cause the lowest calculated hold-up values to be too high. However, this approximation has the important effect of reducing the number of variables in eq. (2) from 3 to 2, which made a rather simple representation possible. Then, however, a close correlation between the two variables of Fig. 5 can no longer be expected. Whereas the experimental results are estimated to have an accuracy within $\pm 5\%$, the mean square error of all the $(\overline{X}_f)_{\text{exp}}/(\overline{X}_f)_{\text{calc}}$ values amounts to about 15%.

It appeared to us impossible to take into account any of the effects mentioned without making the calculations extremely complicated. The experimental results indicate that the effects of the various assumptions and simplifications have, to a great extent, cancelled each other out, leaving only a slight systematic deviation as shown in Figs. 6 and 7. Whether, however, these fortunate conditions persist also for industrial kiln dimensions has to be seen from experience. The following example, taken from SAEMAN's paper gives an indication that the theoretical results are applicable to large scale equipment.

Example. An industrial nodulizing kiln consists of two sections. Section 1 on the discharge side has a length $L_1 = 45$ ft (13·7 m) and radius $R_1 = 3{\cdot}1$ ft (0·95 m). Of section 2 on the feed end, $L_2 = 80$ ft (24·4 m) and $R_2 = 3{\cdot}5$ ft (1·07 m). Further data are:

$\Phi_v = 6{\cdot}1$ cu ft/min ($2{\cdot}88 \times 10^{-3}$ m³/sec)
$\beta = 45°$
$n = 0{\cdot}050$ rev/sec
$\tan \alpha = 0{\cdot}5$ in/ft (0·042)
Measured time of passage $\tau = 40$ min.

From these data we find for section 1:

$$\left.\begin{aligned} N_{\Phi_1} &= 1{\cdot}15 \\ N_{k_1} &= 1{\cdot}17 \end{aligned}\right\} \quad N_{\Phi_1} N_{k_1} = 1{\cdot}35.$$

According to Fig. 5 this value corresponds to $\overline{X}_{f_1} N_{k_1}^{4/3} = 0{\cdot}070$, giving $\overline{X}_{f_1} = 0{\cdot}0565$ and the time of passage in section 1:

$$\tau_1 = 12{\cdot}6 \text{ min}.$$

In order to calculate the hold-up of section 2, the height of the bed h_{L_2} at the junction of the two sections has first to be calculated. Now

$$h_{L_2} = R_2 - R_1 + h_{o_1},$$

where h_{o_1} is the height of material at the entrance of section 1. From Fig. 2 we find $h_{o_1}/R_1 N_{\Phi_1} = 0{\cdot}190$, giving $h_{o_1} = 0{\cdot}21$ m and $h_{L_2} = 0{\cdot}33$ m. Thus for section 2:

$$\left(\frac{h_L}{R N_\Phi}\right)_2 = 0{\cdot}387 \qquad \left.\begin{aligned} N_{\Phi_2} &= 0{\cdot}805 \\ N_{k_2} &= 0{\cdot}742 \end{aligned}\right\} \quad N_{\Phi_2} N_{k_2} = 0{\cdot}60.$$

Using these values and Fig. 4 and 5, we find $\overline{X}_{f_2} N_{k_2}^{4/3} = 0{\cdot}035$, $\overline{X}_{f_2} = 0{\cdot}052$ and so for the time of passage in section 2:

$$\tau_2 = 26{\cdot}2 \text{ min}.$$

The total time of passage $\tau_1 + \tau_2 = 38{\cdot}8$ min agrees closely with the 40 min actually observed.

The authors wish to thank Messrs. L. E. M. MUDDE, E. F. BUNGE, A. STIKKER and A. E. F. VAN CAPPELLE, who assisted in parts of this investigation.

NOTATION

All quantities are expressed in units of the practical system (m, kg-mass, sec).

f_{h_L} = correction factor for end constriction with height h_L
h = depth of bed of material (see Fig. 1)
h_o, h_L = item at feed end and discharge end respectively
k = length of path of cascading particle perpendicular to kiln axis (see Fig. 1)
L = length of the kiln
n = rotary speed of the kiln
R = radius of circular cross-section of the kiln
s = axial component of the path of cascading particle
x = axial distance from feed end
X_f = fraction of cross-section taken in by material, dimensionless
$\overline{X}_f$ = average of X_f over kiln length, relative hold-up, dimensionless
α = angle between kiln axis and horizontal plane
β = angle of repose of material
φ = angle on path k (see Fig. 1)
Φ_v = volumetric flow of material
τ = time of passage through kiln
$N_\Phi = \Phi_v \sin \beta / n R^3 \tan \alpha$, dimensionless
$N_k = R \cos \beta / L \tan \alpha$, dimensionless.

NOTE ADDED IN PROOF

Recently, our attention was drawn to a paper PICKERING, FEAKES and FITZGERALD, "Time for passage of material through rotary kilns" (J. Appl. Chem. 1951 **1** 13). The adopted transport mechanism is the same as in the present paper but the influence of the varying height of the material along the kiln has been neglected. Whereas these authors find a systematic discrepancy of about 10% between their simplified formula and their experimental results, the design equations given in the present paper reduce this difference to 2% on the average.

REFERENCES

[1] SULLIVAN, J. D., MAIER, C. G. and RALSTON, O. C.; U.S. Bur. Mines, Techn. Papers 1927, p. 384. [2] BAYARD, R. A.; Chem. & Met. Eng. 1945 (March) **52** 100. [3] SAEMAN, W. C.; Chem. Eng. Progr. 1951 **47** 508. [4] VÅHL, L.; Chem. Weekbl. 1949 **45** 325. [5] VÅHL, L. and KINGMA, W. G.; Chem. Eng. Sci. 1952 **1** 253.

A new method for predicting the plate efficiency of bubble-cap columns

S. Bąkowski

Imperial Chemical Industries Limited, General Chemicals Division, Research Department, Widnes

(Received August 1952)

Summary—Recent investigation of the mechanism of bubble formation at submerged slots has shown that under the conditions normally existing in distillation columns the vapour may be regarded as flowing through channels, rather than passing in the form of streams of separate bubbles.

By a simplified treatment based on this mechanism an equation has been derived for calculating the local efficiency of a bubble-cap plate. Plate efficiencies calculated by means of this equation have been compared with published experimental data for columns ranging from small pilot-plant units to large stills of several feet diameter as used in the oil industry; data for absorption processes in which the gas film offers the principal resistance to matter transfer have also been examined. Good agreement was found between the predicted and measured efficiencies.

The difference between the local efficiency and the Murphree plate-efficiency for actual plates appears usually to be small, and the new equation can be used in practice to predict the Murphree plate efficiency.

A special application of the new equation to the design of plate columns for vacuum distillation is indicated.

Résumé—Des recherches récentes sur la formation de bulles au travers de fentes immergées ont montré que dans les conditions normales des colonnes de distillation, l'écoulement de la vapeur s'effectue sous forme de canaux continus plutôt que sous forme de chapelets de bulles séparées.

En s'appuyant sur cette hypothèse, l'auteur a établi une équation permettant le calcul de l'efficacité locale d'un plateau à calottes. Les valeurs ainsi obtenues ont été comparées aux résultats publiés pour diverses colonnes (colonnes de petites installations pilotes jusqu'aux colonnes de l'industrie du pétrole de plusieurs pieds de diamètre). L'auteur examine également les données relatives à des opérations d'absorption ou le film gazeux constitue la résistance principale au transfert de matière. Il y a un accord satisfaisant entre les efficacités calculées et celles qui sont mesurées.

Pour des plateaux réels, il y a peu de différence entre l'efficacité locale et l'efficacité suivant Murphree; la nouvelle équation peut être utilisée en pratique pour prédire l'efficacité de Murphree.

L'auteur envisage une application particulière de son équation au calcul des colonnes à plateaux pour distillation dans le vide.

One of the main problems in the design of a bubble-plate column is the proper estimation of plate efficiency. Three different meanings have been attached to this term, when defined in terms of the vapour composition: the most commonly used "overall efficiency" is the ratio between the number of theoretical plates and the actual number of plates required to effect a given separation of the components; the "Murphree efficiency" is the ratio between the actual enrichment of vapour produced by a plate and that which would be obtained if equilibrium between liquid and vapour were reached. If referred to a complete plate in a column the latter is termed the "Murphree plate efficiency", and if referred to a single slot or point on the plate it is termed the "local" or "point" efficiency. Lewis [20] derived analytical expressions showing the relationship between the plate and local efficiencies for three theoretically possible cases.

A great deal of experimental work has been done and several methods for predicting plate efficiencies have been proposed. One of these, originally proposed by Drickamer and Bradford [7] and subsequently modified and developed by O'Connell [25], is based on an empirical relationship between the overall efficiency and the product of the relative volatility and viscosity of the mixture distilled. According to O'Connell the plate efficiency decreases with increase in the value of this product. This method gives fairly good agreement in some cases when applied to distillation of hydrocarbons, but, for instance, the efficiencies predicted for alcohol/water mixtures were found to be considerably lower than those encountered in practice.

A method based on consideration of the diffusion occurring between individual vapour bubbles and the liquid over the slots was proposed by Geddes [9] and recently developed by Ju Chin Chu, Donovan, Bosewell and Furmeister [5]. Although this method gives reasonably good agreement with several experimental results reported in the literature, critical examination shows that the assumptions made by Geddes diverge considerably from the actual conditions in a distillation column. This becomes clear if comparison is made between the high vapour rates on the plates and the small size and low velocities of the bubbles assumed in this treatment.

The mechanism of bubble formation at submerged slots was recently investigated by Spells and Bąkowski [30]. A new method of predicting plate

efficiencies based on the results of these experiments forms the subject of this paper.

Mechanism of Vapour Flow Through Liquid on a Bubble-cap Plate

In preliminary experiments [30] in which bubble-formation at single and multiple slots was studied with the aid of stroboscopic illumination it was found that the properties of the gas and liquid and the shape of the slots had little effect on the apparent size of the bubbles; the main factors were found to be the rate of flow and the slot submergence. There was frequently a discrepancy between the known gas flow-rate and that calculated from the size and frequency of the bubbles, particularly for multiple slots, the former being the greater; this effect was most prevalent for multiple slots for which the bubbles were smaller. This suggested that intermittent channels were formed, connecting the slots directly to the surface of the liquid.

Spells and Bakowski [30] investigated the mechanism further for single slots using high-speed cinematography. It was confirmed that at flow rates and slot submergences normally employed in distillation columns there are few intervals between individual bubbles, these being connected with each other more or less continuously so that direct flow of gas from the slot to the surface of the liquid can take place. Further work by the same authors, not yet published, has revealed the existence of similar continuous channels when gas bubbles are formed at closely-spaced multiple slots as used in distillation columns.

It is clear that under these conditions there is no simple relation between the volume of an individual bubble, the rate of flow, and the time of bubble formation. Each bubble can be regarded as a channel connecting a slot with the surface of the liquid.

The rate of vapour flow through each slot on a bubble plate is directly proportional to the superficial vapour velocity in the column, and therefore to the boil-up rate or vapour load. It is usual to maintain this at the maximum value allowable without causing excessive entrainment of liquid, in order to reduce the diameter of the column as far as possible. Safe values of the vapour load, which depend on the densities of the liquid and vapour and on the plate spacing and depth of liquid seal, can be calculated by one of the conventional methods [2]. The corresponding vapour rate per slot can then be derived for any design of bubble plate. It is evident from Fig. 1 which shows diagrammatically a common arrangement of 3-in. diameter bubble caps at $4\frac{1}{4}$-in. triangular pitch, each having 38 rectangular slots, that the horizontal expansion of the bubbles is limited by those issuing from neighbouring slots. Thus in the case illustrated the free gas passage would be limited to about 0·9 cm² and for a superficial vapour velocity of 60 cm/sec in the column the linear velocity through this cross section would be of the order of 200 cm/sec. This

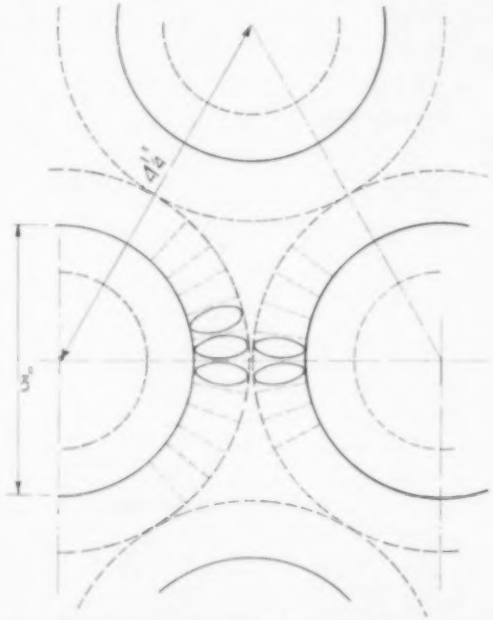

Fig. 1. Typical arrangement of bubble caps. Lateral growth of the bubbles is limited by the bubbles issuing from neighbouring slots.

far exceeds the normal velocities of gas bubbles rising freely in a liquid, and thus also suggests that channels must be formed.

Although increasing the slot submergence has a favourable effect on plate efficiency this should not be carried too far because of the consequent increase in liquid hold-up and pressure drop. In practice the total slot submergence does not usually exceed 5 cm, and a $\frac{1}{2}$-in. (1·27 cm) static seal is often recommended as normal for distillation at atmospheric pressure [6]. Under these conditions, *i.e.* high rates of flow and comparatively low slot-submergence, the formation of separate bubbles is improbable, and the most reasonable assumption seems to be that the vapour flows through channels which may be regarded as short wetted-wall columns in parallel. It will be seen from Fig. 1 that area of the free liquid surface may be expected to be small in comparison with that presented by the walls of the channels.

Prediction of the Local Efficiency Based on the Channelling Mechanism

The process of channelling of vapour through the liquid is actually somewhat complicated and the channels are of irregular cross-section. A simplified mechanism in which the channels are regarded as wetted-wall columns of uniform cross-section was therefore assumed as a basis for further treatment, as illustrated in Fig. 2.

The treatment involves the following assumptions:

(a) The channel length is equal to the total submergence, *i.e.* to the sum of the liquid seal over the slots and the active slot opening, given by the equation:

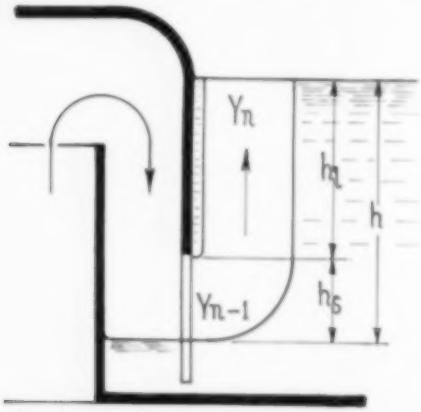

Fig. 2. Idealised channelling mechanism

$$h = h_l + h_s \text{ (cm)} \tag{1}$$

(b) The mean cross-sectional area of the channels can be regarded as approximately constant over the normal range of slot spacings and vapour rates.

(c) The rate of matter transfer through the channel walls is governed by the resistance of the gas film.

(d) The effects of temperature and of the properties of the vapour on the matter-transfer coefficient can be expressed by a convenient approximation based on the elementary kinetic theory, namely that:

$$K_g \propto 1/\sqrt{(M\,T)}$$

where M is the molecular weight

T is the absolute temperature.

The first two assumptions, which concern the dimensions of the channels, are based on actual measurements of the volumes of bubbles formed at slots.

1. Derivation of the general equation

The local or point efficiency for a binary mixture in terms of the partial pressure of the more volatile component, as defined by Murphree, is given by the equation:

$$E_p = \frac{p_n - p_{n-1}}{p_n^* - p_{n-1}} \tag{2}$$

where p_{n-1} = partial pressure of more-volatile component in vapour entering the channel (from plate below)

p_n = partial pressure of more-volatile component in vapour leaving the channel

p_n^* = partial pressure of more-volatile component in equilibrium with the liquid.

Considering the vapour issuing from a single slot: since approximately equimolar quantities of the components are exchanged between the liquid and vapour the vapour rate may be taken as constant and the matter-transfer balance can be expressed by the equation:

$$\frac{V_s\,(p_n - p_{n-1})}{22400} \times \frac{273}{T} = K_g\,A\,\Delta p_m \tag{3}$$

where V_s = vapour rate per slot (cm³/sec)

T = absolute temperature (°K)

K_g = matter-transfer coefficient (g mol/sec . cm² atm)

Δp_m = log mean driving force (atm)

A = surface area of channel (cm²).

Now Δp_m is given by:

$$\Delta p_m = \frac{(p_n^* - p_{n-1}) - (p_n^* - p_n)}{\ln\left(\dfrac{p_n^* - p_{n-1}}{p_n^* - p_n}\right)} \tag{4}$$

and substituting this in eq. (3) gives:

$$\ln\left(\frac{p_n^* - p_{n-1}}{p_n^* - p_n}\right) = \frac{22400\,K_g\,A\,T}{273\,V_s} \tag{5}$$

Combining this with eq. (2) then leads to the following equation for the local efficiency:

$$\ln\left(\frac{1}{1 - E_p}\right) = \frac{22400\,K_g\,A\,T}{273\,V_s} \tag{6}$$

In order to apply this equation in practice it is necessary to express the matter-transfer coefficient and surface area in terms of the operating conditions and the properties of the substances involved.

Taking the rate of matter transfer to be controlled by the gas film the coefficient may be considered to vary with the vapour velocity and the pressure according to an equation similar to that given by Carey and Williamson [4] for a wetted-wall column:

$$K_g = k_g = k_1 \frac{v^{0.75}}{P^{0.25}\,d^{0.25}} \frac{P}{p_f} \tag{7}$$

For equimolar counter-diffusion, however, the drift term P/p_f is unity and can be omitted, so that:

$$K_g = k_1\,v^{0.75}/P^{0.25}\,d^{0.25} \tag{8}$$

where k_1 is a constant depending on the temperature and the properties of the vapour
v is the linear velocity of vapour in the channel (cm/sec)
d is the mean equivalent diameter of the channel (cm)
P is the total pressure (atm).

If the rate of matter transfer is assumed to be proportional to the difference between the numbers of molecules colliding with unit surface in unit time when under the actual and equilibrium partial pressures, it can be shown from the elementary kinetic theory that:

$$k_1 \propto \frac{273}{22\,400\, M^{0.5}\, T^{0.5}} \qquad (9)$$

where M = molecular weight and T = absolute temperature (°K). This relation has been successfully used for calculating rates of matter transfer in high-vacuum evaporation and molecular distillation, and may be expected to hold when the gas film thickness and mean free path of vapour molecules are of the same order of magnitude. It is in reasonable agreement with the experimental data of Johnstone and Pigford [15] in a wetted-wall column. It is convenient to employ this simple relationship in preference to a complex function of viscosity, density and diffusion coefficient as used in the normal treatment of matter transfer, using suitable mean values for the molecular weight.

Introducing now the assumptions based on the simplified channelling mechanism, namely that the channel length h is equal to $h_l + h_s$ and that the mean cross-sectional area of the channel is constant it follows that:

Vapour velocity $v \propto$ the rate per slot V_s.
Interfacial area $A \propto h$.
Equivalent diameter = constant.

Combining eqs. (7), (8) and (9), taking d as constant and substituting values of v and A in terms of d there is obtained on conversion to common logarithms:

$$\log_{10}\left(\frac{1}{1-E_p}\right) = \frac{k\,h\,T^{0.5}}{M^{0.5}\,V_s^{0.25}\,P^{0.25}} \qquad (10)$$

where k is a constant to be evaluated by comparison with experimental data.

2. *Evaluation of the empirical constant*

Preliminary examination of data for a number of distillation processes showed that reasonably constant values of k were obtained. The data of Carey, Griswold, Lewis and McAdams [3] for the systems ethanol/water and benzene/toluene in 15 experiments with rectangular slots of normal width $\frac{1}{8}$ in. (0·32 cm) and $\frac{1}{4}$ in. (0·64 cm) gave a mean value of $k = 0{\cdot}34$.

The final equation for the local efficiency therefore becomes:

$$\log_{10}\left(\frac{1}{1-E_p}\right) = \frac{0{\cdot}34\,h\,T^{0.5}}{M^{0.5}\,V_s^{0.25}\,P^{0.25}} \qquad (11)$$

Comparison with Experimental Data

Published experimental data on plate efficiencies for a range of systems and types of column have been compared with the efficiencies predicted by eq. (11). The constructional details of the columns, the operating conditions and the systems employed are given together with the observed and predicted efficiencies in Table 1. The agreement obtained is illustrated graphically in Figs. 3 to 6, which show the expermental figures together with lines calculated from eq. (11).

The methods used in evaluating the variables in eq. (11) for the experimental conditions and in making the comparison are described in the following sections of the paper.

1. *Vapour rate per slot, V_s*

The flow rate per slot was computed by dividing the total vapour rate in cm³/sec, calculated from the superficial vapour velocity and the area of cross-section of the column, by the number of slots per plate.

2. *Mean molecular weight, M*

This was calculated from the composition of the mixture involved. Since at total reflux the composition of the vapour entering the plate is equal to that of the liquid on the plate the latter composition was used for computing M. When the concentrations of the components were not given M was taken as the arithmetic mean of those of the components.

3. *Total slot submergence, h*

The total submergence h was obtained by adding to the static liquid seal h_l the active slot opening h_s calculated by a modification of the equations of Rogers und Thiele [28]. This modification consisted of neglecting the density of the vapour ϱ_v compared with that of the liquid (*i.e.* assuming $\varrho_l - \varrho_v = \varrho_l$) and expressing the vapour density as a function of pressure, temperature, and molecular weight. The resulting equations are as follows:

For a rectangular slot:

$$h_s = 0{\cdot}038\,(M\,P/T\varrho_l)^{\frac{1}{2}}\,(V_s/W)^{\frac{2}{3}}. \qquad (12)$$

For a triangular slot:

$$h_s = 0{\cdot}2\,(M\,P/T\varrho_l)^{\frac{1}{2}}\,(H\,V_s/W)^{\frac{2}{3}} \qquad (13)$$

where W = width of slot at the base
H = height of slot.

Table 1. Comparison of plate efficiencies determined experimentally and calculated from eq. (11)

Note: Dimensions marked with * estimated from the figures in the original papers. Temperatures and compositions marked with * assumed for calculations.

Author(s)	*Plates*		*Caps*		*Slots*		*Liquid seal h_l*	*System and mol.-% of light component*		*Pressure P*	*Temp.*	*Vapour rate per slot, V_s*	*Efficiency (%)*		*Remarks*
	No. per col.	*Dia. (cm)*	*No. per plate*	*Dia. (cm)*	*No. per cap*	*Dimensions (cm) ($W \times H$)*	*(cm)*			*(atm)*	*(°C)*	*(cm^3/sec)*	*Calculated (E_p)*	*Observed (E_{MV})*	
CAREY [3] *	1	15	1	6·1	32	0·16 × 1·3	0·6	Ethanol-water	30	1	81	36	80	87 (a)	(a) Data taken from Ref. [3] (Fig. 3). In Fig. 3 plate efficiencies are plotted against flow rates. All experiments were done at a constant superficial vapour velocity in the column (6·4 cm/sec)
							1·3						91	93	
							1·9						96	99	
							3·2						99	99·8	
					16	0·32 × 1·3	0·6					72	73	75	
							1·3						87	87	
							1·9						93	95	
							3·2						98	98	
					8	0·63 × 1·3	0·6					145	68	70	
							1·3						83	82	
							1·9						90	90	
							3·2						97	97	
					4	1·27 × 1·3	0·6					290	61	67	
							1·3						77	78	
							1·9						85	87	
							3·2						94	94	
CAREY [3]	1	15	1	6·1	8	0·63 × 1·3	0·6 and 1·8	Ethanol-water	30*	1	81	From 80 to 400	(a) See Fig. 4	See Fig. 4	(a) Experimental data taken from Ref. [3] (Fig. 4). In Fig. 4 plate efficiencies, are plotted against vapour rates
CAREY [3]	1	15	1	6·1	8	0·63 × 1·3	0·8	Benzene-toluene	16	1	103	210	57	55	In Fig. 5a the efficiencies are plotted against benzene concentrations in the mixture
									24		100		57	53	
									36		96		57	56	
									47		93		57	56	
									59		90		57	58	
									68		87		58	59	
									76		85		58	60	

Table 1. (Continued)

Author(s)	*Plates*		*Caps*		*Slots*		*Liquid seal h_l*	*System and mol.-% of light component*		*Pressure P*	*Temp.*	*Vapour rate per slot, V_s*	*Efficiency (%)*		*Remarks*
	No. per col.	*Dia. (cm)*	*No. per plate*	*Dia. (cm)*	*No. per cap*	*Dimensions (cm) ($W \times H$)*	*(cm)*			*(atm)*	*(°C)*	*(cm^3/sec)*	*Calculated (E_p)*	*Observed (E_{MV})*	
Griswold [3], [21]	10	20	1	(a)	48	0·48 × 2·2	1·3	Benzene-toluene	50*	1	92*	40	68	64 (b)	(a) Rectangular 5 cm wide cap extending across the plate (b) Plate efficiency was determined for each plate and an average taken for each run. In Fig. 5a efficiencies are plotted against flow rate
												90	68	66	
												150		73	
												150		68	
												200	69	65	
												220		70	
												250		68	
												260		70	
												310	70	71	
												350		68	
												370		68	
												420	71	66	
												470		65	
												510	70	59	
Carey, Page and Wicker [3]	7	20	1	10·4 (a)	36	0·32 × 1·9 (b)	0·3	Benzene-toluene	50*	1	92*	170 to 490	See Fig. 5c	See Fig. 5c	(a) Outer diameter (b) Height of vertical slot Angle of slot with radii of cap 45°
Page and Wicker [3])	7	20	1	10·4 (a)	36	0·32 × 1·9 (b)	0·3	Carbon tetra-chloride-Toluene	50*	1	94*	327	54	54	
Griswold and Stewart [13]	12	15	2 (a)	6·3	18	0·24 × 1·4 (b)	1·1	Benzene-toluene	50*	1	92*	15 to 300	See Fig. 5b	See Fig. 5b	(a) With a baffle 3·8 cm high between the caps (b) Opposed tangential slots with 0·24 cm minimum width
Peavy and Baker [25]	3	46	10	7·6	38	0·32 × 1·3	0·0	Ethanol-water	50*	1	80*	260*	54	78 66 (a)	(a) Local efficiencies calculated from plate efficiencies assuming $mv/L = 0{\cdot}45$
							1·3						80	89 74	
							2·5						91	104 85	
							5·1						99	118 94	

Table 1. (Continued)

Author(s)	Plates		Caps		Slots		Liquid seal h_l	System and mol.-% of light component		Pressure P	Temp.	Vapour rate per slot, V_s	Efficiency (%)		Remarks
	No. per col.	Dia. (cm)	No. per plate	Dia. (cm)	No. per cap	Dimensions (cm) ($W \times H$)	(cm)			(atm)	(°C)	(cm^3/sec)	Calculated (E_p)	Observed (E_{MV})	
														(c) (d)	
Rhodes and Slachman [27]	3	(a)	1	11 (b)	24	0·32 × 1·1*	0·7*	Ethanol-water	50*	1	80*	160	73	76 72	(a) Column of oval shape cross-section (210 cm^2)
												250	73	71 65	(b) Caps enlarged at bottom (see diagram in Ref. [27])
												310	72	71 67	(c) Determined at total reflux
								Benzene-toluene	50*	1	92*	70	59	66 64	(d) At reflux ratio 1:1
												110	59	67 61	
												140	59	65 57	
Kirschbaum [18]	1	11	1	5·3	24*	0·7 × 0·7* Triangular	0·5	Ethanol-water	55	1	79	40	68	(a) 94	(a) Plate efficiencies higher than 100% were observed probably due to the poor mixing of liquid at low vapour rate (40 cm^3/sec per slot)
							1·0						81	103	
							2·0						93	114	
							3·0						98	116	
							4·0						99	115	
							0·5					200	61	75	
							1·0						72	84	
							2·0						86	92	
							3·0						93	94	
							4·0						96	96	
Kirschbaum [18]	1	40	15	5*	10*	1·5 × 1·5* Triangular	3·0	Ethanol-water	50	1	80	170	94	(a) 96	(a) Data taken from Ref. [18], Fig. 133. In other series of experiments in which plate spacing was 20 cm, a 6 cm layer of 25 mm. Berl saddles was inserted between the plates. The results are plotted in Fig. 5f
												340	93	92	
												500	92	89	
												670	91	88	
												840	90	87	
												1010	90	85	
												1180	90	80	
Kirschbaum [18]	1	40	4	9	18*	1·5 × 1·5* Triangular	3·0	Ethanol-water	50	1	80	350	93	88	Experimental data taken from Ref. [18]. Fig. 153, curve *b*
												700	91	88	
												1050	90	87	
												1400	88	86	
												1750	86	84	

Table 1. (Continued)

Author(s)	Plates		Caps		Slots		Liquid seal h_l	System and mol.-% of light component		Pressure P	Temp.	Vapour rate per slot, V_s	Efficiency (%)		Remarks
	No. per col.	Dia. (cm)	No. per plate	Dia. (cm)	No. per cap	Dimensions (cm) ($W \times H$)	(cm)			(atm)	(°C)	(cm^3/sec)	Calculated (E_p)	Observed (E_{MV})	
KIRSCHBAUM [18]	1	40	1	(a)	150*	0·5 × 0·5* Triangular	3·0	Ethanol-water	50	1	80	340	92	88	(a) Oval shaped cap 136 mm wide, 296 mm long (see Ref. [18], Fig. 152) (b) Ref. [18], Fig. 153, curve *c*
KEYES and BYMAN [7]	4	(a)	1	7·6	38	0·32 × 1·6	3·0	Ethanol-water	54	1	80	26 78 130 180 230	98 96 95 95 95	(b) 95 93 91 90 89	(a) Rectangular plate of free vapour space cross-section 12·7 cm × 12·7 cm (b) Based on actual analyses. Plate No. 1, total reflux. Ref. [17], Table 1, pages 28 and 29
LANGDON and KEYES [19]	4	(a)	1	7·6	38	0·32 × 1·6	3·0	Isopropanol-water	(b) 93 93 85 86 86 70 67 65 63 59 55 55 37 36	1	81 (c)	103 129 103 116 155 129 129 129 129 155 116 155 116 155	(d) 92 91 92 92 92 93 93 93 93 94 94 95 95 95		(a) Rectangular 12·7 × 12·7 cm^2 (b) Arithmetic mean of concentration of liquid entering and leaving the plate (c) Practically constant for all concentrations investigated (d) Efficiency measured on the 1st plate from the bottom at infinite reflux ratio. In Fig. 6c efficiencies measured on all 4 plates are plotted against concentration of liquid leaving the plate.

Table 1. (Continued)

Author(s)	Plates		Caps		Slots		Liquid seal h_l (cm)	System and mol.-% of light component		Pressure P (atm)	Temp. (°C)	Vapour rate per slot, V_s (cm³/sec)	Efficiency (%)		Remarks
	No. per col.	Dia. (cm)	No. per plate	Dia. (cm)	No. per cap	Dimensions (cm) ($W \times H$)							Calculated (E_p)	Observed (E_{MV})	
Gadwa [8]	4	(a)	1	9	38	0·32 × 1·6	3·8	Methanol-water	50*	1	73	230 (c)	98	99	(a) Rectangular 12·7 cm × 22·8 cm
								Propanol-water	43* (b)		88		97	83	(b) Azeotropic mixtures
								Isobutanol-water	33* (b)		89		97	98	(c) Data for higher vapour rates are not included in this table
								Methanol-propanol	50*		80		95	90	
								Methanol-isobutanol	50*		86		95	75	
								Carbon-tetrachloride benzene	50*		78		86	82	
Walter and Sherwood [31]	1	5·1	1	(a)	7	0·24 × 1·3	1·9	Ethanol-water	33	1	81	9	92	88	(a) Segment of a circular cap 5·1 cm in diameter
												98	92	91	See also Fig. 5e
												102	92	89	
												139	92	88	
												189	91	88	
Gerster, Colburn, Bonnet and Carmody [10]	1	33	13	3·8	45	Trapezoidal $W_T = 0.63$ $W = 1.59$ $H = 2.9$	5·4	Air humidification (b)		1	94*	350 (c)	98	93	(a) Total number of slots per plate
											94*	1140 (c)	97	93	(b) Assumed $M = 29$
											94*	350 (d)	98	95	(c) At liquid rate 70 l/min
											94*	1140 (d)	97	99	(d) At liquid rate 230 l/min
															Plate efficiencies were expressed in gas-film transfer units
Walter and Sherwood [31]	1	5·1	1	(a)	7	0·24 × 1·3	1·9	Air humidification (b)		1·0	30	185	89	88	(a) Segment of a circular cap 5·1 cm in diameter
										1·0	30	185	89	88	(b) Assumed for air $M = 29$
										1·0	20	180	89	89	
										1·0	20	180	89	88	
										1·0	27	180	89	85	
										1·0	28	180	89	85	
										1·0	31	180	87	86	

Table 1. (Continued)

Author(s)	Plates: No. per col.	Plates: Dia. (cm)	Caps: No. per plate	Caps: Dia. (cm)	Slots: No. per cap	Slots: Dimensions (cm) (W × H)	Liquid seal h_l (cm)	System and mol.-% of light component		Pressure P (atm)	Temp. (°C)	Vapour rate per slot, V_s cm³/sec	Efficiency (%): Calculated (E_p)	Efficiency (%): Observed (E_{MV})	Remarks
										1·0	27	260	87	85	
										1·0	21	260	87	92	
										1·0	20	250	87	91	
										1·0	22	50	91	92	
										2·0	32	50	88	89	
										3·0	37	45	87	88	
										1·0	24	95	89	90	
										2·0	33	95	87	86	
										3·0	36	95	85	84	
										3·7	39	95	84	81	
										1·0	26	190	88	85	
										2·0	33	195	83	82	
										3·7	40	185	79	78	
Walter and Sherwood [31]	1	46	7	10·1	33	Trapezoidal $W_T = 0{\cdot}32$ $W = 0{\cdot}48$ $H = 1{\cdot}9$	0·95	Absorption of ammonia from air into water (a)		1	14	430	78	70	(a) Assumed for air $M = 29$
												380	78	69	
												240	75	69	
												150	75	69	
												65	74	69	
Gerster, Koffolt and Withrow [11]	3	19	1	7·6	38*	$W = 0{\cdot}32$*	2·5	Methanol-water	89	1	67	230	93	96 (a)	(a) Top plate
									77		69		93	91 (b)	(b) Middle plate
									55		72		94	88 (c)	(c) Bottom plate
									84		68	130	95	96 (a)	Only the results obtained in the runs carried out at total reflux are given in the table
									65		71		95	95 (b)	
									32		78		97	94 (c)	
									81		68	102	96	98 (a)	
									57		72		97	98 (b)	
									21		81		97	94 (c)	
Gerster, Koffolt and Withrow [12]	3	19	2	7·6	38*	$W = 0{\cdot}32$*	2·5	Methanol-water	50*	1	73	64 (a)	64	95	(a) Average value for 8 runs (No. 85–68 and 78) carried out at total reflux

Table 1. (Continued)

Author(s)	Plates		Caps		Slots		Liquid seal h_l (cm)	System and mol.-% of light component		Pressure P (atm)	Temp. (°C)	Vapour rate per slot, V_s (cm³/sec)	Efficiency (%)		Remarks
	No. per col.	Dia. (cm)	No. per plate	Dia. (cm)	No. per cap	Dimensions (cm) ($W \times H$)							Calculated (E_p)	Observed (E_{MV})	
Schoenborn, Koffolt and Withrow [29]	15	20	2	7·6	38*	0·32 × 1·6*	0·7*	Trichloro-ethylene-toluene	50*	1	99	50 50* 100 180 260	52 52 55 58 56	53 52 55 56 56	(a) Badger 19-std caps (b) Only dry runs, without steam, are tabulated. See also Fig. 5d
Nord [24]	10	15	2	5	12	0·63 × 1·3	0·63	Benzene-toluene-xylene	60 (b) 20 (t) 20 (x)	1	100	350	51	60 (b) 55 (t) 53 (d)	(b) of benzene (t) of toluene (x) of xylene (local efficiencies)
Lewis and Wilde [22]	10	274	115 (a)	15·2	32*	0·63 × 2·5	2·5	Naphtha (b)		1	190*	1370	69	65	(a) On 7 upper plates (b) Assumed for plate No. 5 $M = 140$
Gunness [14]	28	127	27	16·5	32	0·63 × 2·5	2·9	Absorption Naphtha (a)		17·9	104 (b)	130	74 82 (c)	80 (d)	(a) From feed composition $M = 61$; $\varrho_l = 0{\cdot}61$ (b) On the feed plate (c) Corrected for weir head (Ep) (d) Local efficiency
McGiffin [23]	30	107	18	11·2	24	Trapezoidal $W_T = 0{\cdot}32$ $W = 1{\cdot}27$ $H = 2{\cdot}9$	2·2	(a) Isopentane-pentane Butane-pentane	50* 50* 50*	9·2 8·4 8·4	116 109 101	630 520 370	65 68 72	63 (b) 69 57	(a) Key components (b) Data taken from Refs. [7] and [25]
									50*	7·4	70	300	73	51	
Brown and Lockhart [1]	20 (a) + 10 (b)	183	34	17·1	24	Trapezoidal $W_T = 0{\cdot}95$ $W = 1{\cdot}27$ $H = 3{\cdot}2$	1·5 (a)	Isobutane Butane (c)	(a) (a) (a) (a) (b) (b) (b) (b)	14·0 17·0 14·3 14·5 14·6 18·1 14·8 15·3	52 64 53 56 134 145 136 137	450 430 680 780 470 550 550 610	61 (d) 76 61 77 57 77 56 77 72 90 69 90 71 89 69 90	58 75 79 75 75 100 102 100	(a) Rectifying section (b) Stripping section (c) $M = 61$ assumed from composition of the mixture (d) Corrected for weir head (E'_p)

For trapezoidal slots it was necessary to solve graphically the equation:

$$V_s = 55\left(\frac{T\,\varrho_l}{P\,M}\right)^{0.5}\left|2{\cdot}5\,W_T\,h_s^{1.5} + \frac{(W - W_T)h_s^{2.5}}{H}\right| \qquad (14)$$

where W_T and W are the widths at the top and bottom of the slot respectively.

At high rates of flow it was sometimes found that the calculated active slot opening exceeded the total height of the slot. In such cases, if the slots were closed by a skirt or the caps rested directly on the plates h_s was taken to be the slot height H; otherwise h_s was corrected for flow of vapour beneath the cap.

Although the slot submergence may be increased by the head of liquid over the exit weir PEAVY and BAKER [26] have shown that liquid is often pumped over by the vapour-lift action of bubbles from neighbouring caps and its level can even be somewhat below the weir. In general therefore only the static liquid seal was taken into account in computing the total submergence.

In some cases, however, a corrected efficiency E' was also calculated using as slot submergence:

$$h' = h_s + h_l + h_w$$

where h_w is the liquid head over the weir, calculated from the well-known Francis formula.

4. Comparison of observed and predicted efficiencies

Since the value of the constant in eq. (11) was based on experiments in a small column with a single cap on each plate it should give the local or point efficiency. In large columns the MURPHREE plate efficiency should be higher owing to cross-flow liquid with incomplete mixing. In some cases where efficiencies greater than unity were observed for instance when recalculating the data of PEAVY and BAKER [26], an attempt was made to derive the local efficiency from the experimental data by means of LEWIS' eq. (20) for Case I (assuming complete mixing of vapour and no mixing of liquid), *i.e.*:

$$E_p = \ln\frac{[E_{MV}\,(m\,V/L) + 1]}{m\,V/L}$$

where E_p = local efficiency
E_{MV} = MURPHREE plate efficiency
m = slope of equilibrium line (dy^*/dx)
V/L = ratio of molar vapour and liquid rates.

In general, however, the differences between the observed values of E_{MV} and the point efficiencies calculated from eq. (11) were found to be small and much lower than would be expected from LEWIS' equations.

DISCUSSION

It will be seen from Table 1 and Figs. 3 to 6 that in most cases the efficiencies calculated from eq. (11) agree well with those determined experimentally. From the results it has been found possible to evaluate the relative importance of the main factors which affect the efficiency of bubble-cap plates: these are the slot dimensions; the properties and composition

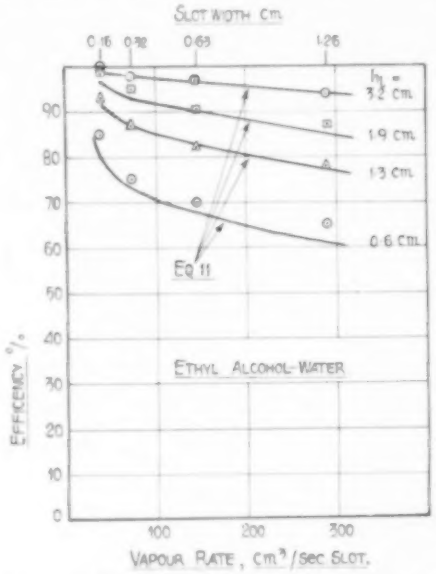

Fig. 3. Variation of efficiency with vapour rate, slot width and liquid seal.

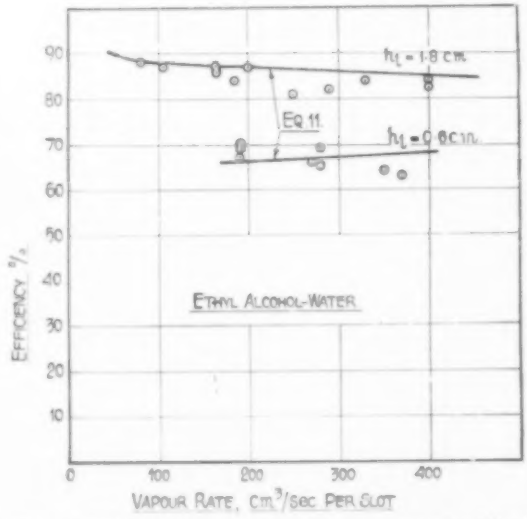

Fig. 4. Variation of efficiency with vapour rate and liquid seal.

of the mixture handled; the operating pressure and temperature; the vapour rate, and the slot submergence.

1. Effect of slot width

The width of the slots seems to have no direct influence on plate efficiency; but there is an indirect effect caused by the change in active slot opening and total

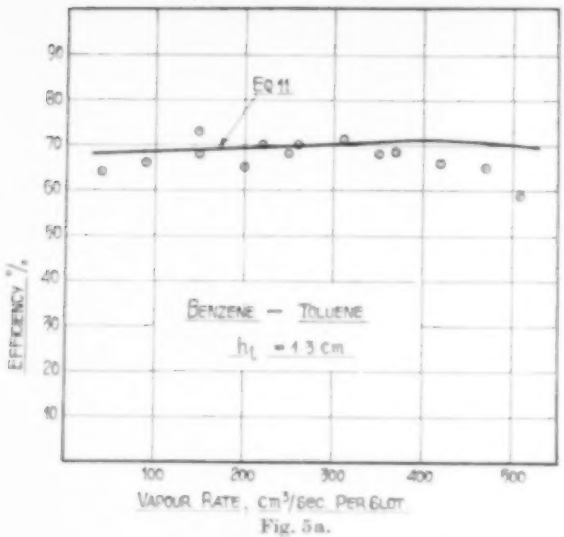

Fig. 5a.

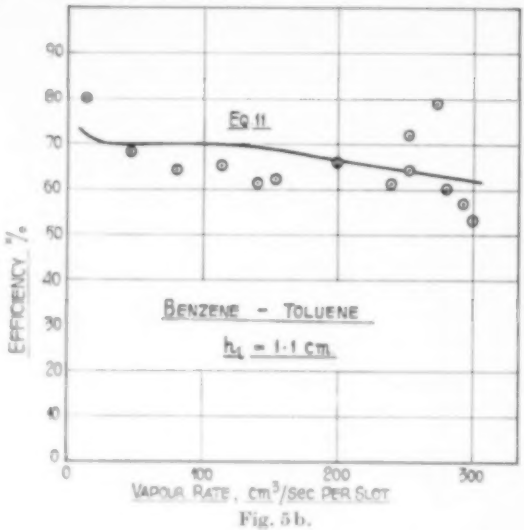

Fig. 5b.

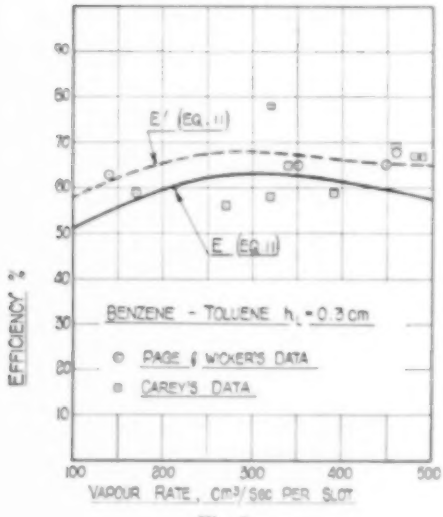

Fig. 5c.

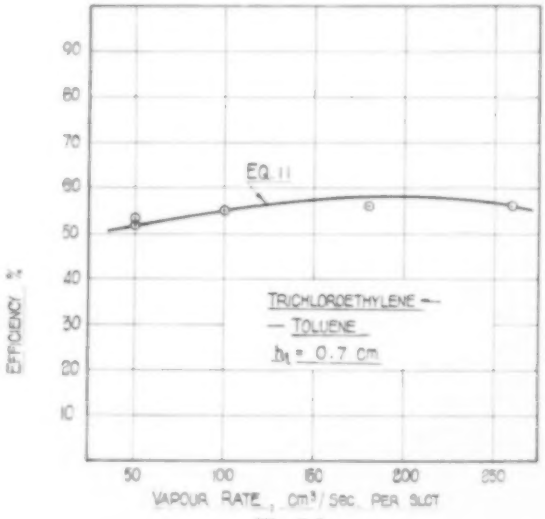

Fig. 5d.

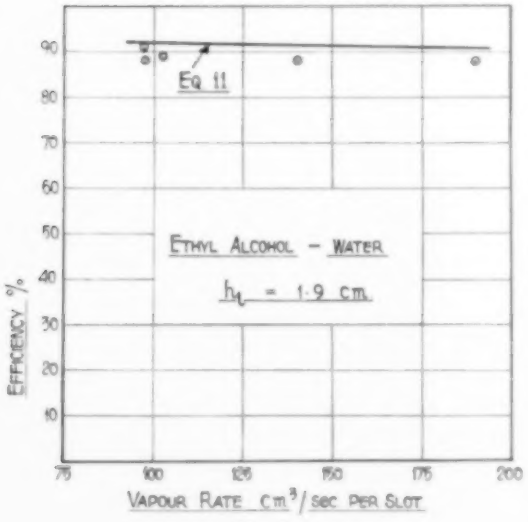

Fig. 5e.

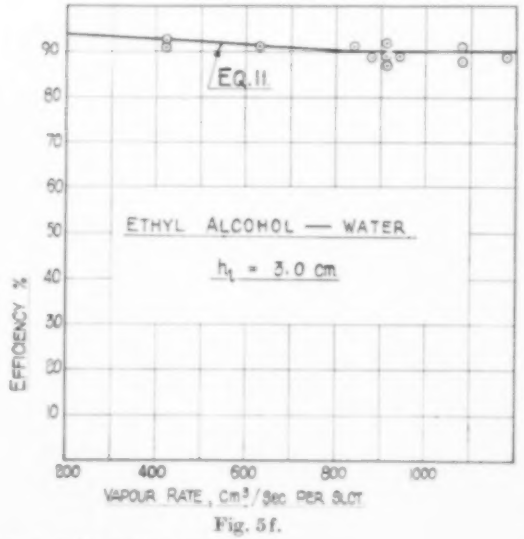

Fig. 5f.

Figs. 5a–f. Variation of efficiency with vapour rate.

VOL. 1 1952

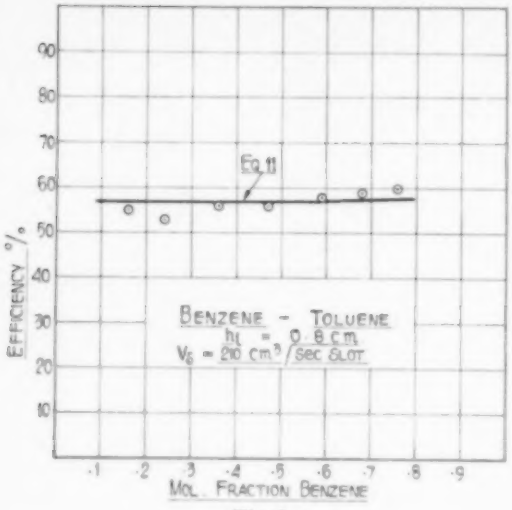

Fig. 6a.

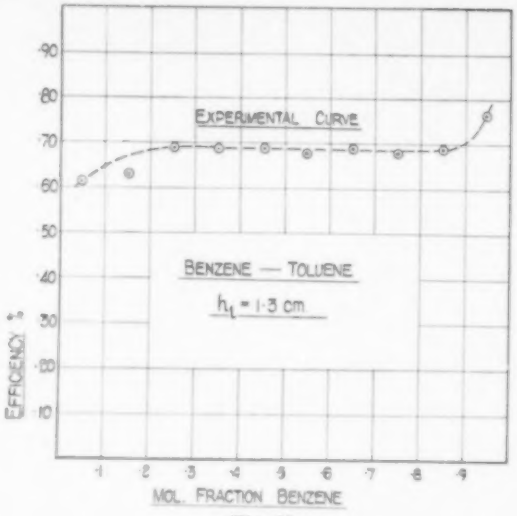

Fig. 6b.

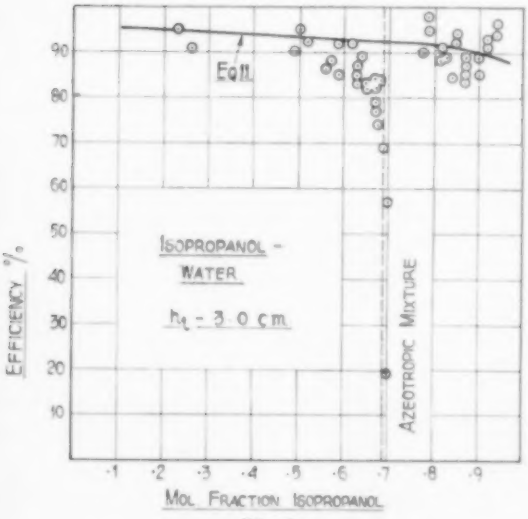

Fig. 6c.

Figs. 6a–c. Variation of efficiency with vapour composition.

submergence at a given vapour rate. This is evident from the work of CAREY *et al.* [3] (Fig. 3) in which the slot width was varied from 1·6 to 12·5 mm. The pitch of the slots in these experiments varied from 6 to 48 mm: even under these conditions the assumption that the vapour passes in the form of channels rather than as separate bubbles appears to be justified.

2. Effect of properties and composition of the mixture

The effect of the properties of the mixture was studied by GADWA [8]; except for mixtures of methanol and isobutanol his results agree fairly well with the predictions of eq. (11). More recently experiments with various liquid mixtures were carried out by WILLIAMS, STIGGER and NICHOLS [32], who, however, reported the results as overall efficiencies. These results are unfortunately too scattered for a comparison with eq. (11) to be made, possibly because the liquid seal employed in this work was low.

Eq. (11) implies that molecular weight and absolute temperature affect the plate efficiency. Since liquid viscosity decreases as the temperature rises and usually increases with molecular weight this may explain the relationship between plate efficiency and viscosity which forms the basis of the correlations of DRICKAMER and BRADFORD [7] and O'CONNELL [25] for overall efficiency.

The effect of the composition of the mixture has been studied by CAREY and GRISWOLD [3] for the benzene/toluene system (see Figs. 6a and b); it is evident that the effect is small, but it would be expected to be greater when the molecular weights of the components differ widely.

The experiments of LANGDON and KEYES [19] with isopropanol/water show good agreement with eq. (11) except when the composition is close to that of the azeotrope (see Fig. 6c). Similar low efficiencies were also reported by KEYES and BYMAN [17] for ethanol/water when close to the azeotropic composition and also for very weak alcohol mixtures. These discrepancies may be attributed to lack of precision in determining the MURPHREE efficiency in these ranges of composition, the results there being very sensitive to experimental errors.

Examination of data for air humidification and absorption of ammonia from air into water [10], [31]

has also shown that eq. (11) gives reasonably good results when applied to absorption and desorption processes in which the gas-film resistance is the limiting factor.

3. Effect of pressure and temperature

The effect of pressure on plate efficiency can be seen in Table 1 for the experiments on air humidification [31] and for tests on columns used in the petroleum industry. Vacuum distillation experiments by Kirschbaum [18] on the system ethanol/water also indicate increased efficiencies at the lower pressures.

At a given vapour rate per slot (cm³/sec) the direct negative effect of increased pressure is compensated to some extent by the increase in active slot opening (h_a) with pressure [eq. (12) and (13)].

The predicted variation with temperature, which appears in eq. (11) as the ratio $(T/M)^{0.5}$, cannot be verified from the data examined since the range of values of this ratio covered is too small.

4. Effect of vapour rate

The effect of vapour rate has been studied by several observers in order to establish the optimum operating conditions. At vapour rates above some critical value depending on the plate spacing entrainment of liquid becomes sufficient to reduce the efficiency. The general conclusion which can be drawn from the published data is that except at very low rates (uneconomic in practice) or at vapour velocities high enough to cause excessive entrainment the plate efficiency varies little with vapour rate.

This conclusion is consistent with eq. (11) which shows that log $[1/(1-E)]$ is proportional to $V_s^{-0.25}$, so that a small decrease in efficiency with vapour rate per slot should occur. This direct effect is compensated by the increase in active slot opening, which gives an increase in total slot submergence. When the static seal (h_l) is low the latter effect should prevail, so that under these conditions there may even be a slight increase in efficiency with vapour rate. A rapid drop in efficiency would be expected for vapour rates exceeding that at which the whole slot opening just becomes active.

5. Effect of slot submergence

The most important factor influencing plate efficiency is the slot submergence, which depends on the static seal provided. At very low submergences quite small variations in liquid level may considerably affect the efficiency; under such conditions the experimental data are somewhat scattered, as may be seen in the Figures 5b and c.

In large columns differences in liquid seal resulting from hydraulic gradient or from faulty levelling of the plates may thus directly affect the efficiency, apart from the reduction caused by the accompanying maldistribution of vapour between unequally submerged caps.

The method outlined in this paper for predicting plate efficiency involves a relation between efficiency and slot submergence, and is therefore considered to be superior to that of O'Connell, which does not take account of this factor. A modification of O'Connell's method incorporating an allowance for liquid seal has however been made recently by Ju Chin Chu *et al.* [5].

Application of the New Equation to the Design of Bubble-cap Columns

Theoretically eq. (11) should give the local efficiency and the Murphree efficiency for whole plates should be somewhat higher. As the observed Murphree plate efficiencies differ little from the values predicted; eq. (11) should be used in practice to predict the Murphree plate efficiency to be expected from a column.

This is not necessarily equal to the *overall efficiency*, defined as the ratio of the number of theoretical plates to the actual number of plates required. They are equal only when the equilibrium and operating lines in a McCabe-Thiele diagram are parallel, *i.e.* when $mV/L = 1$. In important cases of design it is preferable to employ the Murphree efficiency in conjunction with the McCabe-Thiele diagram to obtain directly the number of actual plates necessary. This may be done as illustrated in Fig. 7 by drawing the vertical steps so that the enrichment per plate is E_{MV} times that corresponding to equilibrium. This is most easily done by starting from the reboiler end of the column, but this is not essential.

A special application of the new method may be made in the design of columns for vacuum distillation of heat-sensitive substances, in which the pressure-drop is often limited by the temperature permissible in the reboiler. The pressure drop per plate can be lowered by reducing the liquid seal, but this in turn reduces the efficiency so that more plates are required. If a mean value of the overall efficiency equal to n times E_{MV}, can be taken, the new method can be used to determine the best combination of liquid seal and number of plates, as follows:

VOL. 1 1952

Let N_t = the number of theoretical plates required in the column
N = number of actual plates
Z = specified pressure drop expressed in cm of liquid.

Then, neglecting pressure drop in the caps and risers:

$$N = \frac{N_t}{E_o} = \frac{N_t}{n E_{MV}} = \frac{Z}{h_l + h_s} . \qquad (15)$$

But by eq. (11), taking $E_{MV} = E_p$ and P as the mean absolute pressure:

$$\log_{10} \frac{1}{1 - E_{MV}} = \frac{0{\cdot}34\, T^{0{\cdot}5}\,(h_l + h_s)}{M^{0{\cdot}5}\, P^{0{\cdot}25}\, V_g^{0{\cdot}25}} . \qquad (11)$$

A value of h_l can be found by trial such that both these equations give the same value for the efficiency; insertion of this value in eq. (15) then gives the number of actual plates. If a negative value of h_l is found this indicates that the specified pressure drop is too low and the pressure at the column head will have to be reduced if the desired separation is to obtained.

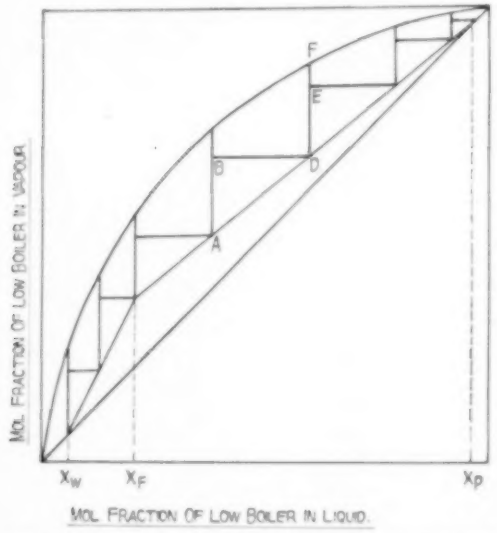

Fig. 7. Modification of McCABE-THIELE diagram to allow for MURPHREE plate efficiency. The vertical steps are taken so that $\frac{AB}{AC} = \frac{DE}{DF} = E_{MV}$.

CONCLUSIONS

1. Recent investigations of the mechanism of bubble formation at submerged slots have shown that under the conditions normally existing in distillation columns the vapour may be regarded as flowing through a channel, rather than passing in the form of a stream of separate bubbles.

2. By a simplified treatment based on this mechanism an equation has been derived for predicting the plate efficiency in bubble-cap columns. The main factor affecting the efficiency is slot submergence; other important factors are vapour rate, pressure, temperature, and the molecular weights of the components.

3. Comparison of experimental data published in the literature with efficiencies calculated from the new equation shows good agrement, apart from a few discrepancies at the extremes at the concentration range and in the neighbourhood of azeotropic mixtures. These are probably due to the lack of precision inherent in the determination of the MURPHREE efficiency in these regions of composition.

4. The method can also be used for absorption processes in which the gas-film controls the rate of absorption.

Acknowledgement—The author desires to acknowledge the assistance of his colleague, Mr. G. A. MORRIS, in the preparation of this paper.

NOTATION

A = interfacial area for matter transfer (cm²)
d = equivalent diameter of channel (cm)
E_{MV} = MURPHREE plate efficiency (based on the change of vapour composition)
E_o = overall efficiency (the ratio of the numbers of theoretical and actual plates required)
E_p = MURPHREE local or point efficiency
H = Total slot height (cm)
h = total slot submergence $(h_l + h_g)$ (cm)
h' = total submergence corrected for weir head (h_{ac}) (cm)
h_l = static liquid seal (cm)
h_s = active slot opening (cm)
h_{ac} = head of liquid over weir (cm)
K_y = overall matter transfer coefficient (g mol/sec . cm² atm)
k_y = gas-film coefficient (g mol/sec . cm² atm)
L = Molar liquid flow (g mol/sec)
M = molecular weight
m = slope of equilibrium line (dy^*/dx)
N = number of theoretical plates
N_t = number of actual plates
P = absolute pressure (atm)
p = partial pressure of more volatile component (atm)
T = absolute temperature (°K)
V = molar vapour flow (g mol/sec)
V_s = vapour rate per slot (cm³/sec)
v = vapour velocity in channel (cm/sec)
W = slot width (cm)
W_T = width at top of trapezoidal slot (cm)
x = mol. fraction in liquid
y = mol. fraction in vapour

y^* = equilibrium mol. fraction in vapour
Z = pressure drop, expressed as liquid head (cm)
ϱ_l = density of liquid (g/cm³)
ϱ_v = density of vapour (g cm³)
Δp_m = log mean driving force for matter transfer (atm)

REFERENCES

[1] BROWN, G. G. and LOCKHART, F. J.; Trans. Amer. Inst. Chem. Eng. 1943 **39** 63. [2] CAREY, J. S.; PERRY's Chemical Engineer's Handbook (3rd Ed.) p. 597. McGraw Hill, 1950. [3] CAREY, J. S., GRISWOLD, J., LEWIS, W. K. and MCADAMS, W. H.; Trans. Amer. Inst. Chem. Eng. 1933–4 **30** 504. [4] CAREY, W. F. and WILLIAMSON, G. J.; Trans. Inst. Mech. Eng. (London) 1950 **163** 41. [5] CHU, J. C., DONOVAN, J. R., BOSEWELL, B. C. and FURMEISTER, L. C.; J. Appl. Chem. 1951 **1** 529. [6] DAVIES, J. A.; Pet. Refiner 1950 **29** (9) 121. [7] DRICKAMER, H. G. and BRADFORD, J. R.; Trans. Amer. Inst. Chem. Eng. 1943 **39** 319. [8] GADWA; Sc.D. Thesis in Chem. Eng., Massachusetts Inst. of Technology, 1936. [9] GEDDES, R. L.; Trans. Amer. Inst. Chem. Eng. 1946 **42** 863. [10] GERSTER, J. A., COLBURN, A. P., BONNET, W. E. and CARMODY, T. H.; Chem. Eng. Prog. 1949 **45** 716. [11] GERSTER, J. A., KOFFOLT, J. H. and WITHROW, J. R.; Trans. Amer. Inst. Chem. Eng. 1943 **39** 37. [12] GERSTER, J. A., KOFFOLT, J. H. and WITHROW, J. R.: Trans. Amer. Inst. Chem. Eng. 1946 **41** 393. [13] GRISWOLD, J. and STEWART, P. B.; Ind. Eng. Chem. 1947 **39** 753. [14] GUNNESS, R. C.; Ind. Eng. Chem. 1937 **29** 1092. [15] JOHNSTONE, H. F. and PIGFORD, R. L.; Trans. Amer. Inst. Chem. Eng. 1942 **38** 25. [16] HUFFMAN, J. R. and TREYBAL, R. E.; Ind. Eng. Chem. (Anal. Ed.) 1940 **12** 745. [17] KEYES, D. B. and BYMAN, L.; Univ. of Illinois Bull. 1941. [18] KIRSCHBAUM, E.; Z.V.D.I. Beiheft Verfahrenstechnik No. 1, 1937, p. 139 and No. 5, 1938, p. 131. "Distillation and Rectification" (Chemical Publishing Co. 1948). [19] LANGDON, W. M. and KEYES, D. B.; Ind. Eng. Chem. 1943 **35** 464. [20] LEWIS, W. K.; Ind. Eng. Chem. 1936 **28** 399. [21] LEWIS, W. K. and SMOLEY, E. R.; Amer. Pet. Bull. 1930 **11** 72. [22] LEWIS, W. K. and WILDE, H. D.; Trans. Amer. Inst. Chem. Eng. 1928 **21** 99. [23] MCGRIFFIN, J. W.; Trans. Amer. Inst. Chem. Eng. 1942 **38** 761. [24] NORD, M.; Trans. Amer. Inst. Chem. Eng. 1946 **42** 863. [25] O'CONNELL, H. E.; Trans. Amer. Inst. Chem. Eng. 1946 **42** 741. [26] PEAVY, C. C. and BAKER, E. M.; Ind. Eng. Chem. 1937 **29** 1056. [27] RHODES, F. H. and SLACHMAN, P. G.; Ind. Eng. Chem. 1937 **29** 51. [28] ROGERS, M. C. and THIELE, E. W.; Ind. Eng. Chem. 1934 **26** 524. [29] SCHOENBORN, E. M., KOFFOLT, J. H. and WITHROW, J. R.; Trans. Amer. Inst. Chem. Eng. 1941 **37** 997. [30] SPELLS, K. E. and BAKOWSKI, S.; Trans. Inst. Chem. Eng. (London) 1950 **28** 38. [31] WALTER, J. F. and SHERWOOD, T. K.; Ind. Eng. Chem. 1941 **33** 493. [32] WILLIAMS, G. C., STIGGER, E. K. and NICHOLS, J. H.; Chem. Eng. Prog. 1950 **46** 7.

VOL. 1 1952

Strömung von Gasen durch feinporige Stoffe

(Flow of gases through micropores)

E. WICKE and W. VOLLMER

Physico-chemical Institute of Göttingen University

Summary—The flow of gases in the transition zone between laminar (POISEUILLE) and molecular (KNUDSEN) flow is of great importance in vacuum technique is finding increasing application in modern chemical industry. Moreover, there are special separation effects in this transition zone*. Our knowledge of the flow through micropores, which often takes place even at atmospheric pressure in this transition zone is lacking. This investigation is concerned with the problem mentioned above. A short discussion is devoted to the transitory flow through single capillaries, while the flow minimum involved is qualitatively explained. The different behaviour of the flow through micropores is attributed to the influence of the pore spectrum, and a new method of determining the "mean pore radius" is given. The effect of the mean gas pressure and of the temperature on this flow is examined, and the sometimes great influence of the slip along the walls and the dependence of the mean free path of the gas molecules on temperature is elaborated. Finally, the conditions are defined under which surface diffusion may come to play an important part in the direct flow through micropores.

Zusammenfassung—Die Strömung von Gasen im Übergangsgebiet zwischen laminarer (POISEUILLE-) und molekulärer (KNUDSEN-) Strömung ist für die Vakuumtechnik, die in den modernen chemischen Betrieb immer stärker Eingang findet, von erheblicher Bedeutung. Auch treten in diesem Übergangsgebiet besondere Trenneffekte auf*. Noch lückenhaft sind unsere Kenntnisse über die Strömung durch feinporige Stoffe, die sich häufig bereits bei Atmosphärendruck in diesem Übergangsgebiet befindet. Die vorliegende Untersuchung befaßt sich mit diesem Problem. — Die Übergangsströmung durch Einzelkapillaren wird kurz besprochen und das dabei auftretende Durchflußminimum qualitativ verständlich gemacht. Das andersartige Verhalten der Strömung durch feinporige Stoffe wird auf den Einfluß des Porenspektrums zurückgeführt und eine neue Methode zur Bestimmung des „mittleren Porenradius" angegeben. Die Abhängigkeit dieser Strömung vom mittleren Gasdruck und von der Temperatur wird untersucht und der unter Um-

* H.-D. BECKEY u. W. E. GROTH, Naturwiss. 1951 **38** 558. Z. Naturforschg. 1952 **7a** 474, entdeckten im Übergangsgebiet an Kapillaren, die sich in einem Temperaturgefälle befanden, einen bisher unbekannten Trenneffekt für Gasgemische, bei dem sich die leichte Komponente am kalten, die schwere am warmen Kapillarenende anreichert („negativer Effekt"). Im Bereich der reinen KNUDSEN-Strömung konnte der Effekt zu einem „positiven" umgekehrt werden.

ständen erhebliche Einfluß der Gleitung sowie der Temperaturabhängigkeit der mittleren freien Weglänge der Gasmolekeln herausgearbeitet. Zum Schluß werden die Voraussetzungen angegeben, unter denen eine Oberflächendiffusion an der direkten Durchströmung feinporiger Stoffe merklichen Anteil gewinnen kann.

1. Problemstellung und Messmethode

a) *Strömung durch Einzelkapillaren*

Für die laminare Strömung von Gasen durch ein einzelnes zylindrisches Rohr bzw. eine einzelne Kapillare gilt bei $\Lambda \ll r$ nach Hagen-Poiseuille:

$$\frac{\dot{n}_p}{\Delta p} = \frac{\pi r^4}{8 \eta L} \cdot \frac{1}{RT} \cdot \bar{p} . \tag{1}$$

$\dot{n}_p/\Delta p$ = Mengenstrom, bezogen auf die Einheit der Druckdifferenz Δp; r, L = Radius bzw. Länge der Kapillare; η = Gaszähigkeit; R = allgemeine Gaskonstante; $\bar{p}$ = mittlerer Gasdruck; T = absolute Temperatur; Λ = mittlere freie Weglänge (m. f. W.) der Gasmolekeln in der Kapillare beim Druck $\bar{p}$.

Bei der Untersuchung der Strömung von Gasen durch Röhren fanden zuerst Kundt und Warburg [1] einen größeren Gastransport als nach obiger Beziehung zu erwarten. Die Autoren konnten diese scheinbare Verringerung der Gaszähigkeit darauf zurückführen, daß an der Wand ein Geschwindigkeitssprung auftritt, der durch die endliche Größe der m. f. W. Λ verursacht wird. Unter Berücksichtigung dieser *Gleitung* läßt sich der Gasdurchsatz genauer erfassen durch die Beziehung:

$$\frac{\dot{n}}{\Delta p} = \frac{\pi r^4}{8 \eta L} \cdot \frac{\bar{p}}{RT} \cdot \left| 1 + \frac{4 \xi}{r} \right| \tag{2}$$

Hierin bedeutet ξ den Gleitungskoeffizienten, der etwa von der Größe der m. f. W. ist:

$$\xi = \text{const} \cdot \Lambda . \tag{2a}$$

Der numerische Wert der Proportionalitätskonstante hängt davon ab, in welcher Weise man die m. f. W. aus den experimentellen Zähigkeitsdaten berechnet [vgl. Gl. (7) und (7a)]. — Da die m. f. W. von Gasen und Dämpfen bei normaler Raumtemperatur und $\bar{p} = 1$ atm in der Größenordnung 10^{-5} bis 10^{-6} cm liegt, übersteigt hier der Einfluß der Gleitung einige Prozente in Poren vom Radius $r \leq 10^{-3}$ bis 10^{-4} cm. Bei feinporigen Substanzen muß daher unter diesen Bedingungen, d. h. auch bereits bei Atmosphärendruck, die Gleitung im allgemeinen berücksichtigt werden.

Ist dagegen die m. f. W. der Gasmolekeln groß gegen den Kapillarradius ($\Lambda \gg r$), so ergibt sich der Gasdurchsatz als sog. Knudsensche Molekularströmung zu:

$$\frac{\dot{n}_k}{\Delta p} = \frac{2}{3} \frac{\pi r^3}{L} \frac{1}{RT} \bar{w} \tag{3}$$

mit

$\bar{w}$ = mittlerer Molekulargeschwindigkeit $= 2 \sqrt{\frac{2RT}{\pi M}}$.

In diesem Falle gilt für die Temperaturabhängigkeit des Mengenstroms zweier Gase verschiedener Molmassen M_1 und M_2:

$$\frac{\dot{n}_{k_1}}{\Delta p_1} \cdot \sqrt{M_1 T_1} = \frac{\dot{n}_{k_2}}{\Delta p_2} \cdot \sqrt{M_2 T_2} . \tag{3a}$$

Mit H_2, O_2 und CO_2 hat Knudsen [2] den Gasdurchsatz durch Glaskapillaren in Abhängigkeit von den verschiedenen Parametern eingehend untersucht. Bei höheren Drucken bestätigte er die Gültigkeit der Gl. (2). Im Gebiet geringerer Drucke stellte er jedoch bei $\Lambda \approx 3r$ ein Minimum des Durchsatzes fest. Zu

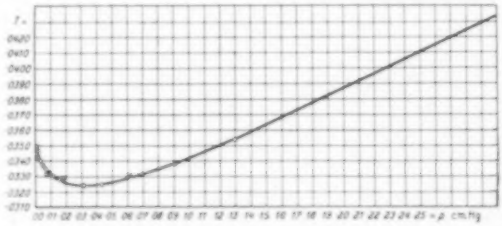

Abb. 1. Strömung von CO_2 durch Glaskapillaren als Funktion des mittleren Druckes nach Knudsen [2]. T ist das durch 24 parallele Kapillaren von 2 cm Länge und $^1/_{200}$ cm Radius unter der Druckdifferenz $\Delta p = 1$ dyn/cm² sekundliche fließende Gasvolumen, letzteres gemessen bei $p = 1$ dyn/cm² und der Kapillarentemperatur.

noch kleineren Drucken hin erfolgte wieder ein Anstieg um etwa 7%, vgl. Abb. 1.

Diese Meßergebnisse konnte Knudsen mit guter Genauigkeit durch eine empirische Formel wiedergeben:

$$\frac{\dot{n}}{\Delta p} = a \bar{p} + b \frac{1 + 0{,}81\, c \bar{p}}{1 + c \bar{p}} \tag{4}$$

mit

$$c = 2{,}47 \sqrt{\frac{M}{RT}} \cdot \frac{r}{\eta} . \tag{4a}$$

Hierin sind die Gln. (2) und (3) als Grenzfälle enthalten:

$$c \bar{p} \gg 1 : \frac{\dot{n}}{\Delta p} = a \bar{p} + 0{,}81\, b \tag{5}$$

$$c \bar{p} \ll 1 : \frac{\dot{n}}{\Delta p} = b . \tag{5a}$$

Durch Vergleich mit den Gln. (2) und (3) ergibt sich:

$$a = \frac{\pi}{8} \cdot \frac{1}{\eta} \cdot \frac{r^4}{L} \cdot \frac{1}{RT} , \tag{6}$$

$$b = \frac{4}{3} \cdot \sqrt{2\pi} \cdot \frac{r^3}{L \sqrt{MRT}} . \tag{6a}$$

In der Form der Gl. (5) kommt besonders deutlich zum Ausdruck, daß es sich bei dem Gleitungsglied $0{,}81 \cdot b$ (mit b nach Gl. (6a)] um einen vom mittleren

Gasdruck unabhängigen Zusatztransport handelt, der mit steigenden Werten dieses Gasdrucks keineswegs verschwindet, sondern lediglich in seinem Verhältnis zum Haupttransport $a \cdot \bar{p}$ immer kleiner und schließlich vernachlässigbar wird. — Setzt man die Gleitungsglieder von Gl. (5) und Gl. (2) einander gleich und benutzt die Beziehung:

$$\eta / \bar{p} = A \cdot \frac{M}{RT} \cdot \bar{w} \cdot \Lambda \,, \tag{7}$$

mit

$$\Lambda = 1 / \left(\sqrt{2}\, N \pi \sigma^2 \right) \tag{7a}$$

(N = Zahl der Partikeln je cm³; σ = gaskinetischer Stoßdurchmesser), so folgt für den Zusammenhang

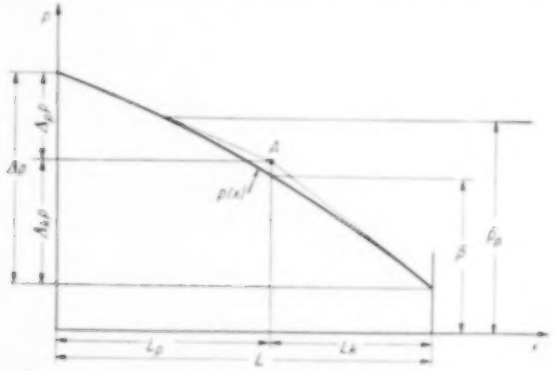

Abb. 1a. Schematische Aufteilung einer Strömungsstrecke in POISEUILLE- und KNUDSEN-Anteil zur Ableitung der Gl. (10).

zwischen Gleitungskoeffizient und m. f. W. bei Strömung durch kreisrunde Röhren [Gl. (2a)]:

$$\xi = 2{,}74 \cdot A \cdot \Lambda \,. \tag{2b}$$

Mit dem aus der gaskinetischen Ableitung der Gl. (7) zu gewinnenden Faktor $A = {}^1/_2$* hat man also in diesem Falle:

$$\xi = 1{,}37 \cdot \Lambda^{**} \,. \tag{2c}$$

b) *Zum Verständnis des Minimums bei der Durchströmung von Einzelkapillaren*

Nach der Methode zur Auffindung von Extremwerten erhält man für den Durchfluß nach Gl. (4) ein Minimum bei $c\,\bar{p} = 1$. Führt man in die Definitions-Gl. (4a) für c die Gaszähigkeit nach Gl. (7) ein (mit $A = {}^1/_2$), so folgt für die m. f. W. im Durchflußminimum:

$$\Lambda_{\min} = 3{,}10 \cdot r \,. \tag{8}$$

* Genauer lautet dieser von S. CHAPMAN, Phil. Trans. Roy. Soc. London A 1915 **216** 279 für reine Gase abgeleitete Faktor $A = 0{,}499$, vgl. auch A. EUCKEN, Lehrb. Chem. Physik, Bd. II, 1, Leipzig 1950, S. 328.

** Für die Strömung zwischen ebenen Platten gilt dagegen $\xi = 2/3 \cdot \Lambda$ (mit Λ nach Gl. (7a)], vgl. A. EUCKEN, *loc. cit.* S. 387; K. F. HERZFELD in Hand- u. Jahrbuch der Chem. Physik, Bd. III, 2, Leipzig 1939.

Das Minimum in Abb. 1 liegt bei einem mittleren Gasdruck von $\bar{p} = 0{,}3$ Torr. Hier berechnet sich die m. f. W. des CO_2 nach Gl. (7a) mit σ nach Tabelle 1 (0° C) zu: $\Lambda_{CO_2} = 9{,}9 \cdot 10^{-3}$ cm. Da der Kapillarradius bei der in Abb. 1 dargestellten Kurve $r = 3{,}3 \cdot 10^{-3}$ cm betrug, wird obige Beziehung gut bestätigt.

Eine strenge Theorie zur Erklärung dieses Durchflußminimums existiert bisher nicht. Es läßt sich jedoch wenigstens qualitativ verhältnismäßig leicht verstehen, wenn man berücksichtigt, daß im Übergangsgebiet von der KNUDSENschen zur POISEUILLEschen Strömung beide Transportarten längs des betreffenden Strömungsweges *hintereinander* geschaltet sind. Das Druckgefälle $\Delta p/L$ für einen bestimmten Mengenstrom $\dot{n}$ nimmt bei POISEUILLE-Strömung nach Gl. (1) mit sinkendem Druck $\bar{p}$ zu. Bei kleinen Drucken wird es daher größer als das Druckgefälle der KNUDSEN-Strömung für den gleichen Mengenstrom, das nach Gl. (3) vom Druck unabhängig ist. Wenn von kleinen Drucken ausgehend sich in Teilen des Strömungsweges mit steigendem Gasdruck POISEUILLEsche Strömung anbahnt, sinkt der auf die Einheit des Druckgefälles bezogene Mengenstrom $\dot{n}/\Delta p$ daher zunächst unter den für reine KNUDSEN-Strömung geltenden Wert ab. Welcher Anteil des gesamten Strömungsweges bzw. Druckabfalls bei einem bestimmten mittleren Gasdruck noch reine KNUDSEN-Strömung enthält, und welcher bereits zur POISEUILLE-Strömung tendiert, hängt wesentlich von dem Verhältnis der m. f. W. bei diesem mittleren Gasdruck zum Kapillarenradius, Λ/r, ab.

Auf Grund dieser Vorstellung kommt man verhältnismäßig einfach zu der KNUDSENschen Beziehung (4). In Abb. 1a stelle $p\,(x)$ schematisch den Druckverlauf längs des Strömungsweges $0 \leq x \leq L$ dar, in dem am linken Ende praktisch reine POISEUILLE-Strömung, am rechten praktisch reine KNUDSEN-Strömung herrschen möge. Extrapoliert man den Druckverlauf von diesen beiden Enden her zur Mitte hin, so teilt der Schnittpunkt A den gesamten Strömungsweg L und den gesamten Druckabfall Δp in je zwei Summanden L_p und L_k bzw. $\Delta_p p$ und $\Delta_k p$, vgl. Abb. 1a. Vereinfachend wird nun angenommen, die POISEUILLE-Strömung erstrecke sich von $x = 0$ bis zum Punkte A ($x = L_p$) heran, von dort ab herrsche dann KNUDSEN-Strömung bis $x = L$. Im POISEUILLEschen Teil gilt dann für den die gesamte Strömungsstrecke L durchsetzenden Mengenstrom:

$$\dot{n} = a \cdot L \cdot \bar{p}_p \cdot \frac{\Delta_p p}{L_p} \,, \tag{9}$$

mit a nach Gl. (6) und $\bar{p}_p$ = mittlerer Gasdruck längs der Strömungsstrecke L_p in Abb. 1a. Im Knudsenschen Teil gilt für denselben Mengenstrom:

$$\dot{n} = b \cdot L \cdot \frac{\Delta_k p}{L_k}, \qquad (9a)$$

mit b nach Gl. (6a). Da nun $L_p/L + L_k/L = 1$ ist, folgt aus (9) und (9a)

$$\dot{n} = a \cdot \bar{p}_p \cdot \Delta_p p + b \cdot \Delta_k p$$

oder

$$\frac{\dot{n}}{\Delta p} = a\,\bar{p} \cdot \frac{\bar{p}_p}{\bar{p}} \cdot \frac{\Delta_p p}{\Delta p} + b \cdot \frac{\Delta_k p}{\Delta p}, \qquad (10)$$

worin jetzt $\bar{p}$ den über die gesamte Strömungsstrecke L gemittelten Gasdruck darstellt.

Wie bereits oben erwähnt, hängt die Einteilung des gesamten Druckabfalles in einen Poiseuilleschen und einen Knudsenschen Anteil vom Verhältnis Λ/r ab (Λ ist hier die m. f. W. beim Druck $\bar{p}$). Da $\Delta_p p/\Delta p$ für große Λ/r-Werte verschwindet, für kleine sich dem Wert 1 nähert, während $\Delta_k p/\Delta p$ sich gerade umgekehrt verhält, liegt hier der Ansatz:

$$\frac{\Delta_p p}{\Delta p} = \frac{1}{1 + \alpha\,\Lambda/r} \quad \text{und} \quad \frac{\Delta_k p}{\Delta p} = \frac{\alpha\,\Lambda/r}{1 + \alpha\,\Lambda/r}$$

nahe, in dem α eine empirische Konstante bedeutet. Der Faktor $\bar{p}_p/\bar{p}$ der mittleren Gasdrucke in Gl. (10) nimmt mit steigendem Λ/r (abnehmendem $\bar{p}$) von dem Wert 1 ausgehend zu. Ähnlich wie dieser Faktor verhält sich der Einfluß der Gleitung, die als druckunabhängiger Paralleltransport zur reinen Poiseuille-Strömung auch bei höheren mittleren Gasdrucken grundsätzlich zu berücksichtigen ist, vgl. Gl. (2). Beide Effekte können gemeinsam durch einen Faktor $(1 + \beta\,\Lambda/r)$ bei dem Poiseuille-Anteil in Gl. (10) berücksichtigt werden, in dem β eine zweite Konstante darstellt. Gl. (10) erhält hiermit die Gestalt:

$$\frac{\dot{n}}{\Delta p} = a\,\bar{p} \cdot \frac{1 + \beta\Lambda/r}{1 + \alpha\,\Lambda/r} + b \cdot \frac{\alpha\,\Lambda/r}{1 + \alpha\,\Lambda/r}. \qquad (10a)$$

Sie läßt sich leicht auf die Form:

$$\frac{\dot{n}}{\Delta p} = a\,\bar{p} + b \cdot \frac{1 + \dfrac{\beta - \alpha}{\alpha} \cdot \dfrac{a}{b} \cdot \bar{p}}{1 + r/\alpha\Lambda} \qquad (11)$$

bringen, die mit der Knudsenschen Beziehung (4) identisch ist. Durch Vergleich hiermit ergeben sich die Konstantenwerte zu: $\alpha = 0{,}322$ $(= 1/3{,}10)$ und $\beta = 5{,}80$, mit denen der Kurvenverlauf in Abb. 1 im gesamten Druckbereich gut wiedergegeben werden kann. Für $\Lambda \ll r$ geht Gl. (10) in die Form der Gl. (2) über, mit $4\,\xi = (\beta - \alpha) \cdot \Lambda$.

Das Minimum des Mengenstroms in Abb. 1 kommt nun dadurch zustande, daß bei geringen Drucken $a\,\bar{p} \ll b$ wird. Dies entspricht dem oben erwähnten Fall, daß die Poiseuille-Strömung bei kleinen Drukken für einen bestimmten Mengenstrom ein höheres Druckgefälle benötigt als die Knudsen-Strömung. Dadurch überwiegt bezüglich des Druckverlaufs in Gl. (11) der Nenner $(1 + r/\alpha\,\Lambda)$, der mit steigendem Druck zunimmt; d. h. der bezogene Mengenstrom $\dot{n}/\Delta p$ sinkt mit steigendem Druck, von $\bar{p} = 0$ ausgehend, zunächst unter den Grenzwert b ab, bevor er mit weiter wachsendem Druck infolge der Zunahme des Gliedes $a\,\bar{p}$ wieder ansteigt*. Im Durchflußminimum selbst ist $a\,\bar{p} = 0{,}049\,b$, wie sich aus den Gln. (8) und (11) ergibt.

Bei der Strömung durch einen Spalt zwischen parallelen Platten (Länge groß gegen m. f. W.) tritt ebenfalls ein Durchflußminimum auf, wie W. Gaede** feststellte, dagegen nicht bei Strömung durch Blenden. In letzterem Falle (Strömungsweg kurz gegen m. f. W.) können sich im Übergangsgebiet die beiden Transportarten nicht in der hier angegebenen Weise überlagern.

* Dies führt zu der gaskinetischen Vorstellung, daß bei den ersten Zusammenstößen der Molekeln im Gasraum mit steigendem Druck, solange deren Zahl noch klein ist gegenüber derjenigen der Wandstöße, zunächst die *Rückstreuung* überwiegt, ähnlich wie bei im Strömungsweg angebrachten Hindernissen. Erst wenn die Zahl der Gasstöße vergleichbar wird mit derjenigen der Wandstöße, überwiegt die sich gleichzeitig anbahnende *gerichtete Bewegung* im Sinne einer hydrodynamischen Strömung, auf Grund deren dann der Durchfluß mit wachsendem Druck wieder ansteigt.

Zusatz bei der Korrektur: Während der Drucklegung erschienen zwei Arbeiten von J. W. Hiby und M. Pahl, Z. Naturforschg. 1952 **7a** 533, 542, in denen der hemmende Einfluß dieser Rückstreuung unter der vereinfachenden Annahme $\Lambda p \ll \bar{p}$ theoretisch behandelt wird (auf Grund einer früher abgeleiteten Streufunktion für Zweierstöße, J. W. Hiby und M. Pahl, Z. Physik 1951 **129** 517, **130** 348 und im Anschluß an die Diffusionstheorie von W. G. Pollard und R. D. Present, Physic. Rev. 1948 **73** 762). Für kreisrunde Kapillaren und ebene Spalte ergibt sich die Abnahme des Megenstroms mit steigendem Mitteldruck links des Minimums in Abb. 1 in Übereinstimmung mit den Meßwerten von Knudsen und Gaede. Die Theorie beschränkt sich auf den Druckbereich, in dem die m. f. W. noch groß ist gegen den Kapillarenradius ($\Lambda \gtrsim 20\,r$) bzw. den Plattenabstand des Spaltes, das eigentliche Übergangsgebiet mit dem Durchsatzminimum wird von ihr nicht erfaßt. Für Lochblenden ergibt sich (unter den Voraussetzungen $\Delta p \ll \bar{p}$, $\Lambda \gg r$) in Übereinstimmung mit der Erfahrung eine stetige Zunahme des Durchsatzes mit steigendem Mitteldruck, was auch noch für kurze Kapillarenstücke gilt; erst oberhalb $L \approx 8r$ liefert die Theorie eine Durchsatzverminderung mit steigendem $\bar{p}$. Im Anschluß hieran führen die Autoren das Fehlen eines Durchsatzminimums bei der Durchströmung poröser Medien darauf zurück, daß in diesem Falle $\Delta L < 8\,r$ gelten dürfte, wenn man unter ΔL die geradlinige Strecke eines Porenstückes zwischen zwei Knicken versteht.

** W. Gaede, Ann. Phys. 1913 (4) **41** 289. Der Autor vermutete als Ursache des Durchflußminimums eine an den Platten haftende Gashaut.

c) *Grundsätzliches zur Strömung durch poröse Substanzen*

Wesentlich schwieriger ist der Gastransport durch poröse Substanzen zu erfassen. Es liegt in der Struktur dieser Körper, daß die Porenradien und -längen oft um Zehnerpotenzen streuen. Immerhin läßt sich aus Messungen des Gasdurchflusses bei verhältnismäßig hohen und bei sehr kleinen mittleren Drucken ein für manche Zwecke nützlicher *Mittelwert des Porenradius* erhalten. Mißt man bei zwei Werten $\bar{p}_1$ und $\bar{p}_2$ höherer Gasdrucke den Durchsatz $\dot{n}_1$ und $\dot{n}_2$ bei gleicher Druckdifferenz Δp, was einer Bestimmung der Neigung der nach rechts auslaufenden Geraden in Abb. 1 entspricht, so läßt sich durch zweimalige Anwendung der Gl. (2) der Gleitungsanteil in erster Näherung eliminieren:

$$\frac{\dot{n}_1 - \dot{n}_2}{\Delta p} = \frac{\pi \cdot (\bar{p}_1 - \bar{p}_2)}{8 \eta R T} \cdot \sum_i Z_i \cdot \frac{r_i^4}{L_i}$$

(Z_i = Zahl der Poren mit dem Radius r_i und der Länge L_i.)

Kombiniert man diese beiden Messungen mit einer dritten, die bei sehr kleinen Drucken im Gültigkeitsbereich der Gl. (3) durchzuführen ist (Druckdifferenz $\Delta_k p$, Mengenstrom $\dot{n}_k$), so erhält man den erwähnten Mittelwert des Porenradius zu:

$$\left.\begin{aligned} &\sum_i Z_i \cdot \frac{r_i^4}{L_i} \Big/ \sum_i Z_i \cdot \frac{r_i^3}{L_i} = \bar{r} \\ &= \frac{16}{3} \eta \cdot \frac{\overline{w}}{\bar{p}_1 - \bar{p}_2} \cdot \frac{\dot{n}_1 - \dot{n}_2}{\Delta p} \cdot \frac{\Delta_k p}{\dot{n}_k} \end{aligned}\right| \qquad (12)$$

Bei mittleren Drucken tritt im allgemeinen laminare Schichtenströmung nach Hagen-Poiseuille, Gleitung, Knudsensche Molekularströmung und gegebenenfalls Oberflächendiffusion an den Porenwandungen zum Teil nebeneinander auf, zum Teil gehen diese verschiedenen Transportarten in verschiedenen Abschnitten einer Pore ineinander über. Was hierbei als höherer, mittlerer oder kleiner Gasdruck anzusprechen ist, hängt weitgehend von dem speziellen Charakter des betreffenden Porengefüges ab. Es kommt hier vor allem auf die Größenordnung des Verhältnisses der m. f. W. zum mittleren Porenradius an, wobei man letzteren etwa aus Gl. (12) oder einer anderen geeigneten Mittelwertsbildung erhalten kann.

In der vorliegenden Arbeit wurden daher die Strömungsverhältnisse in porösen Substanzen nach folgenden Punkten untersucht:

1. Anteil und Einfluß der Gleitung am Gesamttransport bei $\Lambda < \bar{r}$.

2. Druckabhängigkeit des Gesamttransportes bei kleinen Drucken ($\Lambda > \bar{r}$).

3. Einfluß der Temperaturabhängigkeit der m. f. W.

4. Voraussetzungen für einen merkbaren Anteil der Oberflächendiffusion am gesamten Strömungstransport.

d) *Apparatur und Versuchsführung*

Die zur Klärung dieser Fragen benutzte Apparatur war verhältnismäßig einfach, vgl. Abb. 2. Sie bestand im wesentlichen aus zwei auswechselbaren Glaskolben A_1 und A_2, die über ein Leitungssystem und das Strömungsgefäß S miteinander verbunden waren. Verschiedene Vorratsbehälter V enthielten die vorgereinigten Versuchsgase. Als poröse Substanz diente einmal eine Jenaer Glasfritte der Sorte G4 (4,1 mm ⌀, 2 mm stark), deren mittlerer Porenradius mit Hilfe von Gl. (12) zu $2{,}2 \cdot 10^{-4}$ cm bestimmt wurde (Katalogangaben 4,5 bis $7{,}5 \cdot 10^{-4}$ cm). Bei den Messungen mit diesem Filter betrugen die Volumina der Kolben A_1 und A_2 je etwa 6 l. Eine zweite poröse Probe bestand aus feinteiligem Nickelpulver, das aus Nickeloxyd durch vorsichtige Reduktion mit H_2 bei 280°C gewonnen und mit 5000 atm zu einem kleinen Zylinder von 8 mm ⌀ und 8,5 mm Höhe gepreßt worden war. Dieser Preßzylinder mit einer scheinbaren Dichte von 5,0 g/cm³ wurde in das Ende eines Glasrohres eingekittet (an der Stelle F in Abb. 2); für den mittleren Porenradius ergab sich nach der oben geschilderten Methode mit Hilfe von Gl. (12): $\bar{r} = 3{,}0 \cdot 10^{-4}$ cm. In diesem Falle war es zweckmäßig, die Kolben A_1 und A_2 der Meßapparatur (Abb. 2) nur je einen Liter groß zu wählen.

Die Geschwindigkeit der Gasströmung durch die porösen Fritten bzw. Filter wurde durch Verfolgung des Druckausgleichs zwischen den Kolben A_1 und A_2 instationär gemessen. Eine anfänglich am Manometer D (Abb. 2) eingestellte Druckdifferenz Δp_0 setzt eine Ausgleichsströmung in Gang, die mit abnehmender Druckdifferenz dieser proportional abklingt:

$$\dot{n}/\Delta p = -\frac{V_1 V_2}{V_1 + V_2} \cdot \frac{1}{RT} \cdot \frac{1}{\Delta p} \cdot \frac{d(\Delta p)}{dt} = f(\bar{p}, T). \qquad (13)$$

Hierin bedeuten V_1 und V_2 die Volumina der Kolben A_1 und A_2 einschließlich der Rohrleitungen bis zur Strömungsfritte bei F in Abb. 2. Die Größe $f(\bar{p}, T)$ vom Charakter eines Strömungsleitwertes der betreffenden porösen Fritte ist während einer Einzelmessung des Ausgleichsvorganges natürlich konstant, im übrigen abhängig von der Art der Strömungsfritte

VOL. 1 1952

und des Gases sowie vom mittleren Gasdruck und der Temperatur innerhalb des durchströmten Porengefüges. Wird die zur Zeit t gemessene Druckdifferenz $\Delta p(t)$ in der Form $\ln \Delta p(t)/\Delta p_0$ gegen die Zeit t aufgetragen, so erhält man eine Gerade, deren Neigung den Wert von $1/\Delta p \cdot d(\Delta p)/dt$ angibt, der zur Ermittlung des auf $\Delta p = 1$ Torr bezogenen Mengenstroms $\dot{n}/\Delta p$ in Gl. (13) einzusetzen ist.

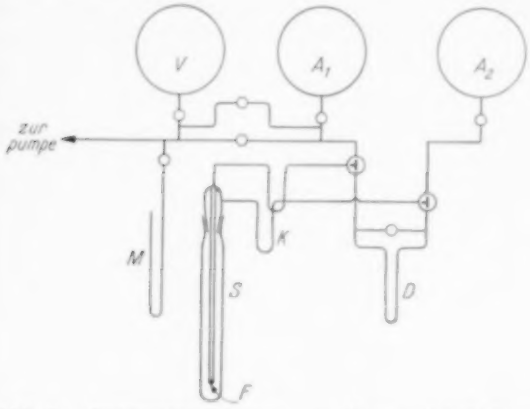

Abb. 2. Strömungsapparatur. V Gasvorratsbehälter; A_1, A_2 Meßkolben; M Manometer für Absolutdrucke; S Strömungsgefäß mit F poröser Probe (Glasfilterfritte oder eingekitteter Preßzylinder aus Ni-Pulver); K Kühlfallen; D Differentialmanometer.

2. Messergebnisse und Auswertung

a) Einfluß der Gleitung auf den Gesamttransport bei $\Lambda < \bar{r}$

Die mit dem Ni-Preßzylinder und dem Jenaer Filter G 4 bei 0° C mit H_2 bzw. N_2 zwischen Atmosphärendruck und 2,5 Torr gemessenen Gasdurchsätze sind in Abb. 3 und 4 dargestellt, und zwar die Größe $\dot{n}/\Delta p = f(\bar{p}, T)$, Gl. (13), gegen den mittleren Gasdruck $\bar{p}$. Nach der Hagen-Poiseuilleschen Gl. (1) sollte die Extrapolation der bei höheren Drucken gemessenen Gerade auf $\bar{p} \to 0$ durch den Koordinatenanfangspunkt gehen. Das Ausmaß der Abweichung von dieser Bedingung zeigt den erheblichen Einfluß der Gleitung an, die nach Gl. (2) für eine Beschreibung der experimentellen Werte herangezogen werden muß.

Das Wort Gleitungs-„Korrektur", das man häufig in der Literatur findet, sei hier absichtlich vermieden. Wie bereits oben betont, handelt es sich bei Porenradien von 10^{-4} cm und kleiner keineswegs um eine Korrekturgröße, sondern um einen Strömungsanteil, der durchaus die Größenordnung des Gesamttransportes bei Atmosphärendruck erreichen kann.

Besonders interessant ist in diesem Zusammenhang eine Untersuchung von W. Brötz und H. Spengler [3], in der die Strömung einer Reihe von Gasen durch eine Probe eines feinporigen technischen Fischer-Tropsch-Katalysators bei $\bar{p} = 350$ Torr gemessen wurde. Tabelle 1 zeigt in den Spalten 1—4 die unter

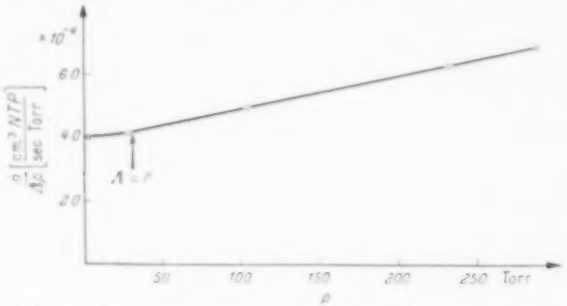

Abb. 3. Strömung von Wasserstoff bei 0° C durch den Ni-Preßzylinder ($\bar{r} = 3{,}0 \cdot 10^{-4}$ cm).

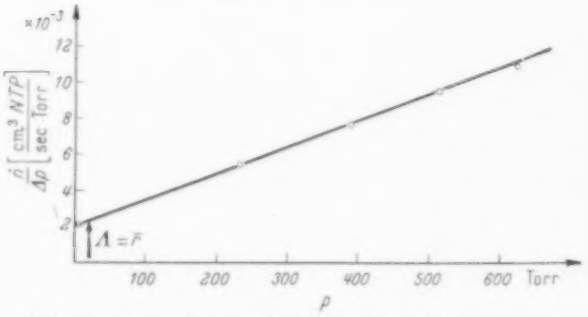

Abb. 4. Strömung von Stickstoff bei 0° C durch die Glasfritte ($\bar{r} = 2{,}2 \cdot 10^{-4}$ cm).

Anwendung von Gl. (1) für reine Poiseuille-Strömung gewonnenen Ergebnisse. Die zunächst unerwartete Streuung der Werte des Ausdrucks $\frac{\dot{n}}{\Delta p} \cdot \eta$

Tabelle 1. Einfluß der Gleitung auf die Strömung verschiedener Gase durch eine poröse Katalysatorprobe bei $\bar{p} = 350$ Torr nach Messungen von Brötz *und* Spengler

1	*2*	*3*	*4*	*5*	*6*
Meßgas	$\frac{\dot{n}}{\Delta p} 10^{11}$ $\frac{\text{mol}}{\text{sec dyn/cm}^2}$	$\eta \cdot 10^6$ *Poise*	$\frac{\dot{n}}{\Delta p} \eta\, 10^{15}$	$1 + 4\frac{\xi}{r}$	$\frac{\dot{n}}{\Delta p} \cdot \eta \cdot 10^{15} : 1 + 4\frac{\xi}{r}$
CH_4	2,34	108	2,52	2,38	1,06
N_2	1,55	175	2,71	2,69	1,01
NH_3	2,56	100	2,56	2,24	1,14
CO_2	1,52	145	2,20	2,11	1,04
H_2	4,82	88	4,23	4,18	1,01
CO	1,67	177	2,96	2,71	1,09

in Spalte 4, der nach Gl. (1) für jedes Meßgas derselbe sein sollte, erweist sich als spezifischer Einfluß der Gleitung. Berücksichtigt man diese durch den in Spalte 5 angegebenen Gleitungsfaktor nach Gl. (2), so ergeben sich die in Spalte 6 verzeichneten Werte, die nun in der Tat als von der Natur des Meßgases unabhängig angesehen werden können.

Zur Berechnung des Gleitungsfaktors wurde hierbei ein mittlerer Porenradius von $\bar{r} = 4{,}50 \cdot 10^{-5}$ cm gewählt, den man aus den Angaben der Autoren durch Anwendung von Gl. (12) erhält. Für den Gleitungskoeffizienten wurde nach Gl. (2c): $\xi = 1{\cdot}37\,\Lambda$ gesetzt. Die Werte für die m. f. W. bei 20° C und $\bar{p} = 350$ Torr wurden aus den in Spalte 3 angegebenen Zähigkeiten nach Gl. (7) berechnet.

b) *Druckabhängigkeit des Gesamttransportes bei kleinen Drucken* ($\Lambda > \bar{r}$)

Der experimentelle Befund für die untersuchten Proben ist bereits in den Abb. 3 und 4 enthalten. Die

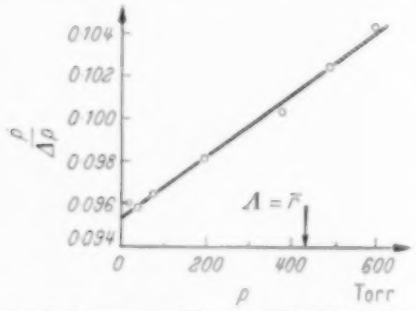

Abb. 5. Strömung von Wasserstoff bei 20° C durch einen Preßling aus Al_2O_3-Pulver ($\bar{r} = 2 \cdot 10^{-5}$ cm) nach CARMAN [4].

dort eingezeichneten Pfeile geben an, bei welchem Druck die m. f. W. gleich ist dem nach Gl. (12) berechneten mittleren Porenradius. Bei dem Ni-Preßzylinder nimmt in der Umgebung dieses Punktes die Neigung der gemessenen Kurve deutlich ab, ein Durchflußminimum wie bei einzelnen durchströmten Kapillaren (Abb. 1) wurde jedoch in keinem Falle beobachtet. P. C. CARMAN [4] stellte bei Untersuchungen über die Strömung von H_2 durch Preßlinge aus feinteiligem Al_2O_3-Pulver fest, daß die im Gebiet höherer Drucke gemessene Gerade in einzelnen Fällen die Meßpunkte bis zu niedrigen Drucken ($\Lambda \gg \bar{r}$) herunter ohne merkbares Abknicken wiedergibt, vgl. Abb. 5.

Bei porösen Stoffen bietet somit die Proportionalität des Strömungsdurchsatzes zum mittleren Druck keine Gewähr dafür, daß es sich um reine POISEUILLE-Strömung handelt. Vielmehr kann hier durchaus eine scheinbare Druckabhängigkeit der KNUDSEN-Strömung ohne Minimum vorliegen, hervorgerufen durch die Überlagerung der verschiedenen hintereinander- und parallelgeschalteten Porenweiten innerhalb der betreffenden Strömungsfritte. Überlagert man z. B. mit Hilfe der KNUDSENschen Beziehung (4) die Strömung durch zwei zylindrische, parallel verlaufende Porensorten, die sich im Radius um eine Zehnerpotenz unterscheiden, so kann im Gesamtdurchsatz das bei der engeren Porensorte auftretende Minimum verschwinden, vgl. Abb. 6.

c) *Einfluß der Temperaturabhängigkeit der m. f. W. Glasfritte G 4* — Die Messungen wurden bei einem mittleren Druck von 3 Torr durchgeführt, dem eine

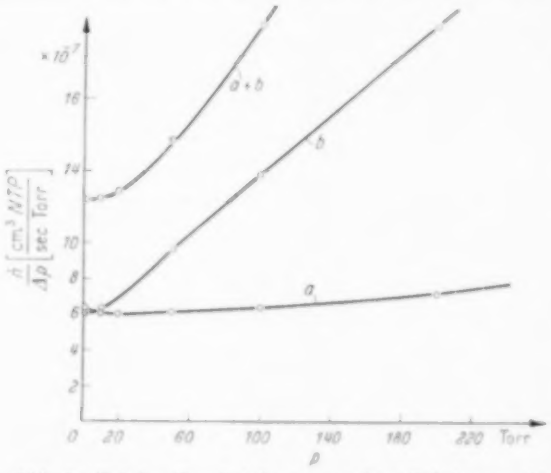

Abb. 6. Bei der Durchströmung poröser Substanzen, in denen Poren verschiedener Weite einander parallel geschaltet sind, kann das von KNUDSEN in einzelnen Kapillaren bei $\Lambda \approx 3r$ festgestellte Durchflußminimum verschwinden. Kurve a: Durchfluß je Einheit des Druckgefälles von H_2 bei einem Gesamtdruck von 760 Torr und 0° C durch 1000 Kapillaren vom Radius 10^{-4} cm und der Länge $L = 1$ cm. Kurve b: Durchfluß durch eine Kapillare vom Radius 10^{-3} cm unter denselben Bedingungen. Kurve $a + b$: Gesamtdurchfluß bei Parallelschaltung beider Porenarten (berechnet mittels Gl. (4)].

m. f. W. von 1 bis $2 \cdot 10^{-3}$ cm der verwendeten Gase entsprach. Tabelle 2 enthält die Ergebnisse der Versuche bei 0° C:

Tabelle 2. Gasströmung durch Glasfritte G 4 bei 0° C und $\bar{p} = 3$ Torr ($\dot{n}_k/\Delta p$ in $cm^3\,NTP/sec\,Torr$)

Gas	$\dot{n}_k/\Delta p \cdot 10^9$	$\dot{n}_k/\Delta p \cdot \sqrt{M}$
H_2	7,54	0,01068
N_2	2,04	0,01080
CH_4	2,68	0,01071
C_4H_{10}	1,46	0,01112

Die Werte der ersten drei Gase passen sich im zulässigen Fehlerbereich der $\sqrt{M}$-Beziehung nach Gl. (3a) an. Aus dem Mittelwert von $(\dot{n}/\Delta p)\cdot\sqrt{M} = 0{,}01073$ ergibt sich dagegen für Butan ein Überschußtransport von 3,8%. WICKE und VOIGT* fanden bei diesem Gas unter Verwendung einer Glasfritte G 5 einen Überschußtransport von 5,3% bei 0° C.

Die Messungen wurden sodann auf ein größeres Temperaturintervall ausgedehnt, um die Abhängigkeit von dem Faktor $\sqrt{MT}$ in Gl. (3a) näher zu prüfen. Wie die in Abb. 7 eingetragenen Meßpunkte zeigen, wurde auch bei N_2 und CH_4 ein mit sinkender Temperatur ansteigender Überschußtransport im Sinne einer Abweichung von der $\sqrt{MT}$-Beziehung festgestellt.

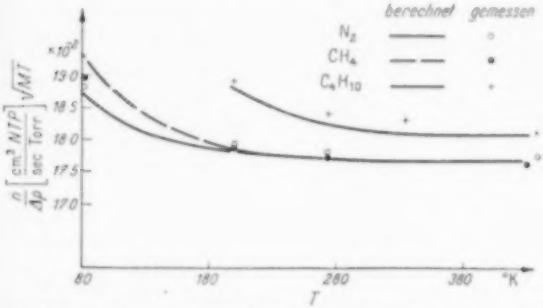

Abb. 7. Temperaturabhängigkeit des Gastransportes durch die Glasfritte, bezogen auf die $\sqrt{MT}$-Beziehung (3a) bei $\bar{p} = 3$ Torr.

Ni-*Preßzylinder* — Bei dem gepreßten Ni-Pulver betrug die m. f. W. der Meßgase bei 0° C und dem gewählten mittleren Gasdruck von 3 Torr ebenfalls noch etwa das Zehnfache des durchschnittlichen Porenradius ($3\cdot 10^{-4}$ cm). In Abb. 8 sind die erhaltenen Meßpunkte eingetragen. Hiernach ist bei tiefen Temperaturen das Produkt $\dot{n}_L/\Delta p\cdot\sqrt{MT}$ auch in diesem Falle nicht konstant, sondern steigt zum Teil erheblich an, beim CH_4 z. B. bei der Temperatur flüssiger Luft um etwa 50% gegenüber 0° C, beim H_2 um etwa 10%.

Diese Zunahme des Strömungsdurchsatzes mit sinkender Temperatur läßt sich in allen hier gemessenen Fällen quantitativ wiedergeben, wenn man die Temperaturabhängigkeit der m. f. W. der betreffenden Gase berücksichtigt. Man stellt sich hierzu zweckmäßig die poröse Fritte in vereinfachender Weise als ein System von Z parallel geschalteten Poren vom gleichen Radius r und der Länge L vor und wendet auf dieses System die vollständige KNUDSENsche Beziehung (4) bzw. Gl. (1) an. Zur unmittelbaren Wiedergabe der Meßwerte bringt man die Gleichung zweckmäßigerweise auf die Form:

$$\left.\begin{aligned}\sqrt{M\,T}\cdot\dot{n}/\Delta p = 520\cdot Z\,r^3/L\,\times\\ \times\left(k\cdot r/\Lambda + 21\cdot\frac{1+0{,}81\cdot kr/\Lambda}{1+kr/\Lambda}\right),\end{aligned}\right\}\qquad(14)$$

in der die Zahlenwerte so gewählt sind, daß $\dot{n}/\Delta p$ den Gasdurchsatz in cm³ NTP je Torr Druckdifferenz und

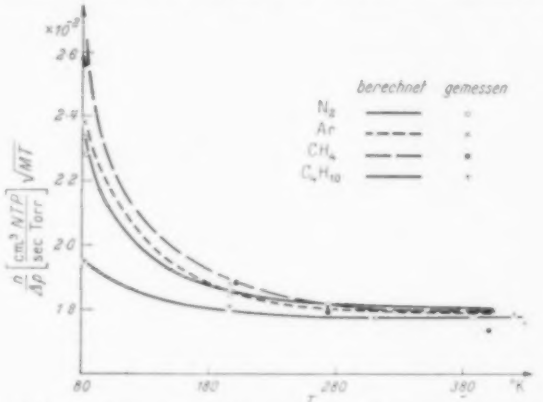

Abb. 8. Temperaturabhängigkeit des Gastransportes durch den Ni-Preßzylinder, bezogen auf die $\sqrt{MT}$-Beziehung (3a) bei $\bar{p} = 3$ Torr.

Sekunde bedeutet. Die Gleichung enthält zwei von der Gasart und der Temperatur unabhängige Konstanten: den Faktor $Z\,r^3/L$ vor der Klammer und die Größe $k\cdot r$, die den Einfluß des ausschlaggebenden Ausdrucks in der Klammer wesentlich bestimmt. Durch Anpassung an die in Abb. 7 und 8 angegebenen Meßpunkte ergaben sich für diese Konstanten bei der Glasfritte G 4 bzw. dem Ni-Preßzylinder die empirischen Werte: $Z\,r^3/L = 1{,}7\cdot 10^{-5}$ cm² bzw. $1{,}73\times 10^{-6}$ cm²; $k\cdot r = 1{,}0\cdot 10^{-3}$ bzw. $2{,}3\cdot 10^{-3}$ cm. Die zur Berechnung der m. f. W. erforderlichen Stoßquerschnitte der Gasmolekeln wurden dem LANDOLT-BÖRNSTEIN, 6. Aufl., Bd. I/1 (1950) entnommen. In Tabelle 3 sind die gaskinetischen Durchmesser der betreffenden Gase zusammengestellt, ferner die SUTHERLAND-Konstanten für den interessierenden Temperaturbereich zwischen 90° und 273° abs. sowie die daraus berechneten m. f. W.

Die ausgezogenen Kurven in den Abb. 7 und 8 sind mit den oben angegebenen Werten nach Gl. (14) berechnet worden. Der mit sinkender Temperatur ansteigende „Überschußtransport" der Gase wird

* E. WICKE und H. VOIGT, Angew. Chem. (B) 1947 **19** 94. Dort wurde dieser Zusatztransport für Oberflächendiffusion gehalten. Wie die nachfolgende Diskussion zeigt, beruht er dagegen tatsächlich auf einer Verschiebung zwischen KNUDSEN- und POISEUILLE-Anteil, hervorgerufen durch die Änderung der m. f. W. mit der Temperatur.

Tabelle 3. Gaskinetische Durchmesser (in 10^{-8} cm), SUTHERLAND-Konstanten und mittlere freie Weglängen bei $p = 3$ Torr (in 10^{-4} cm)

	$\sigma(90)$	$\sigma(273)$	$\sigma(572)$	C °K	$\Lambda(90)$	$\Lambda(273)$	$\Lambda(572)$
H_2	3,06	2,75	2,58	36,4	7,45	28,8	66,3
N_2	4,65	3,78	3,51	91,8	3,23	14,8	36,0
CH_4	5,31	4,18	3,80	118,2	2,47	12,0	30,6
Ar	4,70	3,66	3,34	127,2	3,15	15,85	39,7
C_4H_{10}	6,92[1]	6,71[2]	6,41[3]	280,0[4]	4,75[1]	5,70[2]	7,4[3]

[1] $T = 273$ °K; [2] $T = 333$° K; [3] $T = 397$° K; [4] zwischen 273 und 393° K.

hierdurch sehr gut wiedergegeben und eindeutig geklärt: Bei höheren Temperaturen sind die m. f. W. noch so groß, daß die Beziehung $\dot{n}\sqrt{MT} = \text{const}$ mit guter Näherung gilt (für Butan erst oberhalb des hier überschrittenen Temperaturbereichs zu erwarten). Infolge der erheblichen Zunahme der Wirkungsquerschnitte und Abnahme der m. f. W. nimmt der Gastransport mit sinkender Temperatur jedoch gerade in den Poren mit größeren Querschnitten immer mehr den Charakter einer POISEUILLE-Strömung an, die den in Abb. 7 und 8 gezeigten Anstieg des gesamten Gasdurchsatzes hervorruft.

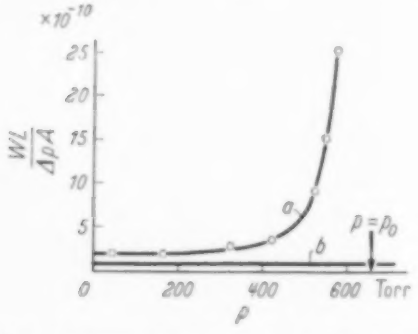

Abb. 9. Strömung von CF_2Cl_2 durch Linde-Silica in Abhängigkeit vom Druck bei −33° C nach CARMAN und MALHERBE *loc. cit.* W Gasstrom in millimol/sec; Δp Druckdifferenz in Torr; L Probendicke in cm; A Probenquerschnitt in cm².

d) *Voraussetzungen für einen merkbaren Anteil der Oberflächendiffusion am gesamten Strömungstransport*

In allen vorangehend besprochenen Meßergebnissen konnten die Abweichungen von dem erwarteten Strömungstransport durch gaskinetische Überlegungen befriedigend erfaßt werden. Ein Einfluß von Oberflächendiffusion trat bei der direkten, von einer Druckdifferenz hervorgerufenen Gasströmung nicht in meßbarer Größenordnung auf. Im Zusammenhang hiermit sind Untersuchungen von CARMAN und MALHERBE [5] von Interesse, in denen Oberflächendiffusion unter Anwendung der Strömungsmethode nachgewiesen werden konnte. Als bestes Beispiel seien die Messungen dieser Autoren an Linde-Silica II bei −33° C angeführt, vgl. Abb. 9 (innere Oberfläche etwa 600 m²/cm³, mittlerer Porenradius etwa 10^{-6} cm).

Als Gas wurde CF_2Cl_2 verwendet, dessen Sättigungsdruck bei der Versuchstemperatur 660 Torr beträgt. Die Kurve a in Abb. 9 gibt den gemessenen Durchsatz des CF_2Cl_2 an. Die Kurve b, die den Anteil der reinen KNUDSEN-Strömung darstellt, beruht auf Strömungsmessungen mit Luft, die mit Hilfe der Molmassen nach Gl. (3a) auf CF_2Cl_2 umgerechnet wurden. Die Differenz zwischen a und b interpretierte CARMAN als Oberflächendiffusion, was qualitativ sicher zutreffen dürfte. In quantitativer Hinsicht ist allerdings zu bemerken, daß ein Teil des mit steigendem Druck auftretenden Zusatztransportes auf ähnliche Ursachen zurückzuführen sein könnte wie der in Abb. 7 und 8 gezeigte Transportanstieg mit sinkender Temperatur. Mit steigendem Druck sinkt die m. f. W. ab und damit nimmt ein Teil des Gastransportes, insbesondere in den weiteren Poren, den Charakter von POISEUILLE-Strömung an, was i. a. bereits einen Zusatztransport hervorruft. Es liegt daher nahe, anzunehmen, daß der steile Ansteig in Abb. 9 zum Teil durch Einflüsse dieser Art verursacht wird. Dies würde zugleich erklären, weshalb der gesamte Zusatztransport schneller als proportional dem Oberflächen-Konzentrationsgradienten ansteigt, was CARMAN als unerwartetes Ergebnis besonders betont.

Wie aus diesen Versuchen folgt, kann die Oberflächendiffusion bei der direkten Durchströmung eines porösen Körpers dann einen meßbaren Transportanteil liefern, wenn die innere Oberfläche von der Größenordnung 100 m²/cm³ poröser Substanz oder größer ist, was mittleren Porenradien von der Größenordnung 10^{-6} cm oder darunter entspricht. Ferner ist es hierfür günstig, wenn der mittlere Druck in der Nähe des Sättigungsdruckes des Versuchsgases liegt, damit die innere Oberfläche eine hohe Adsorptionsbelegungsdichte, möglichst in mehreren Molekellagen, aufweist. Dann wird der dem Druckgradienten im Gasraum entsprechende Gradient der Oberflächenkonzentration sehr hoch, und es kann unter Umständen eine flüssigkeitsähnliche Adsorptionsschicht gleichsam „fließen", was den Gesamtdurchsatz dann wesentlich erhöht.

Solche Verhältnisse lagen bei den hier untersuchten Glasfritten und Ni-Preßlingen in keinem Falle vor.

Der eine von uns dankt der Ruhrchemie AG., Oberhausen-Holten, für eine finanzielle Beihilfe, die ihm die Durchführung voranstehender Untersuchungen im Rahmen seiner Dissertation ermöglichte.

Zusammenstellung der Formelzeichen

C = Sutherland-Konstante °K
i = Index für verschiedene Porensorten
k = Index für Knudsen-Strömung
L = Länge der Strömungsstrecke; cm
M = Molmasse; g/mol
$\dot{n}$ = Gasmengenstrom; mol/sec
(1 cm³ NTP/sec = 1/22415 mol/sec)
N = Partikelzahldichte; cm^{-3}
p, $\bar{p}$, Δp = Druck, mittlerer Druck, Druckdifferenz; dyn/cm^2 (1 Torr = 1333 dyn/cm^2)
p = Index für Poiseuille-Strömung
r, $\bar{r}$ = Kapillarenradius, mittlerer Porenradius; cm
R = allgemeine Gaskonstante = $8{,}315 \cdot 10^7$ $\frac{dyn \cdot cm}{mol \cdot °K}$
t = Zeit; sec
T = absolute Temperatur; °K
$\bar{w}$ = mittlere Molekulargeschwindigkeit; cm/sec
Z = Porenzahl
α, β = Konstanten
η = Gaszähigkeit; $\frac{g}{cm\,sec}$ = Poise
ξ = Gleitungskoeffizient (Gl. 2); cm
Λ = mittlere freie Weglänge [Gl. (7a)]; cm
σ = gaskinetischer Stoßdurchmesser [Gl. (7a)]; cm

Literaturverzeichnis

[1] Kundt, A. und Warburg, E.; Pogg. Ann. 1875 **155** 337, 525. [2] Knudsen, M.; Ann. Phys. 1909 **28** 75; 1911 **35** 389. Vgl. auch Knudsen, M.; Kinetic Theory of Gases, London 1950. [3] Brötz, W. und Spengler, H.; Brennstoffchemie 1950 **7/8** 97. [4] Carman, P. C.; Proc. Roy. Soc. London A 1950 **203** 55. [5] Carman, P. C. und Malherbe, P.; Proc. Roy. Soc. London A 1950 **203** 172.

Book reviews

Walter G. Berl (Editor); **Physical Methods in Chemical Analysis,** Vol. I. Academic Press Inc., Publishers, New York 1950. 664 pp. Price $ 12·00

La publication d'une encyclopédie sur les méthodes physiques applicables à l'analyse chimique répond à un besoin certain, mais la rédaction d'une pareille encyclopédie risque d'échouer devant l'énormité de la tâche, en se perdant dans les détails, ou de ne donner que des notions pratiquement inutilisables sur les méthodes physiques s'appliquant à l'analyse chimique moderne. Les douze chapitres qui forment le volume I répondent d'une façon très satisfaisante à l'objet d'une pareille encyclopédie et fournissent une revue à jour des progrès actuels sans chercher à rivaliser avec des monographies consacrées à chacun des sujets.

Les trois premiers chapitres dûs à G. L. Clark, W. L. Davidson, J. Howsmon traitent des applications des rayons X soit aux phénomènes d'absorption, soit aux phénomènes de diffraction, dans le cas des poudres, métaux ou fibres. Nous avons particulièrement apprécié les pages traitant de l'application des rayons X à l'étude des propriétés physiques (duretés propriétés magnétiques et déformation).

Un chapitre sur la diffraction électronique par L. O. Brockway est plus bref, tout en restant très clair.

Les chapitres sur l'analyse spectrale avec ses diverses branches: spectrophotographie et colorimétrie par W. R. Brode, spectrographie d'émission par J. Sherman, spectroscopie infra-rouge par H. H. Nielsen et Robert A. Oetjen, spectres Raman par J. H. Hibben, condensent d'une façon remarquablement heureuse l'ensemble de ce qu'il faut savoir pour appliquer le spectrographe à l'immense variété des problèmes analytiques qu'il permet de résoudre.

Il reste évidemment moins de place pour des chapitres plus classiques tels que les applications de la lumière polarisée par C. D. West et de la réfractométrie par L. W. Tilton et J. K. Taylor. Mais les 110 pages qui sont consacrées à ces deux branches de l'optique, appliquées depuis longtemps à l'analyse chimique, sont excellentes.

R. D. Heidenreich consacre 50 pages à la microscopie électronique. Elles permettront de s erendre compte des ressources de ce nouveau moyen d'investigation. Mais il serait déraisonnable d'espérer qu'elles suffisent à former les opérateurs auxquels l'on confierait un microscope électronique.

Nous ferons la même remarque sur les chapitres consacrés à la spectrométrie de masse par H. W. Washburn. Ce chapitre donne une idée parfaitement précise de ce que l'on peut attendre de la spectrométrie de masse pour l'analyse des substances complexes.

Le premier volume de la collection doit être particulièrement apprécié par les directeurs de recherches qui tiennent à être tenus au courant des ressources que peuvent leur apporter les méthodes les plus modernes de la physique pour la solution des problèmes analytiques. J. Cathala

W. Jost; **Diffusion in Solids, Liquids, Gases.** Academic Press Inc., Publishers, New York, 1952. 558 pp. Price $ 12·00.

Many readers will remember an earlier book by the same author under the title "Diffusion und Chemische Reaktionen in festen Stoffen", which appeared in 1937. Rather than prepare a second edition of this, Professor Jost has preferred to "treat diffusion processes on a broader basis and to neglect the subject of chemical reaction in solids entirely, except for such cases that could be described in terms of diffusion processes". The result is the present volume.

The first chapter is on the fundamental laws of diffusion and contains an extensive and very useful collection of solutions to the Fick diffusion equation covering most of the experimental conditions met with in practice. This includes solutions not previously published for diffusion in systems containing more than one phase, (in the metallographic sense) a case of considerable importance in industrial practice.

The second chapter describes and gives the theory of the various types of structural defects in solids, particularly those which are responsible for diffusion and ionic conductivity

in solids. This is followed by one on the general theory of diffusion and conductivity processes themselves.

The next two chapters deal at some length with electrolytic conduction and diffusion in ionic crystals and with diffusion in metals and non-polar crystals respectively. Accounts are given of the experimental methods of investigation and, as in all the chapters of the book dealing with the more experimental aspects of the subject, a very large number of numerical results are quoted.

A chapter on solubility, particularly of gases in solids, paves the way for Chapter VII, which is on the permeation and diffusion of gases in solids.

Chapter VIII deals with the electrolytic mobility of ions in solid and molten metals and alloys.

Chapter IX is devoted to surface reactions of metals which involve diffusion such as the growth of oxide and sulphide films and chemical reactions between powdered materials. A number of such reactions are selected for detailed treatment, the experimental methods which have been employed in their study being described and the results obtained discussed in terms of WAGNER's theory, of which a good account is given.

The next two chapters are respectively on diffusion in gases and diffusion in liquids. Both give excellent surveys of the experimental methods and useful collections of experimental results. The theoretical treatment of gaseous diffusion is restricted to the quoting of a number of formulae useful in practical application, for excellent monographs are already available on the subject, but a fuller account is given of the generally less successful attempts that have been made at a theoretical understanding of liquid diffusion.

The book concludes with a useful and interesting chapter on the theory and experimental methods of thermal diffusion in gaseous and condensed phase mixtures.

Extensive bibliographies and references are given at the ends of each chapter.

The emphasis throughout is on the experimental methods of diffusion studies and their results and the book is notable for the large number of numerical results which are quoted; for this reason it forms a most useful source of diffusion data. But in many cases the presentation of data is uncritical, no attempt being made to assess their reliability or accuracy, even when disparent results by different investigators of the same system are quoted side by side.

The summaries that are given of experimental methods are very satisfactory and comprehensive, and the same is generally true of the theoretical sections of the book. There are, however, a number of omissions which are to be regretted in a book of this size. Thus, for example, practically nothing is said of surface diffusion, or of grain boundary diffusion and the important contribution it may make to an observed diffusion flow in polycrystalline materials at low temperatures. Diffusion in aqueous electrolytic solutions only receives very scanty attention, and it is unfortunate that so little space is devoted to the Kirkendall effect and even less to DARKEN's analysis of it for these have been central themes in recent work on diffusion, especially in metals.

However, in spite of these shortcomings the author has largely succeeded in his aim "to assist in planning, evaluating and understanding diffusion experiments, at the same time giving a survey of results to date". Although "to date" is, unavoidably, nearer to 1949 than the present time, references are given in an appendix to papers published as late as 1951.

The printing and binding call for no special comment except for a "misprint" on page 306, the whole of which seems to have been printed from type set up for quite another book! The extensive reader may find the missing page in other publications of the Academic Press, but others will find its omission detracts noticeably from the value of Chapter VII.

The book may be safely recommended to all interested and working in this field as a very useful addition to their shelves, but many may feel that its merits, many though they be, are hardly adequate to justify its very high price.

A. D. LE CLAIRE

A. R. UBBELOHDE; **An Introduction to Modern Thermodynamical Principles.** 2nd Edition, Oxford University Press 1952. 185 pages. 21s.

In this book Professor UBBELOHDE has given a short but comprehensive survey of the main fields of application of statistical thermodynamics. It will be of real value to chemists, engineers and physicists who wish to know the kinds of problem which may be solved by the use of statistical thermodynamics, as a preliminary to studying the more complete treatises. A great deal of ground is covered at a fair pace and almost inevitably there are a few errors and obscurities. For teaching purposes the book could be warmly recommended to those students who have already taken a course of systematic lectures on the foundations of the subject.

The first three chapters are concerned with thermodynamic functions and the fourth and fifth with the Nernst heat theorem. In Chapter VI there is an elementary account of the statistical mechanics of a system of independent particles, using the method of the most probable distribution and STIRLING's theorem. Chapter VII presents a useful survey of the statistical thermodynamics of the solid state, including the DEBYE frequency spectrum, co-operative effects and the BRAGG and WILLIAMS theory of order-disorder transitions in alloys. Chapter VIII is concerned with the methods of attaining very low temperatures.

In Chapter IX there is a short outline of EINSTEIN-BOSE and FERMI-DIRAC statistics. This chapter does not connect up very well with the earlier discussion in Chapter VI of the BOLTZMANN statistics and in particular there is no discussion of the important factor $\log n!$ in the formulae for free energy and entropy. However it is notoriously difficult to carry out a really satisfactory treatment, at an elementary level, of the quantum statistics of non-localised particles.

Chapter X is concerned with rotational and vibrational contributions to the thermodynamic properties of gases and also with the subject of ortho- and para-hydrogen. The three following chapters present very short accounts of the statistical thermodynamics of radiation, adsorption and lattice defects.

Chapter XIV, on melting and crystal structure, is one of the best in the book and is based to a large extent on Prof. UBBELOHDE's own researches. The last two chapters are concerned with isotopes and exchange equilibria and with molecular flexibility and the statistical theory of rubber.

There are certainly very few of the applications of statistical thermodynamics which are not included in this interesting and useful survey.

K. G. DENBIGH

END